이학박사 학위논문

신경세포 특이적 βPix isoform의 발현이 결여된 쥐의 신경생물학적 특징과 βPix-d에 의한 미세소관 안정화 및 신경돌기 발달에 관한 연구

Studies on the characterization of neuronal βPix isoform knockout mouse and the role of βPix-d in microtubule stabilization and neurite outgrowth

2019년 8월

서울대학교 대학원

생명과학부

권 영 희

ABSTRACT

Studies on the characterization of neuronal βPix isoform knockout mouse and the role of βPix-d in microtubule stabilization and neurite outgrowth

Younghee Kwon

School of Biological Sciences

The Graduate school

Seoul National University

βPix activates Rho family small GTPases, Rac1 and Cdc42 as a guanine nucleotide exchange factor. Although overexpression of βPix in cultured neurons indicates that βPix is involved in spine morphogenesis and synapse formation *in vitro*, the *in vivo* role of βPix in neuron is not well understood. Recently, we generated βPix knockout mice that showed lethality at embryonic day 9.5. Here, we investigate the neuronal role of βPix using βPix heterozygous mice that are viable and fertile. βPix heterozygous mice show decreased expression level of βPix proteins in various tissues including brain. Cultured hippocampal neurons from βPix heterozygous mice show a decrease in neurite length and complexity as well as in synaptic density. Both excitatory and inhibitory synapse densities are decreased in these neurons. Golgi-staining of hippocampal tissues from the brain of these mice show reduced dendritic complexity and spine density in the hippocampal neurons. Expression levels of NMDA- and AMPA- receptor subunits and Git1 protein in hippocampal tissues are

also decreased in these mice. Behaviorally, βPix heterozygous mice exhibit impaired social interaction. Altogether, these results indicate that βPix is required for neurite morphogenesis and synapse formation, and the reduced expression of βPix proteins results in a defect in social behavior.

Among alternatively spliced βPix isoforms, βPix-b and βPix-d are expressed specifically in neurons, however their neuronal functions are poorly understood. Here, we generated neuronal βPix isoform knockout (KO) mice in which expression of the neuronal isoforms, βPix-b and βPix-d, are deleted. Loss of the neuronal βPix isoforms leads to reduced Rac1 and Cdc42 activities, decreased dendritic complexity and spine density, and increased GluN2B and CaMKIIα expression in the hippocampus *in vivo*. The defects in neurite development and dendritic spine maturation in cultured neuronal βPix isoform KO hippocampal neurons are recovered by expression of βPix-b or βPix-d. Furthermore, the neuronal βPix isoform KO neurons display decreased excitatory and inhibitory synaptic densities, which are rescued by expression of βPix-b or βPix-d. Neuronal βPix isoform KO mice have defects in long-term potentiation and showed impaired novel object recognition, startle response and prepulse inhibition, and low anxiety levels. Taken together, our research highlights that neuronal βPix isoforms are required for normal development of neuronal structures, synapse formation and behaviors in hippocampus.

Microtubules are one of the major cytoskeletal components of neurites including axons and dendrites. The regulation of microtubule stability is important for appropriate neurite morphogenesis during neuronal development, which in turn is critical for establishment of functional neuronal connections. In neurons, βPix-b plays a role in dendritic spine morphogenesis that mainly involves reorganizations

of actin filaments, but the neuronal role of βPix-d has not been revealed. In addition, the role of neuronal βPix isoforms during neurite outgrowth is not well understood. Here, we unveil a novel mechanism for βPix-d to regulate microtubule stabilization and neurite outgrowth. At DIV4, hippocampal neurons cultured from neuronal βPix isoform KO mice show defects in neurite length and complexity, and microtubule stability. Treatment of taxol that stabilizes microtubules alleviates the impairment of neurite morphology and microtubule stability in the neuronal βPix isoform KO neurons. Neuronal βPix isoforms increase microtubule stability and βPix-d stabilizes microtubules more than βPix-b. We also find the localization of βPix-d on microtubules. In addition, the neuronal βPix isoform KO neurons have a deficit in phosphorylation level of Stathmin1, a microtubule severing protein, at Ser16. Neuronal βPix isoforms recover the impairments of neurite morphology and phosphorylation level in Stathmin1 shown in the neuronal βPix isoform KO neurons and the levels of those recoveries are greater in expression of βPix-d than βPix-b. Furthermore, those recoveries by βPix-d in the neuronal βPix isoform KO neurons are not observed by inhibition of PAK1 activity that phosphorylates Stathmin1 at Ser16. Taken together, our present study show that βPix-d stabilizes microtubules and phosphorylates Stathmin1 at Ser16 with PAK1 more than βPix-b, and is consequently involved in neurite morphogenesis.

Key Words: βPix; βPix heterozygous mice; neuronal βPix isoform knockout mice; βPix-d; neurite; dendritic spine; microtubule stabilization; Stathmin1

Student Number: 2012-23056

TABLE OF CONTENTS

LIST OF FIGURES

BACKGROUND

1. βPix

βPix (beta-PAK (p21-activated kinase) interacting exchange factor) is identified as a protein localized in focal adhesions (Oh et al., 1997) and later demonstrated to act as a guanine nucleotide exchange factor (GEF) for Rac1 and Cdc42 (Koh et al., 2001). Rho family members of small GTPases, including Rac, Cdc42 and Rho, perform distinct roles in the regulation of actin cytoskeleton such as actin polymerization and actomyosin contractility (Etienne-Manneville and Hall, 2002). The Rho GTPases function as molecular switches, cycling between active GTP-bound forms and inactive GDP-bound forms. Among regulatory proteins of Rho GTPases activity, GEFs activate the GTPases by enhancing the exchange of bound GDP for GTP (Bos et al., 2007).

We previously identified various βPix isoforms by alternative splicing (Kim et al., 2000) and translation (Rhee et al., 2004). Depending on the location of expression, βPix can be divided into ubiquitous isoform, βPix-a and neuronal isoforms, βPix-b and βPix-d, containing an insert (INS) domain (Figure 1). βPix acts as an important regulator of cell migration and direction sensing in immune system (Eitel et al., 2008; Volinsky et al., 2006) and cell adhesion, spreading and cell-cell contact formation in cancer cells (Ahn et al., 2003; Flanders et al., 2003; Stevens et al., 2014).

In neurons, βPix is found in both excitatory and inhibitory synapses that are required for precise establishment of neural circuits. The neuronal role of βPix has been identified as a regulator of spine morphogenesis and synapse formation. βPix

Figure 1. Schematic structure of *ARHGEF7* gene encoding βPix with exons corresponding to key domains and domain structure of βPix-a, βPix-b and βPix-d isoforms.

SH3 = Src homology 3 domain, DH = Dbl homology domain, PH = Pleckstrin homology domain, PRD = Proline-rich domain, GBD = GIT1-binding domain, LZ = Leucine zipper domain, INS = novel insert region, 11 a.a. = addition of 11 amino acids region. A red box marks the deleted exon within Insert domain.

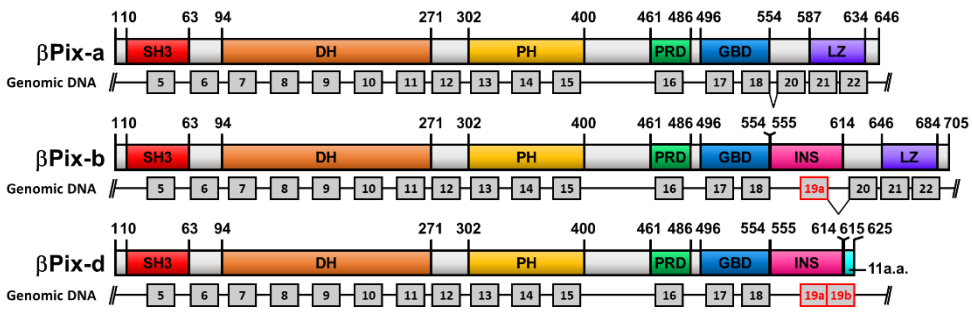
βPix-a
110 63 94 271 302 400 461 486 496 554 587 634 646
SH3 DH PH PRD GBD LZ
Genomic DNA
5 6 7 8 9 10 11 12 13 14 15 16 17 18 20 21 22
βPix-b
110 63 94 271 302 400 461 486 496 554 555 614 646 684 705
SH3 DH PH PRD GBD INS LZ
Genomic DNA
5 6 7 8 9 10 11 12 13 14 15 16 17 18 19a 20 21 22
βPix-d
110 63 94 271 302 400 461 486 496 554 555 614 615 625
SH3 DH PH PRD GBD INS
11a.a.
Genomic DNA
5 6 7 8 9 10 11 12 13 14 15 16 17 18 19a 19b

and Git1 are reported to promote the formation and stabilization of mature dendritic spines together with Rac1 and PAK3 (Zhang et al., 2003; Zhang et al., 2005), CaMKs (Saneyoshi et al., 2008) and K-Cl co-transporter 2 proteins (Llano et al., 2015) in mouse hippocampal neurons, and in *Drosophila* (Parnas et al., 2001). Also, βPix interacts with Shank family in post synaptic density and contributes to synaptic function (Park et al., 2003). In addition to those excitatory synaptic function, βPix and Git1 are essential for $GABA_A$ receptor synaptic stability and inhibitory neurotransmission (Smith et al., 2014). βPix also contributes to presynaptic function by regulating vesicle targeting (Sun and Bamji, 2011).

There are several reports about βPix genetic manipulation in various model organisms. In *C. elegans*, *pix-1* and *pak-1* can control early elongation, which controls remodeling of apical junction and basolateral protrusions via control switch between Rac1- and RhoA-like morphogenetic programs (Martin et al., 2016). In zebrafish, *bubblehead* mutant, with a genetic mutation in βPix, exhibits multiple hemorrhages in brain and defective cerebral vascular stabilization via PAK2a, Git1, and Integrin αvβ8 signaling (Liu et al., 2012). And βPix knockdown in zebrafish with injection of anti-sense morpholino-oligonucleotide yielded embryos with delayed epiboly and with shortened antero-posterior axes (Tay et al., 2010). Recently, Omelchenko *et al.* reported that βPix knockout embryos have a defect in collective cell migration of anterior visceral endoderm cells, leading to developmental defects in embryo morphology and size and embryonic lethality at about embryonic day 8.5 (E8.5) (Omelchenko et al., 2014).

2. Neuronal development

Neurons are one of the most highly polarized cell types, as they possess structurally and functionally different processes, axons and dendrites that extend from the soma to mediate information flow through the nervous system. This polarization underlies the directional flow of information in the central nervous system, so the establishment and maintenance of neuronal polarization is crucial for correct development and function (Takano et al., 2015).

Banker and colleagues established dissociated rodent hippocampal and described in detail the morphological changes that occur during polarization (Dotti et al., 1988). The morphological changes of cultured neurons are divided into five stages (Figure 2A and 2B). Upon isolation, hippocampal neurons retract their processes, so that their development *in vitro* begins with round spheres that spread filopodia (stage 1; shortly after plating). These neurons subsequently form several minor neurites (stage 2; days 0.5-1.5), which show characteristic alternations of growth and retraction. The major polarity event occurs when one of these equivalent minor neurites grows rapidly to become the axon (stage 3; days 1.5-3). The next steps are the morphological development of the remaining short minor neurites into dendrites (stage 4; days 4-7) and the functional polarization of axons and dendrites, including dendritic spine formation (stage 5; >7 days in culture) (Takano et al., 2015). Over the past several years, it has become clear that the Rho family of GTPases and related molecules play an important role in various aspects of neuronal development, including neurite outgrowth and differentiation, axon pathfinding, and dendritic spine formation and maintenance (Govek et al., 2005).

Figure 2. Establishment of polarity and stages of neuronal development in hippocampal neurons.

(A) Schematic representation of neuronal polarization in cultured rat embryonic hippocampal neurons (Arimura and Kaibuchi, 2007). (B) Immunocytochemical images of WT hippocampal neurons at 12 h, 36 h, 4 d and 6 d after plating. Those neurons were stained by F-actin (red), β3-Tubulin (green) and DAPI (blue).

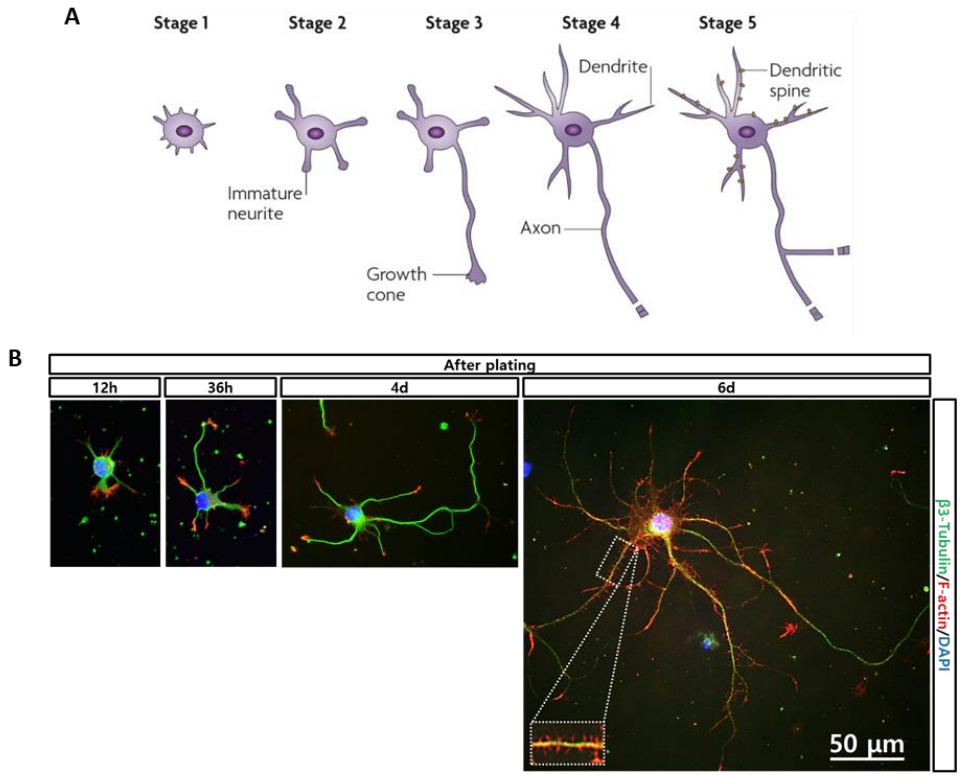
A
Stage 1
Stage 2
Stage 3
Stage 4
Stage 5
Dendrite
Dendritic spine
Immature neurite
Axon
Growth cone
B
After plating
12h
36h
4d
6d
β3-Tubulin/F-actin/DAPI
50 μm

3. Neuronal structures and brain disorders

Neuronal complexity, specifically dendrite branching and morphology, facilitates and allows individual neurons to carry out specialized brain functions and cognitive behaviors, such as social networking, learning, and memory. The dynamic nature and plasticity of the CNS (Dailey and Smith, 1996). The dendrites help the nervous system to effectively process all information it receives from internal and external cues to generate appropriate responses. The branching pattern and the extent of dendrite branching are directly associated with the number and distribution of inputs that the neuron receives and processes. Neuronal networking and neuron-to-neuron communication occurs at specialized junctions called synapses. Precise synapse development is important for accurate neuronal network activity and normal brain function (Kulkarni and Firestein, 2012).

Alterations in dendrite morphology or defects in neuronal development, including changes in dendrite branching patterns, fragmentation of dendrites, retraction or loss of dendrite branching, and changes in spine morphology and number, contribute to several neurological and neurodevelopmental disorders, such as autism spectrum disorders (ASDs), Alzheimer's disease (AD), schizophrenia, Down syndrome, Fragile X syndrome, Rett syndrome, anxiety and depression. Similarly, miscommunication between neurons is also a major underlying cause of many neurological and cognitive disorders, such as mental retardation, schizophrenia, Parkinson's disease, autism and AD ((Kulkarni and Firestein, 2012; Penzes et al., 2011); (Figure 3A and 3B)).

Figure 3. Abnormal neuronal morphology in neurological disorders.

(A) Schematic representation of neuron depicting atrophies in dendrite morphology and spines in brains of individuals with the disorders (Kulkarni and Firestein, 2012). (B) Putative lifetime trajectory of dendritic spine number in the in a normal subject (black), in ASD (pink), in schizophrenia (SZ, green) and in AD (blue) (Penzes et al., 2011).

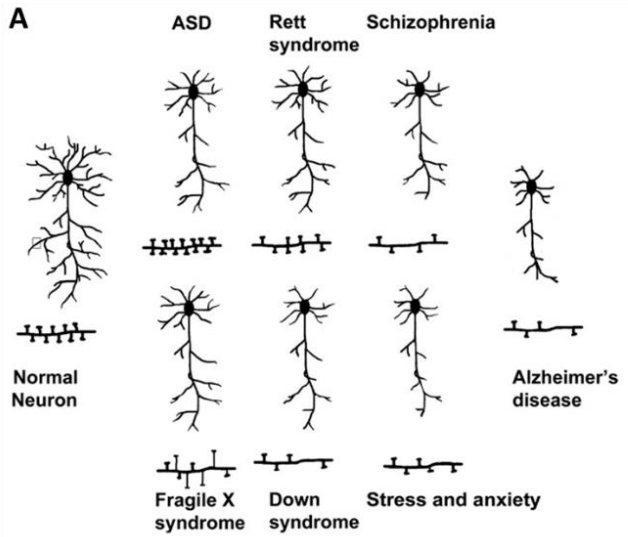
A
ASD
Rett syndrome
Schizophrenia
Normal Neuron
Alzheimer's disease
Fragile X syndrome
Down syndrome
Stress and anxiety

B

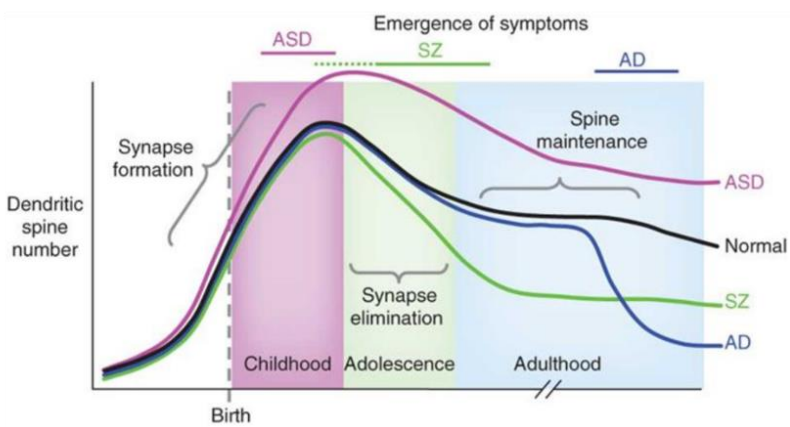
Emergence of symptoms
ASD
SZ
AD
Synapse formation
Spine maintenance
Dendritic spine number
ASD
Normal
SZ
AD
Synapse elimination
Childhood
Adolescence
Adulthood
Birth

4. Microtubule stabilization in neurites

Microtubules are dynamically assembled polymers of α– and β–tubulin that are present in all eukaryotic cells (Janke and Kneussel, 2010) and abundant in neurons, occupying axons and dendrites. The microtubule arrays provide a structural backbone for axons and dendrites that allows them to acquire and maintain their specialized morphologies. The stability properties of neuronal microtubules are commonly discussed in the biomedical literature as crucial to the development and maintenance of the nervous system, and have recently gained attention as central to the etiology of neurodegenerative diseases. A balance between dynamic and stable microtubule fractions contributes to the morphological stability of cells, with a greater proportion of the microtubule mass being stable in cells with relatively stable morphologies, such as neurons ((Baas et al., 2016); (Figure 4A and 4B)).

During the differentiation and maturation of neurons, there are also changes in microtubule associated proteins in different neuronal subcellular domains. The essential and dynamic reorganization phases of the microtubule network during the successive phases of neuronal morphogenesis rely on the tight control of microtubule dynamicity as well as of their fragmentation, transport and stabilization. While most of them act directly on microtubules to stabilize them or promote their assembly, depolymerization or fragmentation, others are now emerging as essential regulators of neuronal differentiation by controlling the amount of free tubulin and hence modulate microtubule dynamics (Poulain and Sobel, 2010).

Microtubule defects cause a wide range of nervous system abnormalities and several human neurodevelopmental disorders have been linked to altered microtubule-meditated processes. Mutations in microtubule-related genes encoding

Figure 4. Post-translational modifications of tubulin and microtubules vary in different regions of a neuron and change during neuronal differentiation.

(A) Schematic representation of how different patterns of tubulin post-translational modifications might specify microtubule functions in neurons (Song and Brady, 2015). (B) Immunocytochemical image of WT hippocampal neurons stained with tα-Tyrosinated α-Tubulin (green), α-Acetylated α-Tubulin (red) and DAPI (blue) at DIV4. Tyrosinated tubulin is relatively enriched in the dendrites, soma and growth cone microtubules. Acetylated tubulin is relatively enriched in the axonal shaft.

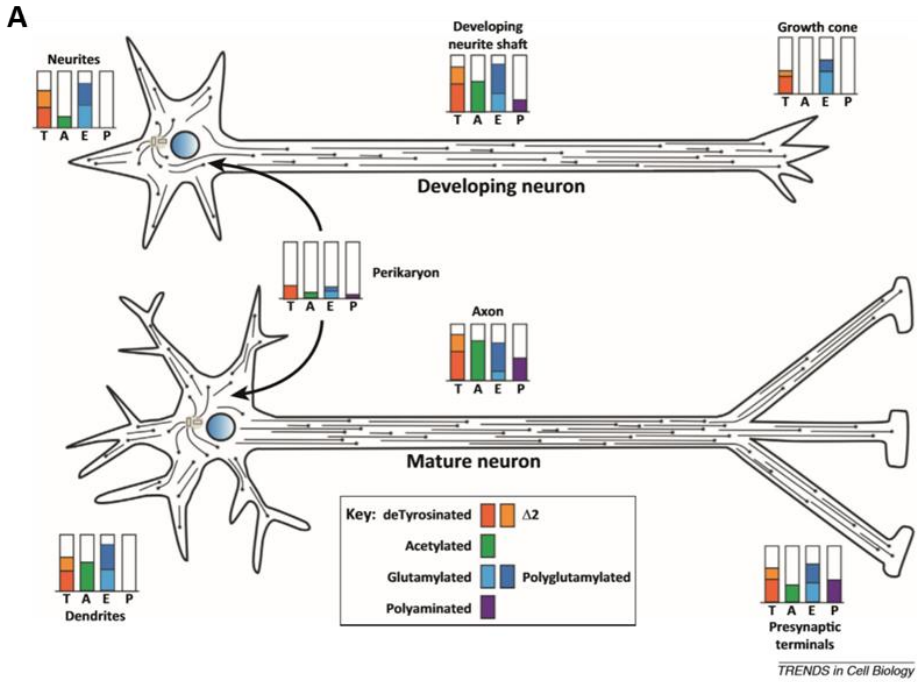
A
Neurites
T A E P
Developing neurite shaft
T A E P
Growth cone
T A E P
Developing neuron
Perikaryon
T A E P
Axon
T A E P
Mature neuron
Key: deTyrosinated
Δ2
Acetylated
Glutamylated
Polyglutamylated
Polyaminated
T A E P
Dendrites
T A E P
Presynaptic terminals
TRENDS in Cell Biology

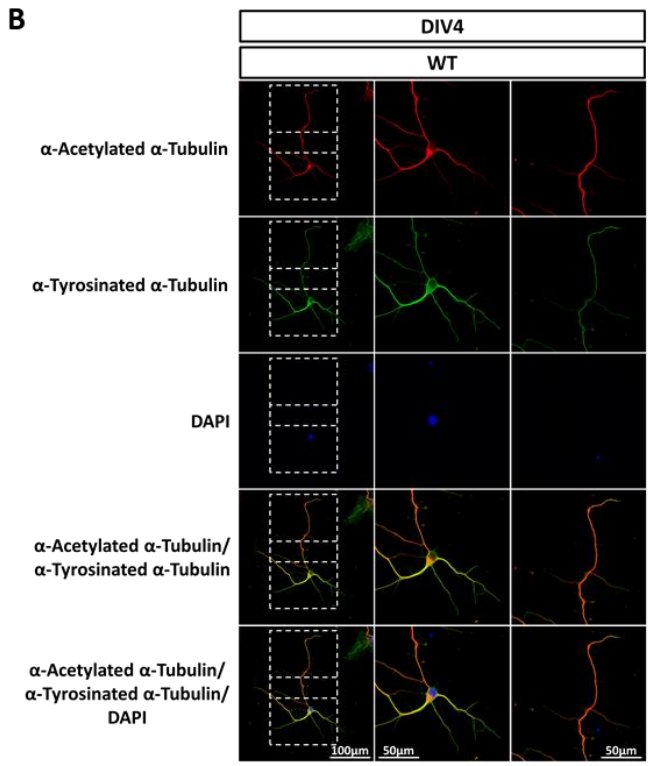
B
DIV4
WT
α-Acetylated α-Tubulin
α-Tyrosinated α-Tubulin
DAPI
α-Acetylated α-Tubulin/
α-Tyrosinated α-Tubulin
α-Acetylated α-Tubulin/
α-Tyrosinated α-Tubulin/
DAPI
100μm
50μm
50μm

for microtubule-associated proteins, microtubule severing proteins, motor proteins and motor associated regulators are associated with various neurodevelopmental problems (Kapitein and Hoogenraad, 2015; Lasser et al., 2018).

5. Stathmin1

Phosphoproteins of the Stathmin family, originally identified as intracellular signal relay proteins, are mostly or exclusively expressed in the nervous system with a high level of expression during brain development. One of the most abundant sources of Stathmin1 is the nervous system, where it is highly expressed and regulated in neurons during development (Chneiweiss et al., 1992). At the molecular level, the best characterized function of Stathmin1 is its capacity to bind tubulin in a phosphorylation dependent manner, and hence its functional contribution to the intracellular regulation of microtubule dynamics (Ravelli et al., 2004). When Stathmins were phosphorylated, Stathmins release tubulin dimers allowing microtubules to be formed. Expression of Stathmins is upregulated during neuronal differentiation and plasticity, and altered in numerous neurodegenerative diseases ((Chauvin and Sobel, 2015); (Figure 5)). In addition, Stathmin has linked to fear, cognition and aging in rodent and human studies (Brocke et al., 2010; Shumyatsky et al., 2005).

Figure 5. Conceptual model for the catastrophe-promoting mechanism by which Stathmin depolymerizes microtubules.

1) Binding of Stathmin (green) to tubulin promotes microtubule catastrophe by sequestering free tubulin (1a) (nFRET hotspots) and by acting on protofilaments at microtubule plus ends, thus destabilizing the tips and increasing the likelihood of catastrophe (1b). 2) Binding of pSer25-/pSer38-Stathmin (orange) to microtubule wall constitutes a pool of inactive Stathmin (2a) (nFRET hotspots), possibly a scaffold with phosphatases, dephosphorylated and contributing to catastrophe; or phosphorylation of Ser25 and/or Ser38 of Stathmin by kinases may change curved to straight T2S complex so it can be incorporated into the growing microtubule (2b). 3) Fully phosphorylated Stathmin detaches from tubulin/microtubules and is unable to either sequester tubulin or promote microtubule disassembly.

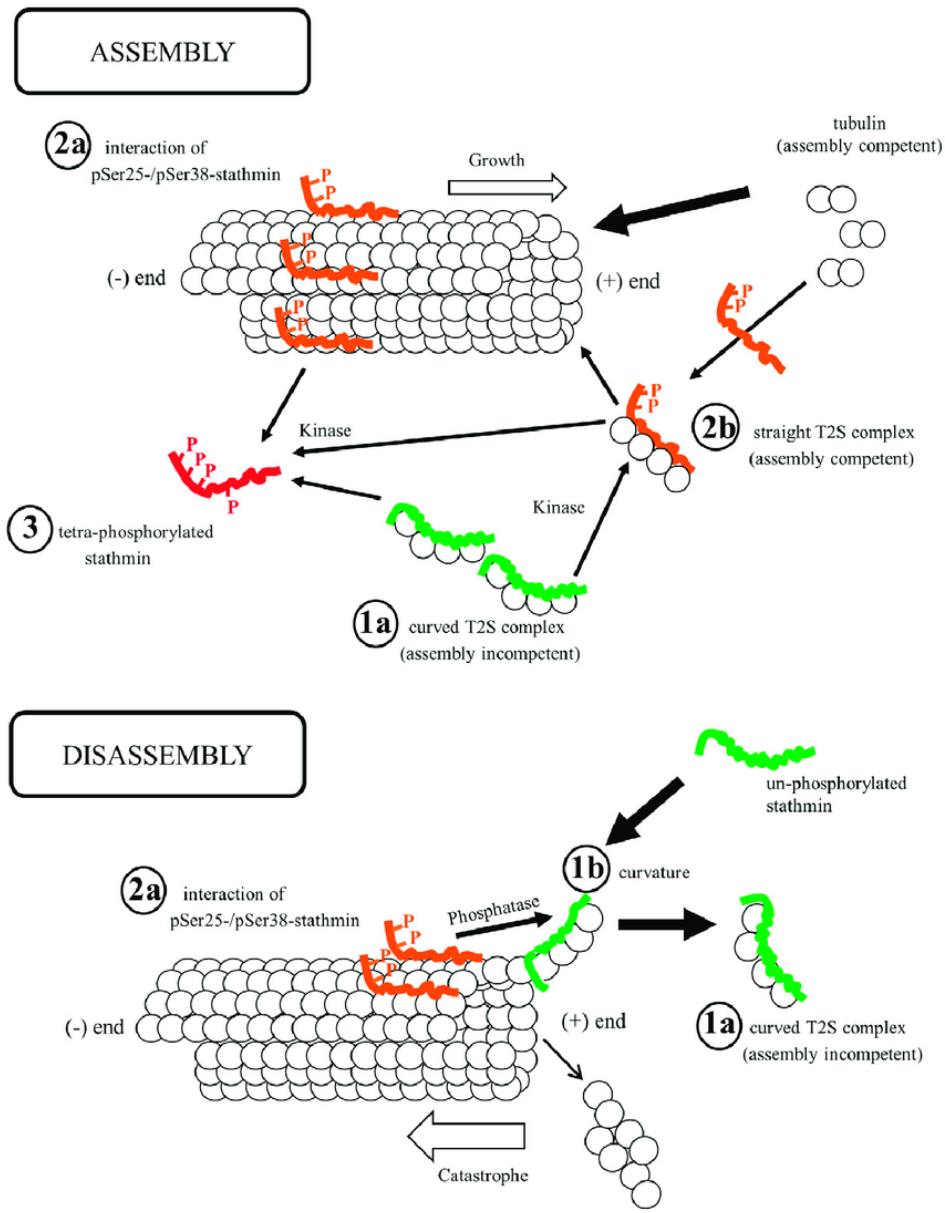
ASSEMBLY
2a interaction of pSer25-/pSer38-stathmin
Growth
tubulin (assembly competent)
(-) end
(+) end
Kinase
2b straight T2S complex (assembly competent)
Kinase
3 tetra-phosphorylated stathmin
1a curved T2S complex (assembly incompetent)
DISASSEMBLY
un-phosphorylated stathmin
1b curvature
2a interaction of pSer25-/pSer38-stathmin
Phosphatase
(-) end
(+) end
1a curved T2S complex (assembly incompetent)
Catastrophe

MATERIALS AND METHODS

1. Mice

Genomic fragment of mouse *ARHGEF7* gene was cloned by screening a CITB mouse BAC clone library (Invitrogen). To generate a gene-targeting vector for *ARHGEF7*, a 3.1 kb and a 3.4 kb fragments flanking exon 19 of this gene were cloned into Os.Dup/Del vector respectively, which carries a neomycin-resistance ($Neo^{R)}$ cassette that replaces the exon 19 and a thymidine kinase cassettes (Figure 6A). J-1 embryonic stem cells were maintained and electroporated with the targeting vector and neomycin-selected. Survived clones were analyzed for proper recombination after digestion with either EcoRI or SacI. Targeted embryonic stem cells were microinjected into the blastocysts of C57BL/6J mice. Resulting founders were mated with C57BL/6J mice (Charles River Breeding Laboratories) and germ line transmission was confirmed by Southern blotting and PCR of genomic DNA. βPix knockout (KO) mice have lethality phenotype at E9.5 and βPix heterozygous (HET) mice, that were viable and fertile, had decreased βPix expression in mRNA and protein level (Figure 6B and 6C). For experiments, interbreeding of βPix HET mice was performed. Genotypes were determined by PCR using following primer pairs (Figure 6D): forward primer 5'-GAC CAC TCT TTC CCT TTG TTC ACA CG-3', wild-type (WT) specific reverse primer 5'-TCG TCA TCA GCC AAG ACG TGA TTA TG-3' and targeted specific reverse primer 5'-TAT CAG GAC ATA GCG TTG GCT ACC CG-3'. Genomic DNA was extracted from mouse tail, and Taq polymerase (Takara) was used for PCR reaction. Annealing temperature was 57.3˚C and PCR products were amplified through 40 cycles.

Figure 6. Generation of βPix heterozygous mice.

(A) Gene targeting strategy for βPix heterozygous mice. (B) RT-PCR analysis for βPix-a and βPix-b mRNA levels in brain, thymus and spleen from 8 weeks WT and βPix heterozygous mice. Locations of PCR primers were presented in arrow in the lower panels. (C) Expression patterns of βPix-a, βPix-b and βPix-d in brain, testis, lung, spleen and heart in 8 weeks WT and βPix heterozygous mice. Equal amounts of 30 μg proteins (homogenates) were loaded per lane and probed with SH3 antibody. 3 independent experiments for (B) and (C). (D) PCR genotyping for WT, βPix HET and βPix KO mice. Genotypes were determined by PCR on tail DNA. Locations of PCR primers are presented in lower panels in (B) (arrow).

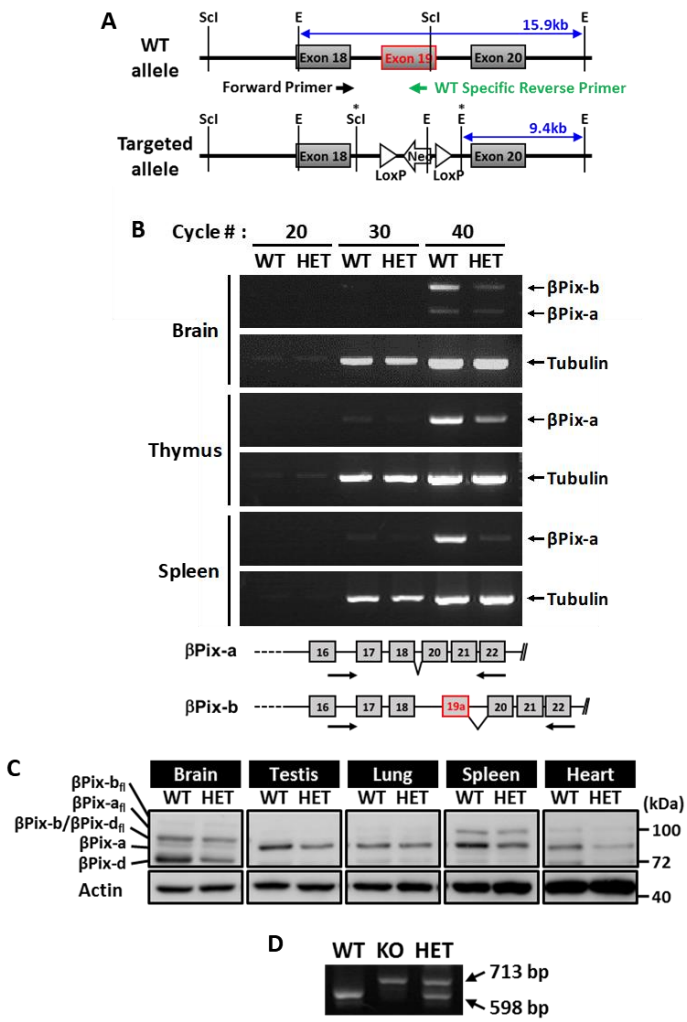
A
WT allele
ScI
E
ScI
E
15.9kb
Exon 18
Exon 19
Exon 20
Forward Primer
WT Specific Reverse Primer
Targeted allele
ScI
E
*
ScI
E
*
E
9.4kb
E
Exon 18
Neo
Exon 20
LoxP
LoxP
B
Cycle # :
20
30
40
WT HET WT HET WT HET
Brain
βPix-b
βPix-a
Tubulin
Thymus
βPix-a
Tubulin
Spleen
βPix-a
Tubulin
βPix-a
16
17
18
20
21
22
βPix-b
16
17
18
19a
20
21
22
C
Brain
Testis
Lung
Spleen
Heart
WT HET WT HET WT HET WT HET WT HET
(kDa)
βPix-bfl
βPix-afl
βPix-b/βPix-dfl
βPix-a
βPix-d
Actin
100
72
40
D
WT KO HET
713 bp
598 bp

To generate neuronal βPix isoform KO mice, exon 19 of *ARHGEF7* gene encoding mouse βPix protein was replaced with a Neo^R cassette. Cre-mediated excision of the neomycin-resistant gene flanked by LoxP sites was performed *in vivo* by crossbreeding with mice harboring a Sox2 promotor driven Cre transgene (Figure 7A). Because the exon 19 is specific to the mRNA of βPix-b and βPix-d isoforms, the knockout resulted in removal of the neuronal βPix isoforms, while maintaining the expression of βPix-a in mRNA (Figure 7B) and protein (Figure 7C) level. After initial confirmation of the deletion of Neo^R gene, neuronal βPix isoform heterozygous mice were established and maintained by backcrossing to C57BL/6 mice for more than five generations. For experiments, interbreeding of neuronal βPix isoform heterozygous mice was performed. Genotypes were determined by PCR using following primer pairs and gave rise to a band of 1,323 bp for WT allele and 960 bp for neuronal βPix KO allele (Figure 7D): forward primer 5'-AGC ACA GTT GAC GTT GCT TTC TGT C-3', WT specific reverse primer 5'- AAA GCC CAT CAG GTA CTC ACT GGA C-3' and neuronal βPix isoform KO specific reverse primer 5'- AAA CTA TCA GTC TGC CCT CAC CCA C-3'. Genomic DNA was extracted from each mouse-tail, and nTaq polymerase (Enzynomics) was used for PCR reaction. Annealing temperature was 58˚C and PCR products were amplified through 40 cycles.

All mice were bred and kept in specific pathogen-free animal facilities at Seoul National University and all procedures were approved by the committees on Animal Research at Seoul National University (SNU-160321-2-5). Mice were fed ad libitum and housed 4-5 by genotype per cage at a constant temperature of 23±1˚C and humidity of 40-60% under a 12 hours light/dark cycle.

Figure 7. Generation of neuronal βPix isoform KO mice.

(A) Gene targeting strategy for neuronal βPix isoform KO mice. (B) RT-PCR analysis for βPix-a and βPix-b mRNA levels in whole brain from WT and neuronal βPix isoform KO mice. Locations of PCR primers were presented in arrow in the lower panels. (C) Expression patterns of βPix-a, βPix-b and βPix-d in brain, liver, lung, thymus, spleen and testis in 4 weeks WT (+/+), neuronal βPix isoform HET (+/Δ) and neuronal βPix isoform KO (Δ/Δ) mice. Equal amounts of 15 μg protein (homogenates) were loaded per lane and probed with the SH3 antibody. 3 independent experiments for (B) and (C). (D) PCR genotyping for +/+, +/Δ and Δ/Δ mice. Genotypes were determined by PCR on tail DNA. Locations of PCR primers are presented in lower panels in (B) (arrow).

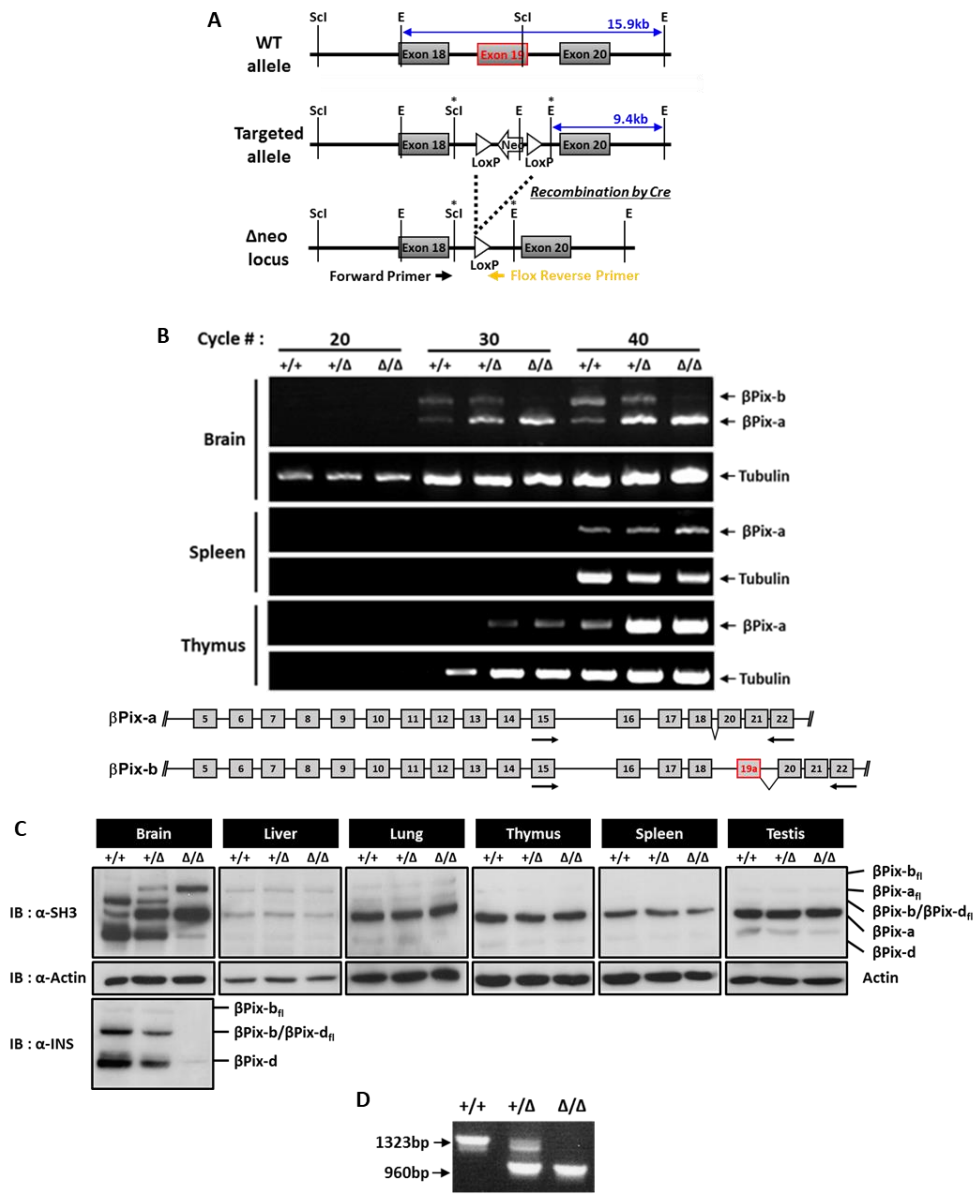
A
WT allele
Targeted allele
Δneo locus
ScI
E
15.9kb
9.4kb
Exon 18
Exon 19
Exon 20
Neo
LoxP
Recombination by Cre
Forward Primer
Flox Reverse Primer
B
Cycle # :
20
30
40
+/+
+/Δ
Δ/Δ
Brain
Spleen
Thymus
βPix-b
βPix-a
Tubulin
βPix-a
βPix-b
C
Brain
Liver
Lung
Thymus
Spleen
Testis
IB : α-SH3
IB : α-Actin
IB : α-INS
βPix-b$_{fl}$
βPix-a$_{fl}$
βPix-b/βPix-d$_{fl}$
βPix-a
βPix-d
Actin
D
1323bp
960bp

2. Reagents and antibodies

For generation of polyclonal rabbit antibodies detecting all βPix isoforms, neuronal βPix isoforms and βPix-d, GST fusion proteins of SH3, INS domain and 11 a.a. (Figure 1A) were respectively purified by glutathione affinity column, as described previously (Kim et al., 2000; Oh et al., 1997). The following antibodies used for the Western blots and immunostainings were commercially purchased: monoclonal mouse antibody against acetylated Tubulin (clone 6-11B-1, Sigma), monoclonal rabbit antibody against Acetyl-α-Tubulin (clone D20G3, Cell Signaling), monoclonal mouse antibody against Actin (clone AC-40, Sigma), monoclonal mouse antibody against CaMKIIα (clone CBα-2, Zymed Laboratories), monoclonal mouse antibody against Cdc42 (clone 44/CDC42, BD Transduction LaboratoriesTM), monoclonal mouse antibody against Gephyrin (clone mAb7a, Synaptic Systems), monoclonal mouse antibody against GFP (clone B-2, Santa Cruz), monoclonal mouse antibody against Git1 (clone 13/p95PKL, BD Transduction Laboratories), monoclonal mouse antibody against GluA1 (clone N355/1, Abcam), monoclonal mouse antibody against GluA2 (clone 6C4, Zymed Laboratories), monoclonal rabbit antibody against GluA4 (Cell Signaling), polyclonal rabbit antibody against GluN2B (Chemicon), polyclonal rabbit antibody against MAP2 (Cell Signaling), monoclonal mouse antibody against Myc (clone 9E10, Santa Cruz), polyclonal rabbit antibody against phopho-PAK1 (Ser199/204) / PAK2 (Ser192/197) (Cell Signaling), polyclonal rabbit antibody against PAK1 (Santa Cruz Biotechnology, Inc.), monoclonal mouse antibody against PSD-95 (clone 7E3-1B8, Thermo Scientific), monoclonal mouse antibody against Rac1 (clone 23A8, Millipore), monoclonal rabbit antibody against Stathmin1 (EP1573Y, Abcam), polyclonal rabbit antibody

against Stathmin1 (phospho S16) (Abcam), monoclonal mouse antibody against Synaptophysin (clone SY38, Chemicon), monoclonal mouse antibody against Tyrosine Tubulin (clone TUB-1A2, Sigma), monoclonal mouse antibody against Tau (clone Tau-5, Chemicon), monoclonal mouse antibody against α-Tubulin (clone DM1A, Abcam), monoclonal mouse antibody against Tubulin, beta III isoform (clone TU-20, Chemicon), polyclonal guinea pig antibody against VGAT (Synaptic Systems) and polyclonal rabbit antibody against VGLUT1 (Synaptic Systems). Taxol was purchased from Sigma.

3. Western blot analysis

For tissue homogenates, the tissues were briefly homogenized in ice-cold homogenization buffer (1 μM aprotinin, 1 μM leupeptin and 1 μM pepstatin in phosphate-buffered slaline (PBS)) with homogenizer and incubated at 4˚C for 30 min after addition of Triton X-100 at 1%. The homogenates were centrifuged at 22,250 g for 30 min at 4˚C. The supernatant was used as lysates for immunoblotting. Protein concentrations were measured by Bradford assay. Equal amounts of protein were resolved by SDS-PAGE and transferred to a PVDF membrane (Millipore). Blots were blocked with 5% skim milk or 3% bovine serum albumin in 0.1% Triton X-100 in PBS (0.1% PBS-T) for 50 min. The blots were incubated with primary antibodies for 1 h at room temperature. Then, the blots were incubated with horseradish peroxidase-conjugated secondary antibodies (Jackson ImmunoResearch Laboratories, Inc.) and analyzed by enhanced chemiluminescence. α-Actin or α-Tubulin was used as loading controls.

4. Nissl staining

12 weeks WT and βPix heterozygous mice were anesthetized and perfused with intracardiac injection of 10 ml PBS followed by 30 ml 3.7% paraformaldehyde (PFA) in PBS. After fixation, the brains were removed and post fixed in 3.7% PFA in PBS for 4 h. The brains were cryoprotected in 30% sucrose in PBS at 4˚C and were embedded and frozen in optimal cutting temperature compound (Tissue-Tek). 25 μm serial sagittal sections cut by a cryostat (Leica, CM1900) were mounted on gelatin-coated slides. Then, the sections were dehydrated with ascending series of ethanol concentrations (75, 95 and 100%), treated with xylene for 5 min and rehydrated in descending series of ethanol concentrations (100, 95 and 75%) and in MilliQ water. They were stained with 1% cresyl violet (Sigma) solution for 3 min. Finally, the stained sections were dehydrated in ascending series of ethanol (75, 95 and 100%), treated with xylene and coverslipped using PermountTM mounting medium (Fisher Scientific). Images were acquired by Zeiss Lumar V12 (Germany) using a 0.8 x (NeoLumar S) objective lens.

5. Primary hippocampal neuron culture and transfection

Mouse hippocampal cultures were prepared from postnatal day 0-1 (P0-1) mouse pups of either sex as previously described (Beaudoin et al., 2012). Dissociated hippocampi tissues were treated with papain (20 μg/ml) and DNase (10 units/μl) for 20 min at 37 °C. The tissues were then mechanically dissociated by tituration with a glass Pasteur pipette. Hippocampal neurons ($2x10^5$ cells / 60 mm dish) were plated in MEM (Welgene) supplemented with 0.6% glucose, 1 mM sodium pyruvate, 1% penicillin-streptomycin (Gibco), 2 mM L-glutamine and 10% certified fetal bovine

serum (c-FBS) (Gibco) for 4 hours before exchange with Neurobasal media (Gibco) supplemented with 0.5 mM L-glutamine and B27 supplement (Gibco). The cells were maintained in a 5% CO_2 incubator at 37 °C. Every four to seven days, half of the original media was discarded and replaced with fresh Neurobasal media supplemented with 0.5 mM glutamine and B27 supplement. When hippocampal neurons were transfected at DIV3, Lipofectamine 2000 (Invitrogen) was used according to the manufacturer's instructions, and when transfected at DIV7, a modified calcium phosphate method using CalPhos Transfection Kit (Calbiochem) was performed (Ryan et al., 2005).

6. Immunocytochemistry

Mouse hippocampal neurons seeded on 12 mm or 18 mm coverslips were fixed for 10 min in 3.7% PFA in PBS at room temperature. The neurons were permeabilized with 0.5% PBS-T for 10 min and then incubated in blocking solution (10% c-FBS, 0.5% gelatin and 0.1% PBS-T) for 30 min. The coverslips were then incubated with primary antibodies diluted in blocking solution for 1 h at room temperature. After washing with 0.1% PBS-T, coverslips were stained with FITC-conjugated or TRITC-conjugated anti-mouse or anti-rabbit IgG (Jackson ImmunoResearch Laboratories, Inc.), AMCA-conjugated anti-rabbit IgG (Jackson ImmunoResearch Laboratories, Inc.) or Alexa Fluor 350-conjugated anti-mouse IgG (Invitrogen) for 1 h. Following incubation, coverslips were washed with 0.1% PBS-T and mounted with Vectashield (Vector Laboratories). The stained neurons were observed with a Zeiss LSM700 confocal microscope equipped with a 20x, 0.8 Plan-Apochromat objective lens and a 40x, 1.20 C-Apochromat objective lens. Imaging settings were kept constant

throughout all images in the same experiment and Z-stacked images were converted to maximal projection. The images were quantified using ImageJ software (NIH) in a blinded manner and the measured values were transferred to Excel program (Microsoft).

7. Analysis of neuronal morphology and synapse density in cultured hippocampal neurons

Neurite complexity was quantified by Sholl analysis, as follows (Sholl, 1953). A transparent grid with equi-distant (10 μm) concentric rings was placed over the dendritic tree tracings. The numbers intersecting the concentric rings and neurites were measured manually. To analyze the protrusion morphology and the synapse densities in transfected neurons, three or more dendritic segments that are longer than 10 μm were randomly selected from secondary or tertiary dendrites. Protrusion length was defined as the length from the base of the neck to the furthest end of the spine head and width was measured as the head diameter perpendicular to the spine neck. The protrusions with a length of 3 μm or more and a width of 0.3 μm or less were categorized as filopodial structures whereas the rest was categorized as dendritic spines. For synapse density, hippocampal neurons were stained with antibodies against post-synaptic marker PSD-95 and pre-synaptic marker VGLUT for excitatory synapse, and post-synaptic marker Gephyrin and pre-synaptic marker VGAT for inhibitory synapse. Each synapse was classified by counting colocalization of signal of these pre- and post-synaptic markers. Neuron J and Synaptcount J plugins in ImageJ software were used for counting synapses.

8. Golgi staining

5 and 12 weeks WT and βPix heterozygous mice were anesthetized and perfused with intracardiac injection of 10 ml PBS followed by 30 ml 3.7 % PFA in PBS. After fixation, the brains were removed and stained by standard Golgi-Cox impregnation using the FD Rapid GolgiStain kit (NeuroTechnologies). 150 μm thick serial sagittal sections were obtained using a vibratome, collected on clean gelatin-coated microscope slides and mounted with PermountTM mounting medium (Fisher Scientific). Z-stack images that were converted to maximal projection were acquired by Zeiss Axiovert 200M microscope equipped with a Zeiss Axiocam HRm CCD camera using a 40 x, 0.6 LD Achroplan objective lens and 100 x, 1.40 Plan-Apochromat objective lens, respectively. The images were quantified using ImageJ software in a blinded manner and the measured values were transferred to Excel program.

9. Sholl analysis and analysis of spine density in Golgi stained tissues

Pyramidal neurons from CA1 hippocampal regions were readily identified by their characteristic triangular soma-shape and subjected to analyses on their basal dendrites. Sholl analysis for dendritic complexity and analysis of spine density were performed as described for cultured hippocampal neurons shown above. In order to analyze mature dendritic spines, immature filopodia with a length of 2 μm or more and a width of 0.2 μm or less are excluded.

10. *In vivo* glutathione S-transferase (GST) pull-down assay

For whole brain and hippocampus homogenates, brains of 5 weeks mice were

briefly homogenized in ice-cold homogenization buffer (50 mM HEPES, pH 7.4, 150 mM NaCl, 15 mM NaF, 1 mM Na3VO4, 1 μM aprotinin, 1 μM leupeptin and 1 μM pepstatin) with homogenizer and incubated at 4˚C for 30 min after addition of 0.5% NP-40. The homogenates were centrifuged at 22,250 g for 30 min at 4˚C. The supernatant was used as lysates for GST pull-down assays. Protein concentrations were measured by the Bradford assay (Biorad). 700-800 μg lysates were incubated with 10 μg GST-Rac/Cdc42 (p21) binding domain (PBD) proteins pre-bound to 50% slurry of Glutathione Sepharose 4B (Amersham Pharmacia) for 1 hour at 4 ˚C. After the incubation, the resins were washed three times to remove unbound proteins and then subjected to 12% SDS-PAGE and immunoblotting. GST-PBD was detected by Coomassie Brilliant Blue staining.

11. Postsynaptic density (PSD) preparation from mouse brain

Whole brain and hippocampal tissues were obtained from 5 and 12 weeks mice and experiments were performed as described previously (Peca et al., 2011). For hippocampus samples, tissues from three mice were pooled to generate one sample. Brain or hippocampal tissues were homogenized in ice-cold homogenization buffer (320 mM Sucrose, 4 mM HEPES, pH 7.4, 2 mM EGTA, 50 mM NaF, 0.5 mM Na_3VO_4, 1 μM aprotinin, 1 μM leupeptin and 1 μM pepstatin) by glass homogenizer with 15-20 strokes. Homogenates were centrifuged for 15 min at 1,000 g at 4°C. Collected supernatants were centrifuged again for 15 min at 10,000 g at 4°C. Next, the resulting pellets were resuspended in the homogenization buffer and were centrifuged for 15 min at 1,000 g at 4°C to obtain the crude synaptosomal fraction. The pellet was dissolved in hypo-osmotic buffer (2 mM EGTA, 50 mM NaF, 0.5 mM

Na_3VO_4, 1 μM aprotinin, 1 μM leupeptin and 1 μM pepstatin) by manually applying 5-7 strokes using a tissue grinder and then followed by addition of 1 M HEPES, pH 7.4. Then the hypo-osmotic synaptosomal fraction was rotated for 1 hour at 4°C. Hypo-osmotic synaptosomal fractions were centrifuged for 20 min at 25,000 g at 4°C and the pellets were snap frozen on dry ice. The pellets were resuspended in PSD preparation buffer (50 mM HEPES, pH 7.4, 2 mM EDTA, 2 mM EGTA, 50 mM NaF, 0.5 mM Na_3VO_4, 1 μM aprotinin, 1 μM leupeptin and 1 μM pepstatin). To prepare the PSD fraction, 10% Triton X-100 was added in the resuspended pellets and they were incubated for 30 min at 4°C. Then, they were centrifuged for 20 min at 32,000 g at 4°C and the pellets were resuspended in the PSD preparation buffer to obtain PSD-1T fractions. The PSD-1T fractions were divided in half and 10% Triton X-100 was added in one of the two. In the same way, they were incubated for 30 min at 4°C. Then, they were centrifuged for 15 min at 200,000 g at 4°C and the pellets were resuspended in the PSD preparation buffer to obtain PSD-2T fractions. Using the bicinchoninic acid protein assay (Thermo Scientific Pierce), protein concentrations were measured for each sample.

12. Immunohistochemistry

5 weeks WT mice were deeply anesthetized by carbon dioxide and perfused with intracardiac injection of 10 ml PBS followed by 30 ml 3.7% PFA in PBS. After fixation, the brains were removed from mice and post-fixed in 3.7% PFA in PBS for 4 hours at room temperature. The brains were placed with 30% sucrose in PBS at 4 ˚C to remain more pliable and less prone to fracture, and were embedded and frozen in a gel like medium called optimal cutting temperature (O.C.T.) compound (Tissue-

Tek). 25 μm serial sagittal sections cut by cryostat (Leica, CM1900) were mounted on gelatin-coated slides. Then, the sections were permeabilized with 0.5% PBS-T for 10 min and then incubated in blocking solution (10% c-FBS, 0.5% gelatin and 0.1% PBS-T) for 30 min. The sections were then incubated with primary antibodies diluted in blocking solution during overnight at 4 °C. After washing with 0.1% PBS-T, the sections were stained with Alexa Fluor® 555 donkey anti-rabbit IgG and Alexa Fluor® 488 donkey anti-mouse IgG (Invitrogen) for 1 hour. Following incubation, the sections were washed with 0.1% PBS-T, mounted with Vectashield that was mixed with DAPI. We observed with Zeiss LSM700 confocal microscope equipped with a 10x, 0.45 Plan-Apochromat objective, a 20x, 0.8 Plan-Apochromat objective and a 40x, 1.20 C-Apochromat objective. All image settings were kept constant in the same experiment and Z-stacked images were converted to maximal projection. For co-localization analysis, we used co-localization plugins in ImageJ software.

13. Constructs

Expression vectors were cloned by PCR-based strategy into pEGFP-N1 vector (Clontech) and pcDNA3.1 myc/his vector (Invitrogen). To generate GFP-βPix-a, GFP-βPix-b or GFP-βPix-d, coding regions of βPix-a, βPix-b or βPix-d were subcloned into pEGFP-N1 by PCR and to generate Myc-PID, 83-149 a.a. of PAK1 coding regions which inhibits all group I PAKs were subcloned into pcDNA3.1 myc/his vector by PCR.

14. Statistics

All analyses were completed from a minimum of three independent experiments.

All data are expressed as mean ± standard error of the mean. *P* values (* $P<0.05$, ** $P<0.01$ and *** $P<0.001$) are statistically evaluated from two-tailed student's t-test.

CHAPTER I

Studies on the characterization of βPix heterozygous mouse and neuronal βPix isoform knockout mouse

Abstract

βPix activates Rho family small GTPases, Rac1 and Cdc42 as a GEF. In neurons, βPix regulates axon formation, dendritic spine morphogenesis and synapse formation. The formation and plasticity of dendritic spines are essential processes for normal brain function. Among alternatively spliced βPix isoforms, βPix-b and βPix-d are expressed specifically in neurons. Although previous studies on the role of βPix in neurons have shown *in vitro*, the neuronal role of βPix *in vivo* is not well understood. Here, we generated βPix heterozygous mice and neuronal βPix isoform KO mice, and investigated neuronal structures and synapse formation in those mice. Firstly, βPix heterozygous mice have reduced expression of βPix in brain and show abnormal morphology of neurite and spine *in vitro* and *in vivo*. Also, cultured hippocampal neurons from βPix heterozygous mice have decrease in synapse density. The expression levels of NMDA- and AMPA-receptor subunits and Git1 protein are decreased in hippocampus from βPix heterozygous mice. Behaviorally, βPix heterozygous mice exhibit impaired social interaction. Altogether, these results indicate that βPix is required for morphogenesis of neurite and dendritic spine and the decreased βPix expression causes defective social behavior. Next, in neuronal βPix isoform KO mice, loss of neuronal βPix isoforms leads to reduced Rac1 and Cdc42 activities, decreased dendritic complexity and spine density, and increased GluN2B and CaMKIIα expression in the hippocampus *in vivo*. The defects in neurite development and dendritic spine maturation in cultured neuronal βPix isoform KO hippocampal neurons are recovered by expression of βPix-b or βPix-d. Furthermore, neuronal βPix isoform KO neurons display decreased excitatory and inhibitory

synaptic densities, which are rescued by expression of βPix-b or βPix-d. Our electrophysiological analysis shows reduced long-term potentiation in Schaffer collateral-CA1 synapses of neuronal βPix isoform KO hippocampus and in behavioral studies, neuronal βPix isoform KO mice exhibit robust deficits in novel object recognition. In addition, neuronal βPix isoform KO mice show impaired startle response and prepulse inhibition, and low anxiety levels. Taken together, our study suggests that neuronal morphogenetic signaling by neuronal βPix isoforms contribute to the hippocampal synaptic function and behavior.

Introduction

Neurons communicate with one another via excitatory or inhibitory synapses that regulate neuronal activity. Dendritic spines are actin-rich protrusive structures that mainly mediate excitatory synaptic transmission (Matus et al., 1982). Immature dendritic protrusions, classified as filopodia, are long and thin, whereas mature dendritic protrusions, classified as spines, tend to have well-defined head and neck structures (Newey et al., 2005). The morphogenesis of dendritic spines is particularly important during synaptic plasticity underlying normal cognitive functions such as learning and memory (Alvarez and Sabatini, 2007; Nimchinsky et al., 2002). Impairments in their morphogenesis are associated with numerous neurological disorders including ASD, attention deficit hyperactivity disorder (ADHD) and schizophrenia (Penzes et al., 2011).

The morphological plasticity of dendritic spines involves actin cytoskeleton reorganization (Luo, 2002). Rho family members of small GTPases, including Rac, Cdc42 and Rho, perform distinct roles in the regulation of actin cytoskeleton such as actin polymerization and actomyosin contractility (Etienne-Manneville and Hall, 2002). The Rho GTPases function as molecular switches, cycling between active GTP-bound forms and inactive GDP-bound forms. The precise spatio-temporal control of Rho GTPase signaling is regulated by GEFs, which activates Rho GTPases by catalyzing the exchange of GDP for GTP (Schmidt and Hall, 2002), and GTPase activating proteins (GAPs), which inhibit Rho GTPases by facilitating GTP hydrolysis (Moon and Zheng, 2003). Interestingly, recent studies suggest that GEFs modulate neuronal morphology, synaptic plasticity and cognitive function (De

Filippis et al., 2014; Miller et al., 2013).

βPix was identified as a protein localized in focal adhesions (Oh et al., 1997) and was later demonstrated to act as a Rho GEF that specifically activates Rac1 and Cdc42 (Bagrodia et al., 1998; Koh et al., 2001). βPix acts as an important regulator of cell migration and direction sensing in immune systems (Eitel et al., 2008; Volinsky et al., 2006) and cell adhesion, spreading and cell-cell contact formation in cancer cells (Ahn et al., 2003; Flanders et al., 2003; Stevens et al., 2014). In neurons, βPix has been identified as a regulator of spine morphogenesis and synapse formation (Park et al., 2003; Saneyoshi et al., 2008; Zhang et al., 2005). We previously identified alternatively spliced isoforms of βPix: βPix-a, βPix-b and βPix-d (Figure 1). While βPix-a is ubiquitously expressed in most tissues, βPix-b and βPix-d are mainly expressed in brain, specifically in neurons (Kim et al., 2000; Oh et al., 1997; Rhee et al., 2004). Until now, most studies on the neuronal role of βPix have studied only using *in vitro* models. In addition, there has so far been no documentation of neuronal function for each of neuronal βPix isoform.

In order that we systematically investigate the neuronal roles of neuronal βPix isoforms on neuronal structures and synapse formation *in vivo*, we generated two types of mice lacking βPix expression, βPix heterozygous mice and neuronal βPix isoform KO mice. Firstly, we identify that βPix heterozygous mice have decreased expression level of βPix in various tissue including brain. Cultured hippocampal neurons from βPix heterozygous mice have decreased length and complexity of neurite and dendritic spine density. Both excitatory and inhibitory synapse density are decreased in the hippocampal neurons from βPix heterozygous mice. Golgi-stained hippocampal neurons from βPix heterozygous mice have defects in dendritic

complexity and dendritic spine density. In hippocampus from βPix heterozygous mice, expression level of NMDA and AMPA receptor subunits and Git1 protein are decreased. Next, Rac1 and Cdc42 activities are decreased in hippocampus from the neuronal βPix isoform KO mice and pyramidal neurons in that region have simplified dendritic arbors and reduced dendritic spine density *in vivo*. Interestingly, expression level of NMDA receptor subunit and CaMKIIα proteins were increased in hippocampus from neuronal βPix isoform KO mice. *In vitro* analyses of hippocampal neurons from neuronal βPix isoform KO mice showed impaired development of neurite, dendritic spine and synapses, and those defects are recovered by expression of the neuronal βPix isoforms. Furthermore, neuronal βPix isoform KO mice exhibited a significant decrease in long-term potentiation (LTP) and deficits in novel object recognition. Behaviorally, neuronal βPix isoform KO mice have impaired startle response and PPI, and decreased anxiety-like behavior in elevated plus maze. These data suggest that the neuronal βPix isoforms are required for normal development of neuronal structures and functions in hippocampus, affecting hippocampal-related synaptic transmissions and behaviors.

Results

1. Characterization of βPix heterozygous mouse

1.1. βPix heterozygous mice have decreased βPix expression level in brain.

There were no differences between WT and βPix heterozygous mice in body weight (Figure 8A) and gross anatomy of the brain (Figure 8B). Meanwhile, in various tissue of βPix heterozygous mice, the level of βPix expression was decreased to approximately half of that of WT mice (Figure 6C). In central nervous system, several neuronal βPix isoforms including βPix-b and βPix-d are expressed in addition to the ubiquitous βPix-a isoform (Kim et al., 2000; Shin et al., 2019). In βPix heterozygous mice, expression of all the βPix isoforms in various brain regions and spinal cord were reduced (Figure 9). These results suggest that βPix heterozygous mice can be used as an appropriate mouse model to study the effects of βPix deficiency in the brain.

1.2. Cultured hippocampal neurons from βPix heterozygous mice show defects in the development of neurite, dendritic spine and synapse.

Previous reports showed that βPix can affect neuronal structures, such as dendritic branches and spines (Llano et al., 2015; Lopez Tobon et al., 2018; Saneyoshi et al., 2008; Shin et al., 2019; Zhang et al., 2005). To determine the effects of the reduced βPix level on neuronal morphogenesis *in vitro*, hippocampal neurons from WT and βPix heterozygous mice were cultured and the morphology of neurite and dendritic spine of mature neurons at DIV14 were analyzed. The hippocampal neurons from βPix heterozygous mice had shorter neurites and less branches than the WT neurons

Figure 8. βPix heterozygous mice show normal body weight and gross anatomy of the brain.

(A) Body weight revealed no genotype differences in 5 and 12 weeks WT and βPix heterozygous mice. (B) Nissl stained sagittal sections of hippocampus and cerebellum from 12 weeks mice. 4 mice were analyzed in each group for (A).

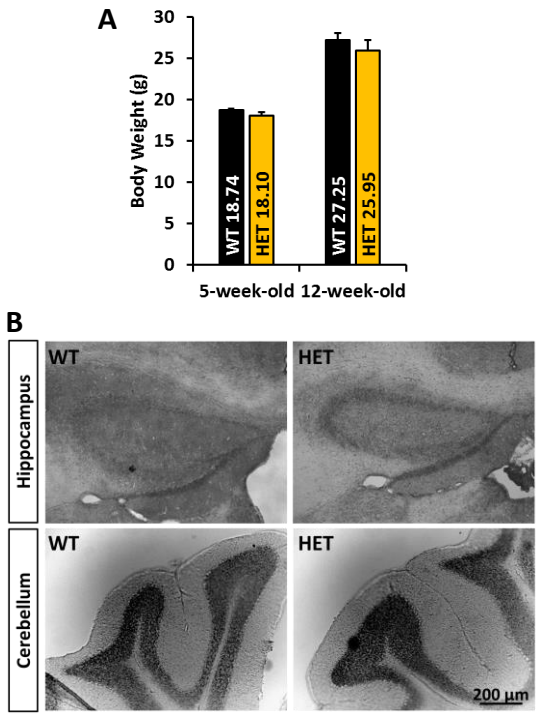
A
Body Weight (g)
30
25
20
15
10
5
0
WT 18.74
HET 18.10
WT 27.25
HET 25.95
5-week-old
12-week-old
B
Hippocampus
Cerebellum
WT
HET
WT
HET
200 µm

Figure 9. Expression levels of βPix isoforms are reduced in brain and spinal cord of βPix heterozygous mice.

Expression patterns of βPix in olfactory bulb, frontal cortex, striatum, hippocampus, cerebellum, brain stem and spinal cord from 12 weeks WT and βPix heterozygous mice. Equal amounts of 15 μg protein (homogenates) were loaded per lane and probed with the SH3 antibody.

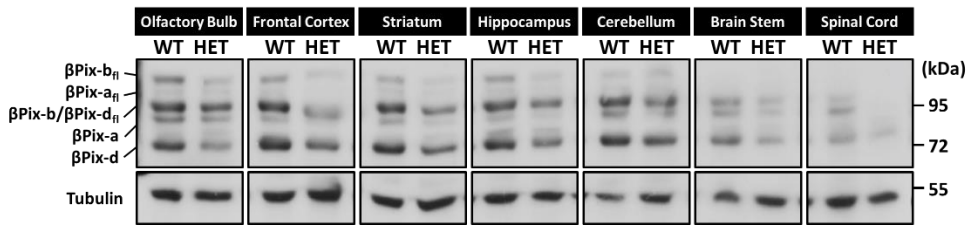
Olfactory Bulb
Frontal Cortex
Striatum
Hippocampus
Cerebellum
Brain Stem
Spinal Cord
WT HET
βPix-bfl
βPix-afl
βPix-b/βPix-dfl
βPix-a
βPix-d
Tubulin
(kDa)
95
72
55

(Figure 10A). Quantitatively, total neurite length per neuron had 55% decrease in βPix heterozygous mice, compared with that in WT mice (Figure 10B). By Sholl analysis, βPix heterozygous mice had reduced neurite complexity, compared with βPix WT mice (Figure 10C). Based on previous studies, immature dendritic protrusions, classified as filopodia, are long and thin, whereas mature dendritic protrusions, classified as spines, tend to have well-defined head and neck structures (Newey et al., 2005). βPix heterozygous neurons hade more long and thin protrusions on dendritic shaft than WT neurons (Figure 11A-11C). Among all protrusions from dendritic shafts, the hippocampal neurons from βPix heterozygous mice had 72% increase in filopodia, but 22% decrease in dendritic spine, compared with the WT neurons (Figure 11D). Indeed, dendritic spine density have 41% decrease in βPix heterozygous neurons, compared with WT neurons (Figure 11E). These results indicate that βPix plays an important role in neuronal morphogenesis. To assess whether the defects in dendritic development due to βPix deficiency also affect synapse formation, we analyzed the densities of excitatory and inhibitory synapses by immunostaining with synaptic markers (Figure 12A and 12C). Compared to WT mice, βPix heterozygous mice had 58% decrease for excitatory synapse density (Figure 12B) and 34% decrease for inhibitory synapse density (Figure 12D). Altogether, these data indicate that βPix is critical for neurite and spine development and synapse formation.

1.3. Dendritic complexity and spine density are decreased in hippocampal neurons of βPix heterozygous mice *in vivo*.

To investigate the role of βPix in neuronal morphogenesis *in vivo*, dendrite and

Figure 10. βPix heterozygous mice have defects in neurite morphology in cultured hippocampal neurons.

(A) Representative images of cultured hippocampal neurons transfected with GFP at DIV7 and analyzed by tracing GFP fluorescence at DIV14. (B) Total neurite length was significantly shorter in the hippocampal neurons from βPix heterozygous mice than from WT mice. (C) Sholl analysis revealed simplified dendritic arborizations of βPix heterozygous mice, compared to WT mice. 45-64 neurons were analyzed in each group.

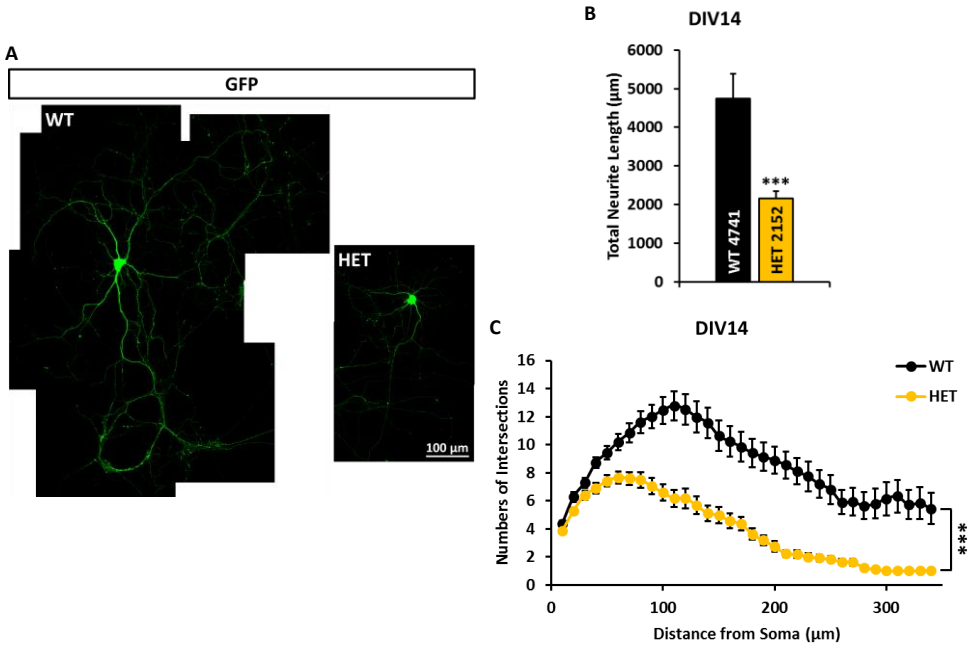
A
GFP
WT
HET
100 µm
B
DIV14
Total Neurite Length (µm)
6000
5000
4000
3000
2000
1000
0
WT 4741
HET 2152
***
C
DIV14
Numbers of Intersections
16
14
12
10
8
6
4
2
0
0
100
200
300
Distance from Soma (µm)
WT
HET
***

Figure 11. βPix heterozygous mice have defects in dendritic spine morphology in cultured hippocampal neurons.

(A) Representative images of cultured hippocampal neurons transfected with GFP at DIV7 and analyzed by tracing GFP fluorescence at DIV14. (B) The length of protrusions was significantly longer in βPix heterozygous mice than in WT mice. (C) The width of protrusions was significantly thinner in βPix heterozygous mice than in WT mice. (D) Percentage of filopodia and spine on the dendrites of cultured hippocampal neurons from WT and βPix heterozygous mice. Filopodia percentage of βPix heterozygous mice was significantly higher than that of WT mice. (E) Dendritic spine portion was significantly decreased in βPix heterozygous mice than in WT mice. 1412-1493 protrusions were analyzed in each group.

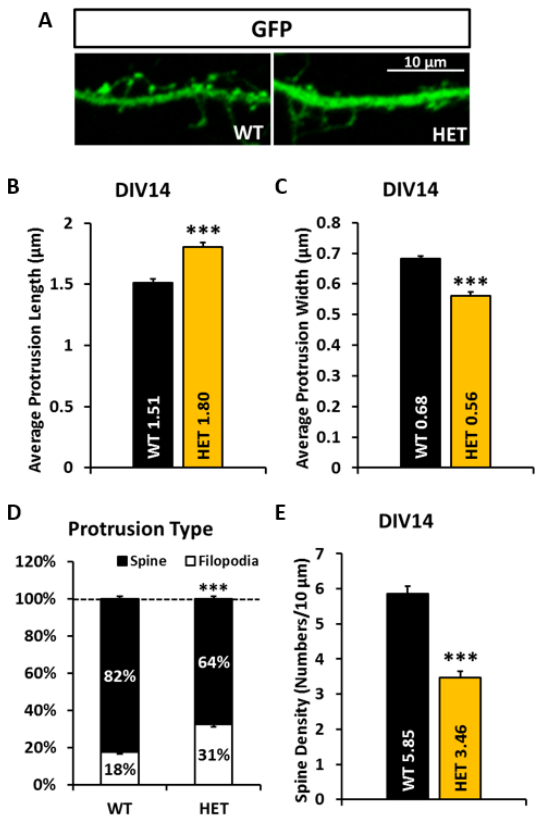
A
GFP
10 µm
WT
HET
B
DIV14
Average Protrusion Length (µm)
2
1.5
1
0.5
0
***
WT 1.51
HET 1.80
C
DIV14
Average Protrusion Width (µm)
0.8
0.7
0.6
0.5
0.4
0.3
0.2
0.1
0
***
WT 0.68
HET 0.56
D
Protrusion Type
Spine
Filopodia
120%
100%
80%
60%
40%
20%
0%
***
82%
18%
64%
31%
WT
HET
E
DIV14
Spine Density (Numbers/10 µm)
7
6
5
4
3
2
1
0
***
WT 5.85
HET 3.46

Figure 12. βPix heterozygous mice have decreased synapse density in cultured hippocampal neurons.

(A) Representative images of cultured hippocampal neurons stained for excitatory synapse at DIV14. Empty arrowheads point to the VGLUT1-positive PSD-95 indicating excitatory synapse. Quantification in (B). (B) Excitatory density was decreased in cultured hippocampal neurons from βPix heterozygous mice, compared with WT mice. (C) Representative images of cultured hippocampal neurons stained for inhibitory synapse at DIV14. Arrowheads point to the VGAT-positive Gephyrin indicating inhibitory synapse. Quantification in (D). (D) Inhibitory density was decreased in cultured hippocampal neurons from βPix heterozygous mice, compared with WT mice. 92-104 dendritic segments were analyzed in each group.

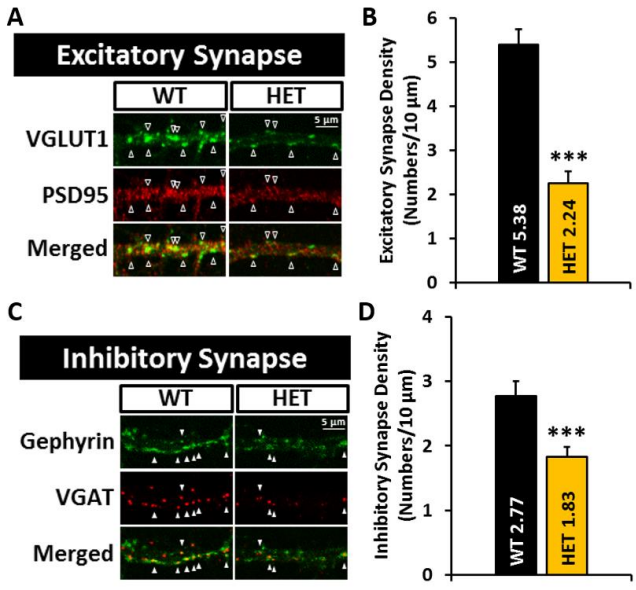
A
Excitatory Synapse
WT
HET
VGLUT1
PSD95
Merged
5 μm
B
Excitatory Synapse Density (Numbers/10 μm)
0
1
2
3
4
5
6
WT 5.38
HET 2.24
***
C
Inhibitory Synapse
WT
HET
Gephyrin
VGAT
Merged
5 μm
D
Inhibitory Synapse Density (Numbers/10 μm)
0
1
2
3
4
WT 2.77
HET 1.83
***

dendritic spine of hippocampal neurons in the Golgi-stained brains of WT and βPix heterozygous mice were analyzed. Brains of 5 and 12 weeks mice were Golgi-stained for juvenile and for adult, respectively. Sholl analysis revealed that 5 weeks βPix heterozygous mice had a reduced complexity in basal dendrites of CA1 pyramidal neurons, compared to WT mice (Figure 13A and 13B). However, in 12 weeks mice, there was no significant difference in the neuronal complexity between the genotypes (Figure 13C). Next, we found that both 5 and 12 weeks βPix heterozygous mice displayed a significant decrease in dendritic spine density on pyramidal neurons of CA1 and CA3 region and granule neurons of DG region (Figure 14A and 14B). Taken together, these results show that the reduced dendritic complexity in the juvenile due to βPix deficiency can be compensated in the adult by some unknown mechanisms, but the reduced spine density is maintained throughout the adult period, highlighting an important *in vivo* role for βPix in the development of hippocampal neurons.

1.4. Adult βPix heterozygous mice have decreased protein levels of glutamate receptor subunits and Git1.

As described in previous and present studies ((Shin et al., 2019; Zhang et al., 2005); Figure 11 and 14), βPix has been proposed as a key regulator of dendritic spine where the glutamatergic synapses are located. To determine how the defects in the spine and synapse formation due to βPix deficiency affect expression of glutamate receptor subunits, the expression levels of various glutamate receptor subunits were quantitatively analyzed by western blotting in hippocampal tissues (Figure 15A).

Figure 13. βPix heterozygous mice have reduced dendritic complexity in hippocampal neurons *in vivo*.

(A) Representative images of basal dendrites of pyramidal neurons in hippocampal CA1 regions from 5 and 12 weeks WT and βPix heterozygous mice. (B) In 5 weeks mice, Sholl analysis revealed decreased neuronal complexity of βPix heterozygous mice, compared to WT mice. (C) In 12 weeks mice, the neuronal complexity of βPix heterozygous mice was similar to that of WT mice. 40-50 neurons were analyzed in each group.

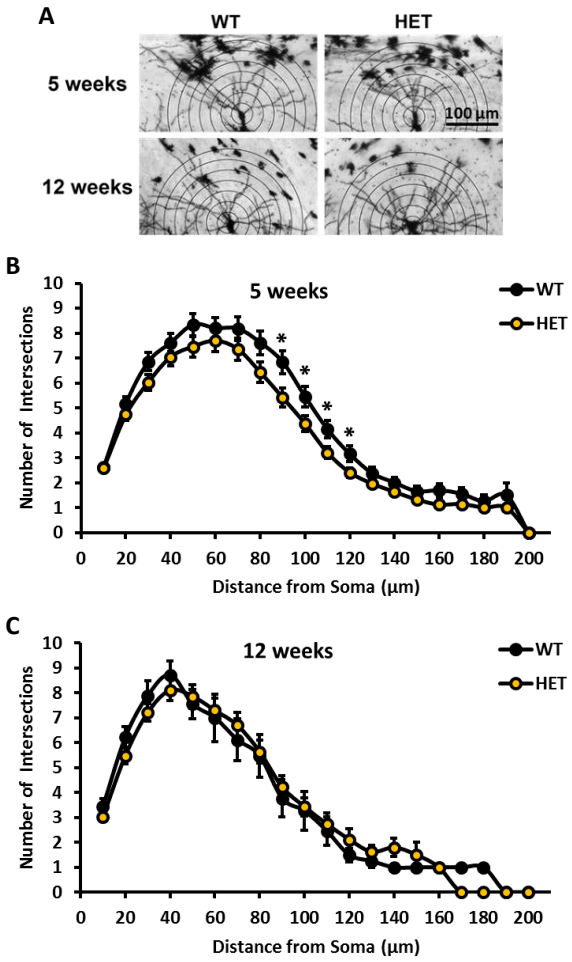
A
WT
HET
5 weeks
12 weeks
100 µm
B
5 weeks
WT
HET
Number of Intersections
Distance from Soma (µm)
C
12 weeks
WT
HET
Number of Intersections
Distance from Soma (µm)

Figure 14. βPix heterozygous mice have reduced dendritic spine density in hippocampal neurons *in vivo*.

(A and B) Representative images (A) and quantitation (B) of dendritic spine of hippocampal neurons from 5 and 12 weeks mice. 40-50 neurons were analyzed for each group.

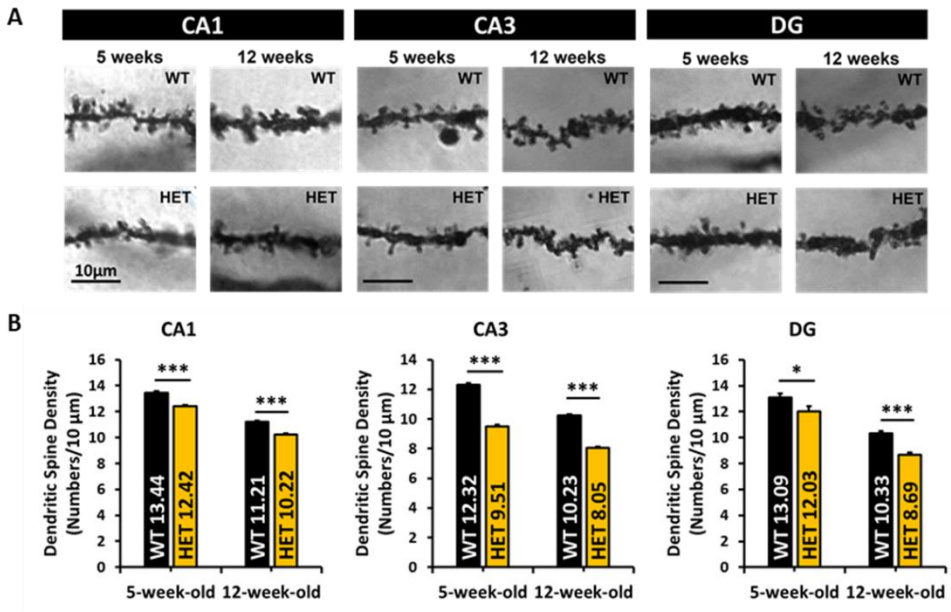
A
CA1
CA3
DG
5 weeks
12 weeks
WT
HET
10μm
B
CA1
CA3
DG
Dendritic Spine Density (Numbers/10 μm)
WT 13.44
HET 12.42
WT 11.21
HET 10.22
WT 12.32
HET 9.51
WT 10.23
HET 8.05
WT 13.09
HET 12.03
WT 10.33
HET 8.69
5-week-old
12-week-old
***
*

Figure 15. βPix heterozygous mice have decreased glutamate receptor subunits and Git1 expression levels in hippocampal tissue.

(A-C) Representative western blots for synaptic proteins (A). Quantification of relative protein levels are shown in (B) and (C).

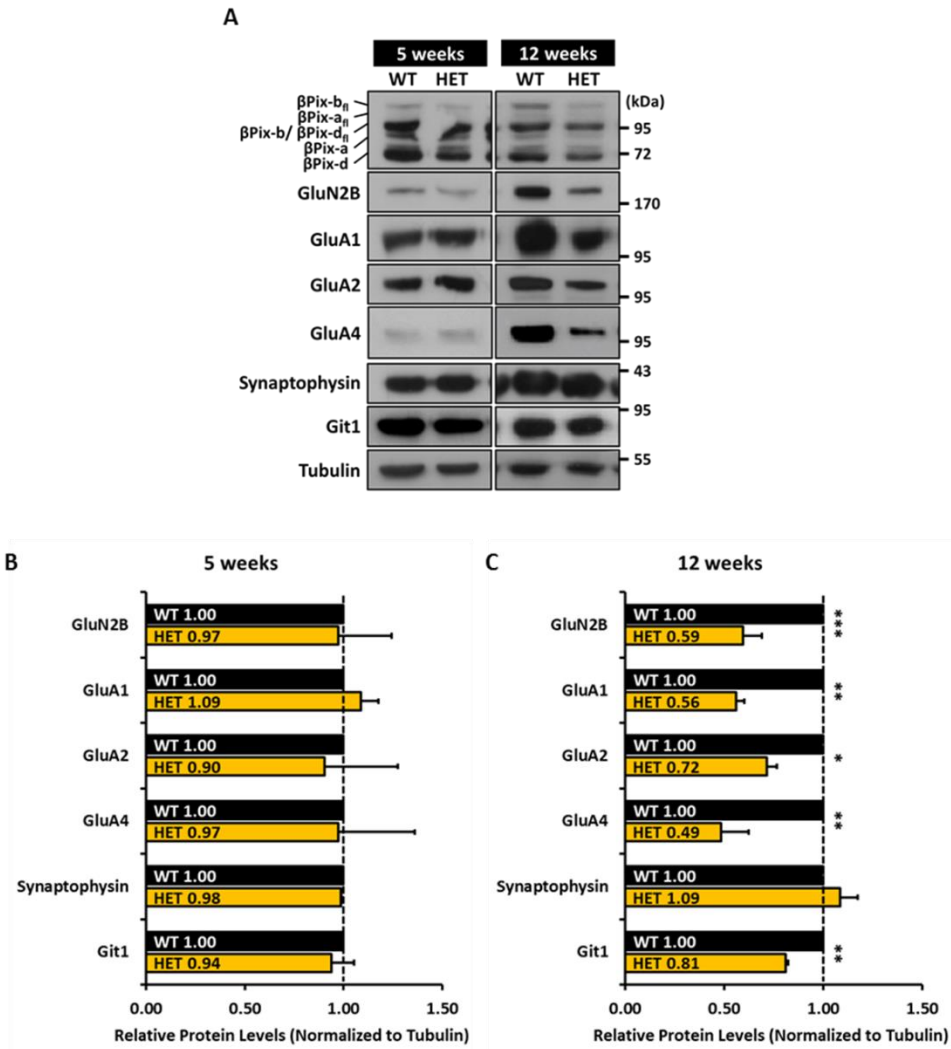
A
5 weeks
12 weeks
WT HET WT HET
(kDa)
βPix-b/ βPix-b$_{fl}$ βPix-a$_{fl}$ βPix-d$_{fl}$ βPix-a βPix-d
95
72
GluN2B
170
GluA1
95
GluA2
95
GluA4
95
Synaptophysin
43
Git1
95
Tubulin
55
B
5 weeks
GluN2B WT 1.00 HET 0.97
GluA1 WT 1.00 HET 1.09
GluA2 WT 1.00 HET 0.90
GluA4 WT 1.00 HET 0.97
Synaptophysin WT 1.00 HET 0.98
Git1 WT 1.00 HET 0.94
0.00 0.50 1.00 1.50
Relative Protein Levels (Normalized to Tubulin)
C
12 weeks
GluN2B WT 1.00 HET 0.59 ***
GluA1 WT 1.00 HET 0.56 **
GluA2 WT 1.00 HET 0.72 *
GluA4 WT 1.00 HET 0.49 **
Synaptophysin WT 1.00 HET 1.09
Git1 WT 1.00 HET 0.81 **
0.00 0.50 1.00 1.50
Relative Protein Levels (Normalized to Tubulin)

There was no difference in 5 weeks between WT and βPix heterozygous mice (Figure 15B). However, in 12 weeks βPix heterozygous mice, there was a significant reduction of GluN2B subunit of NMDA receptor, and GluA1, GluA2 and GluA4 subunits of AMPA receptor (Figure 15C). βPix tightly associates with Git1 and the signaling of βPix and Git1 is involved in spine morphogenesis (Zhang et al., 2005). In 12 weeks, but not in 5 weeks, βPix heterozygous mice also showed a significant decrease in Git1 expression (Figure 15B and 15C). Altogether, these data suggest that the reduced level of βPix expression causes morphological and molecular defects in neurons in βPix heterozygous mice.

1.5. βPix heterozygous mice have deficits in social interaction.

Abnormal social behaviors are the most recognizable manifestation in certain psychiatric disorders containing schizophrenia and autism (Couture et al., 2006; Silverman et al., 2010), that are associated with alterations in neuronal morphology (Kulkarni and Firestein, 2012; Penzes et al., 2011). To determine whether the reduced level of βPix expression affects social interaction, we performed social preference test, as measured the time spent in interaction zone where before and after target mouse was placed (Figure 16A). WT mice had more time in the interaction zone when there was a target mouse than when there was no target. In the same procedure performed, βPix heterozygous mice elicited no changes in the time spent in the interaction zone (Figure 16B). During the test, there were no significant differences in velocity between genotypes (data not shown). These results show that βPix heterozygous mice display socially avoidance.

Figure 16. βPix heterozygous mice have impaired social interaction.

(A) Experimental scheme of social preference test. (B) Social-interaction time in the presence of a social target for 12 weeks mice. 9 mice were analyzed in each group. Experiments were performed in laboratory of Prof. Daesoo Kim (KAIST).

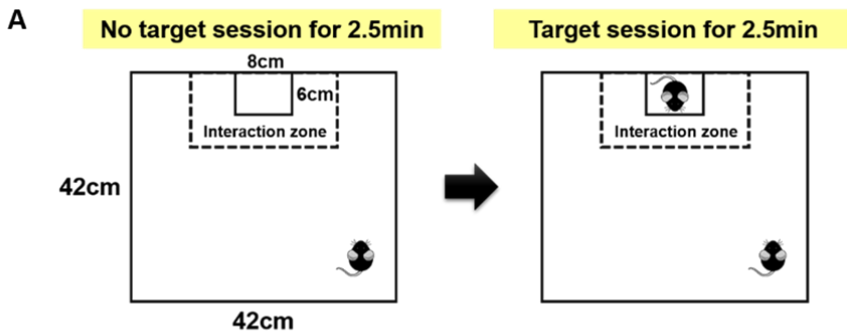
A
No target session for 2.5min
Target session for 2.5min
8cm
6cm
Interaction zone
42cm
42cm
Interaction zone

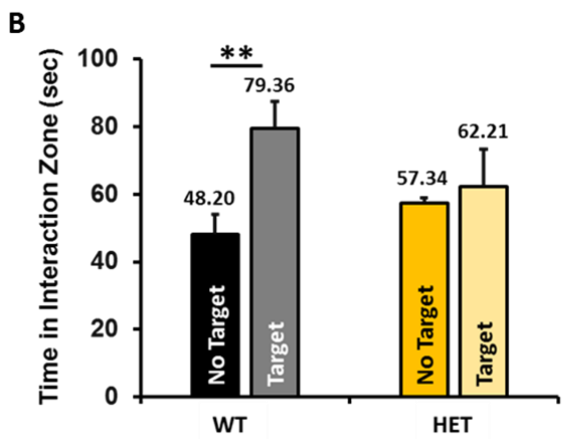
B
Time in Interaction Zone (sec)
100
80
60
40
20
0
**
79.36
48.20
62.21
57.34
No Target
Target
No Target
Target
WT
HET

2. Characterization of neuronal βPix isoform knockout mouse

2.1. Neuronal βPix isoform KO mice display loss of βPix-b and βPix-d in brain.

Although the neural expression of βPix-b and βPix-d suggests that these isoforms may have neuronal functions, the specific roles of βPix-b and βPix-d in neurons remain poorly understood. To investigate the neuronal βPix isoform-dependent phenotypes, we generated neuronal βPix isoform KO mice (KO, Δ/Δ). The targeting construct was designed to delete exon 19 of the mouse *ARHGEF7* gene that encodes the INS domain, which is specific to the neuronal βPix isoforms (Figure 1). Both the LoxP site and the Neo^r gene were introduced into the target locus through homologous recombination. The excision of the neo^r gene *in vivo* was then accomplished by breeding the floxed mice with a transgenic line expressing Sox2-Cre (Figure 7A) (Hall et al., 2009). We confirmed that βPix-b mRNA is not produced in the brain of neuronal βPix isoform KO mice, while βPix-a mRNA is more expressed than in that of WT mice (Figure 7B). Also, Western blot analysis of whole brain extracts from neuronal βPix isoform KO mice showed complete loss of βPix-b and βPix-d using the INS antibody and increased expression of βPix-a using the SH3 antibody (Figure 7C). These βPix expression patterns are similar in the central nervous system and cultured hippocampal neurons, and there is no significant difference in those patterns during neuronal development (Figure 17A and 17B). These data indicate that deletion of the INS domain causes compensatory increases in the level of βPix-a in brain from neuronal βPix isoform KO mice. In the tissues except brain, βPix-a expression level in neuronal βPix isoform KO mice is similar to that in WT mice (Figure 7B and 7C). In addition, body weight, one of developmental milestones and general health measures did not differ across genotypes in both 5 and

Figure 17. Lack of βPix-b and βPix-d expression in various brain regions, spinal cord and hippocampal neurons from neuronal βPix isoform KO mice.

(A) Expression patterns of βPix in 5 and 12 weeks whole brain and hippocampus, and DIV5 and DIV14 hippocampal neurons from WT and neuronal βPix isoform KO mice. Equal amounts of 15 μg protein (homogenates) were loaded per lane and probed with the SH3 antibody. (B) Expression patterns of βPix in olfactory bulb, frontal cortex, striatum, hippocampus, cerebellum, brain stem and spinal cord from 5 weeks WT and neuronal βPix isoform KO mice. Equal amounts of 15 μg protein (homogenates) were loaded per lane and probed with the SH3 and INS antibody. Data are representative of 3 independent experiments.

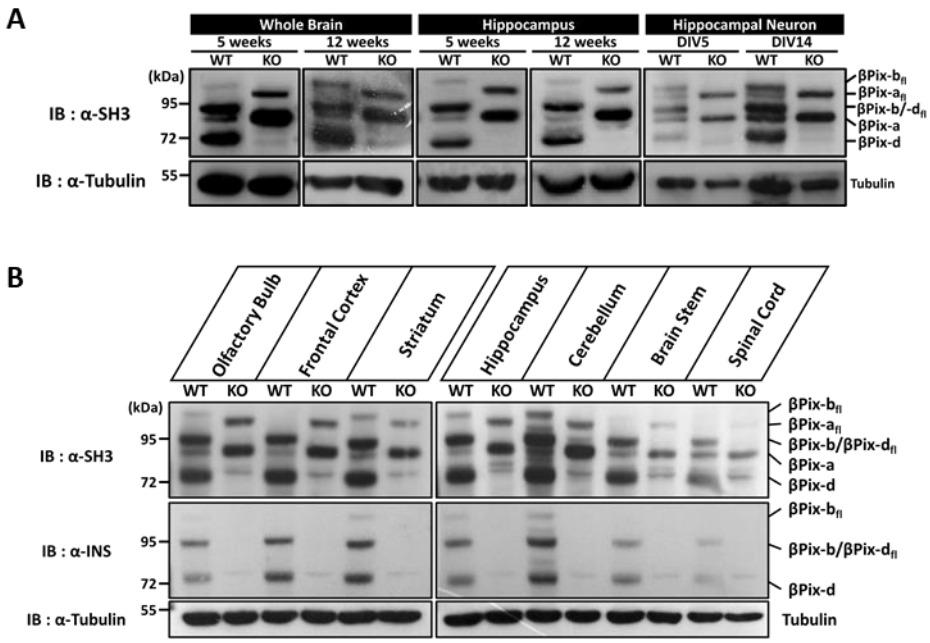
A
Whole Brain
Hippocampus
Hippocampal Neuron
5 weeks
12 weeks
5 weeks
12 weeks
DIV5
DIV14
WT KO WT KO WT KO WT KO WT KO WT KO
(kDa)
95
72
55
IB : α-SH3
IB : α-Tubulin
βPix-bfl
βPix-afl
βPix-b/-dfl
βPix-a
βPix-d
Tubulin
B
Olfactory Bulb
Frontal Cortex
Striatum
Hippocampus
Cerebellum
Brain Stem
Spinal Cord
WT KO WT KO WT KO WT KO WT KO WT KO WT KO
(kDa)
95
72
IB : α-SH3
95
72
IB : α-INS
55
IB : α-Tubulin
βPix-bfl
βPix-afl
βPix-b/βPix-dfl
βPix-a
βPix-d
βPix-bfl
βPix-b/βPix-dfl
βPix-d
Tubulin

12 weeks mice (Figure 18A). The neuronal βPix isoform KO mice are viable and fertile, and the brain weight and size did not differ between WT and neuronal βPix isoform KO mice (Figure 18B and 18C). Also, the neuronal βPix isoform KO mice did not display any gross anatomical and histological abnormality in cortex and hippocampus (Figure 18D). Taken together, we suggest that this mouse model is suitable for researches on the function of βPix-b and βPix-d in neurons.

2.2. Active Rac1 and Cdc42 are reduced in hippocampus of neuronal βPix isoform KO mice.

Since βPix has guanine-nucleotide exchange activity toward Rac1 and Cdc42, we further examined whether the loss of neuronal βPix isoforms affects the levels of GTP-bound Rac1 and Cdc42 in hippocampus. The hippocampi of neuronal βPix isoform KO mice showed Rac1-GTP levels decreased by 56% (Figure 19A and 19B) and Cdc42-GTP levels decreased by 51% (Figure 19C and 19D). Taken together, these results indicate that the loss of neuronal βPix isoforms causes reduction in Rac1 and Cdc42 signaling in the hippocampus, thereby suggesting an impairment in morphogenesis of hippocampal neurons.

2.3. Dendritic complexity and spine density are decreased in hippocampal pyramidal neurons of neuronal βPix isoform KO mice.

Dendrites receive and process neural information, and display highly branched structures with patterns of characteristic arborization. The complexity of dendritic tree correlates with number and distribution of synaptic inputs that a neuron receives and consequently, has important effects on the synaptic plasticity and computation

Figure 18. Neuronal βPix isoform KO mice show normal body weight and gross anatomy of the brain.

(A) Body weight revealed no genotype differences in 5 and 12 weeks WT and neuronal βPix isoform KO mice. (B) Brain weight revealed no genotype differences in 5 and 12 weeks WT and neuronal βPix isoform KO mice. (C) 12 weeks neuronal βPix isoform KO mice had normal brain size compared to littermate WT mice. (D) Images of Nissl stained sagittal sections showed normal cytoarchitecture in cortex and hippocampus of 13 weeks male littermate mice. 7 for 5 weeks and 6 for 12 weeks male littermate mice were analyzed from 3 independent experiments.

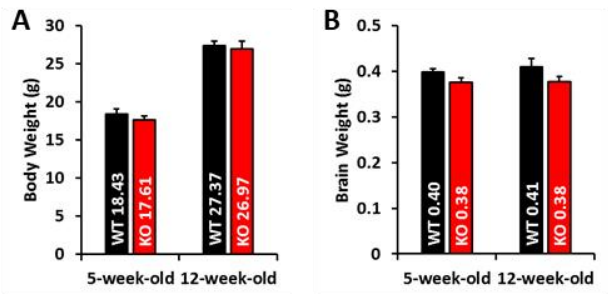
A
Body Weight (g)
30
25
20
15
10
5
0
WT 18.43
KO 17.61
WT 27.37
KO 26.97
5-week-old
12-week-old
B
Brain Weight (g)
0.5
0.4
0.3
0.2
0.1
0
WT 0.40
KO 0.38
WT 0.41
KO 0.38
5-week-old
12-week-old

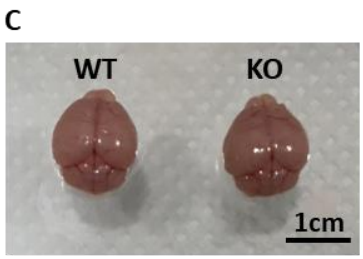
C
WT
KO
1cm

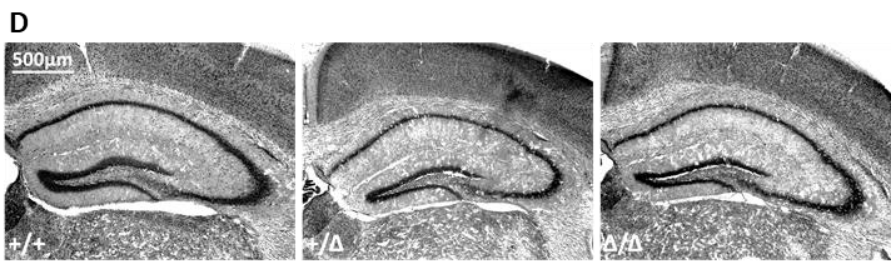
D
500μm
+/+
+/Δ
Δ/Δ

Figure 19. Absence of neuronal βPix isoforms leads to a significant reduction in active Rac1 and Cdc42 in hippocampal tissue.

(A) Representative blots for GTP-bound Rac1 by pull-down assay in the hippocampus from 5 weeks male mice. (B) Quantification of (A). Neuronal βPix isoform KO mice had reduced ratio of GTP-Rac1 and total level of Rac1 in the hippocampus. (C) Representative blots for GTP-bound Cdc42 by pull-down assay in the hippocampus from 5 weeks male mice. (D) Quantification of (C). Neuronal βPix isoform KO mice had reduced ratio of GTP-Cdc42 and total level of Cdc42 in the hippocampus. Data are representative of 4 independent experiments for (A) and (B) and 3 independent experiments for (C) and (D).

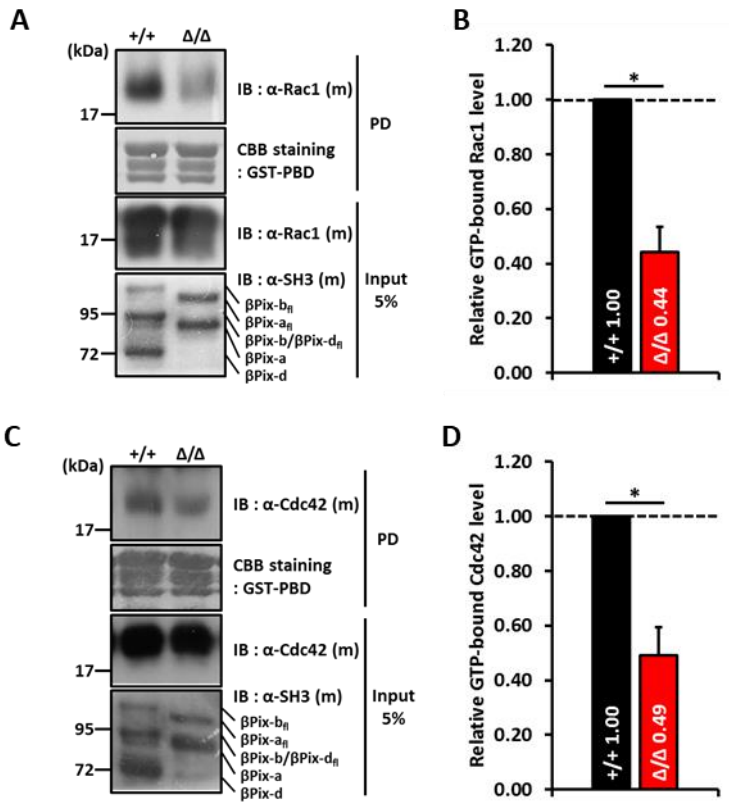
A
+/+
Δ/Δ
(kDa)
17
IB : α-Rac1 (m)
PD
CBB staining
: GST-PBD
17
IB : α-Rac1 (m)
IB : α-SH3 (m)
Input
5%
95
72
βPix-bfl
βPix-afl
βPix-b/βPix-dfl
βPix-a
βPix-d
B
Relative GTP-bound Rac1 level
1.20
1.00
0.80
0.60
0.40
0.20
0.00
*
+/+ 1.00
Δ/Δ 0.44
C
+/+
Δ/Δ
(kDa)
17
IB : α-Cdc42 (m)
PD
CBB staining
: GST-PBD
17
IB : α-Cdc42 (m)
IB : α-SH3 (m)
Input
5%
95
72
βPix-bfl
βPix-afl
βPix-b/βPix-dfl
βPix-a
βPix-d
D
Relative GTP-bound Cdc42 level
1.20
1.00
0.80
0.60
0.40
0.20
0.00
*
+/+ 1.00
Δ/Δ 0.49

(Jan and Jan, 2001; Poirazi and Mel, 2001). The Rac1 and Cdc42 GTPases have emerged as important determinants of dendritic structure, particularly with respect to dendritic branching and remodeling (Newey et al., 2005). Previously, βPix has been shown to control neurite extension in *Xenopus* spinal neurons and chick neural retinal cells (Santiago-Medina et al., 2013; Za et al., 2006). The effects of neuronal βPix isoforms deficiency on dendritic growth and branching were determined using Sholl analysis, which quantifies the number of dendrites from a neuron cross concentric circles of increasing diameter. Using this analysis for the basal dendrites of CA1 pyramidal neurons in Golgi-stained hippocampus (Figure 20A), we found a simplification of dendritic tree in 5 weeks neuronal βPix isoform KO animals compared to that in WT mice (Figure 20B), whereas 12 weeks WT and neuronal βPix isoform KO mice did not significantly differ in the dendritic arborizations (Figure 20C).

Next, we investigated the role of neuronal βPix isoforms in dendritic spine formation. Most neurons have small and specialized protrusions that extend from their dendrites, called dendritic spines. Involvements of RhoA, Rac1 and Cdc42 GTPases in dendritic spine formation have also been demonstrated (Tashiro and Yuste, 2008). Previous studies have shown that βPix mediates spine morphogenesis by regulation of actin filaments (Llano et al., 2015; Zhang et al., 2005). Hence, we measured dendritic spine density in Golgi-stained hippocampal CA1 pyramidal neurons from WT and neuronal βPix isoform KO mice. We found that 5 and 12 weeks neuronal βPix isoform KO mice displayed a significant decrease in dendritic spine density (Figure 21A and 21B). Taken together, our data suggest that reduced levels of active Rac1 and Cdc42 in the hippocampus of neuronal βPix isoform KO

Figure 20. Neuronal βPix isoform KO mice have decreased dendritic complexity in hippocampal neurons *in vivo*.

(A) Representative images of basal dendrites of pyramidal neurons in hippocampal CA1 regions from 5 and 12 weeks WT and neuronal βPix isoform KO mice. (B) In 5 weeks mice, Sholl analysis revealed decreased neuronal complexity of neuronal βPix isoform KO mice, compared to WT mice. (C) In 12 weeks mice, neuronal βPix isoform KO mice had decreased in neuronal complexity, compared to WT mice. 55-57 neurons were analyzed in each group from 3 independent experiments.

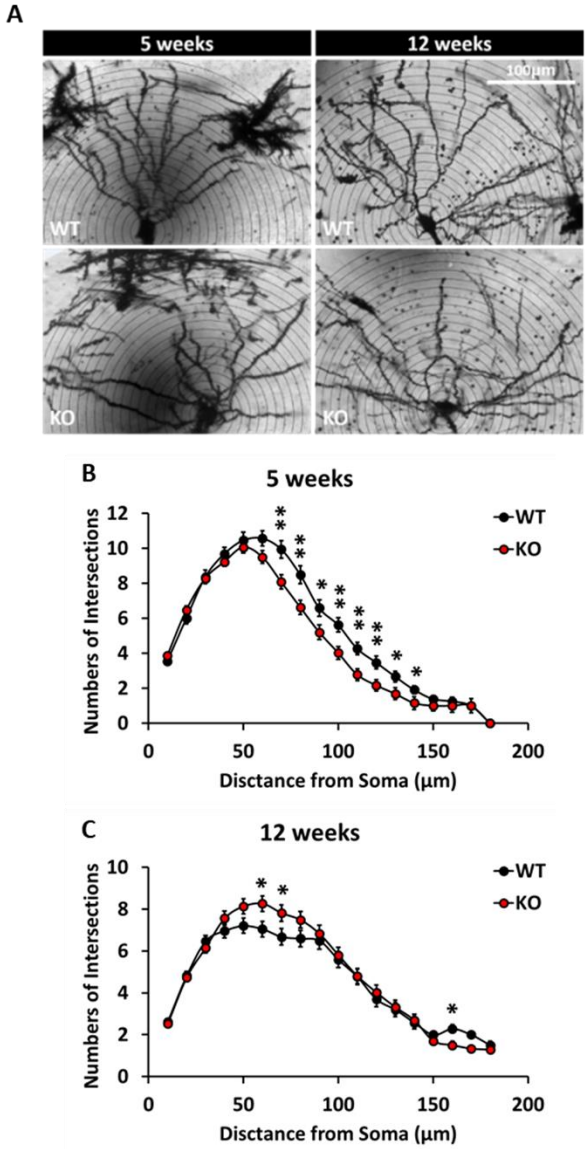
A
5 weeks
12 weeks
100μm
WT
WT
KO
KO
B
5 weeks
Numbers of Intersections
Disctance from Soma (μm)
WT
KO
C
12 weeks
Numbers of Intersections
Disctance from Soma (μm)
WT
KO

Figure 21. Neuronal βPix isoform KO mice have decreased dendritic spine density in hippocampal neurons *in vivo*.

(A) Representative images of dendritic spine of pyramidal neurons in hippocampal CA1 regions from 5 and 12 weeks WT and neuronal βPix isoform KO mice. (B) In CA1 pyramidal neurons, 5 and 12 weeks neuronal βPix isoform KO mice had significantly lower spine density than WT mice.

A

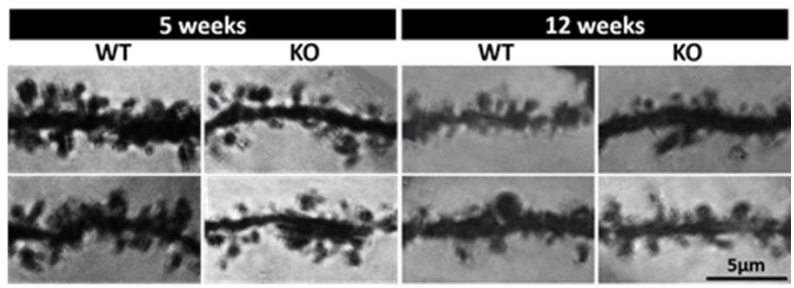
5 weeks
12 weeks
WT
KO
WT
KO
5μm

B

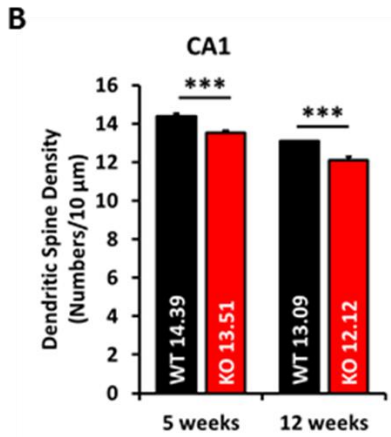
CA1
***
***
Dendritic Spine Density (Numbers/10 μm)
16
14
12
10
8
6
4
2
0
WT 14.39
KO 13.51
WT 13.09
KO 12.12
5 weeks
12 weeks

mice result in the neuronal morphological alterations. These results highlight a critical *in vivo* role of the neuronal βPix isoforms in the normal development of hippocampal pyramidal neurons.

2.4. Juvenile KO mice have increased levels of GluN2B and CaMKIIα expression.

Dendritic spines usually receive excitatory input from axons of other neurons. Glutamate is the most common excitatory neurotransmitter involved in synaptic transmission and the dendritic spines express glutamate receptors that are anchored by cytoskeletal elements at the postsynaptic density (Matus et al., 1982). Given a decreased spine density in the hippocampal CA1 pyramidal neurons from neuronal βPix isoform KO mice, we sought to examine whether proteins involved in excitatory neurotransmission were affected. We used hippocampal homogenates from WT and neuronal βPix isoform KO mice and performed Western blotting (Figure 22A). We observed that GluN2B, one of NMDA receptor subunits had a significantly increased expression levels in the hippocampus of 5 weeks neuronal βPix isoform KO mice compared to those in WT tissue (Figure 22B), but not in that of 12 weeks neuronal βPix isoform KO mice (Figure 22C). Furthermore, in the hippocampus of 5 weeks neuronal βPix isoform KO mice, we observed an increased expression level of CaMKIIα, a kinase activated by Ca^{2+} influx through NMDARs (Figure 22B), but not in that of 12 weeks neuronal βPix isoform KO mice compared to the levels in WT mice (Figure 22C). We did not observe any changes in the levels of GluA1 and GluA2 that are subunits of AMPA receptor in the hippocampal homogenates from both 5 and 12 weeks mice (Figure 22B and 22C). Notably, βPix-

Figure 22. Neuronal βPix isoform KO mice have increased GluN2B and CaMKIIα expression levels in hippocampal tissue.

(A) Representative blots for synaptic proteins detected by specific antibodies in hippocampus from 5 and 12 weeks WT and neuronal βPix isoform KO mice. (B) Protein levels of GluN2B and CaMKIIα were increased in hippocampus from 5 weeks neuronal βPix isoform KO mice. (C) There was no difference between WT and βPix heterozygous mice in protein levels, in 12 weeks neuronal βPix isoform KO mice. Data are representative of 3 independent experiments and quantification of relative levels of synaptic proteins as normalized to tubulin expression.

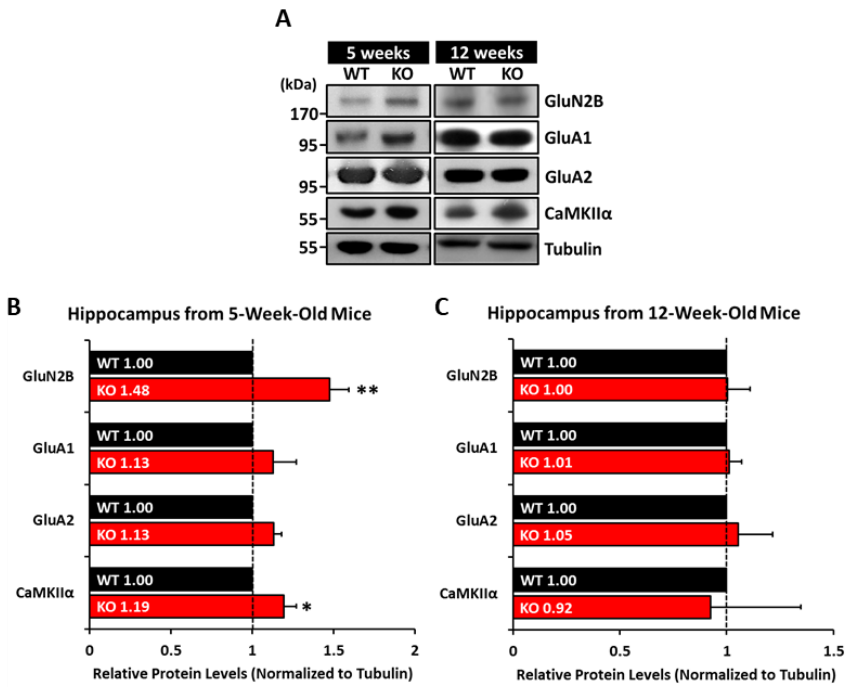
A
5 weeks
12 weeks
WT
KO
WT
KO
(kDa)
170
95
95
55
55
GluN2B
GluA1
GluA2
CaMKIIα
Tubulin
B
Hippocampus from 5-Week-Old Mice
GluN2B
WT 1.00
KO 1.48
**
GluA1
WT 1.00
KO 1.13
GluA2
WT 1.00
KO 1.13
CaMKIIα
WT 1.00
KO 1.19
*
0
0.5
1
1.5
2
Relative Protein Levels (Normalized to Tubulin)
C
Hippocampus from 12-Week-Old Mice
GluN2B
WT 1.00
KO 1.00
GluA1
WT 1.00
KO 1.01
GluA2
WT 1.00
KO 1.05
CaMKIIα
WT 1.00
KO 0.92
0
0.5
1
1.5
Relative Protein Levels (Normalized to Tubulin)

b and βPix-d were detected in synaptosomes and synaptic membrane fractions and in 5 weeks mice, GluN2B was enriched higher in the PSD fractions from neuronal βPix isoform KO hippocampus than in the WT hippocampal PSD (Figure 23A and 23B). Therefore, our data suggest that the morphological and molecular defects in the dendritic spines of neuronal βPix isoform KO mice may cause impaired synaptic transmission in the hippocampus during adolescent development.

2.5. βPix-b and βPix-d are required for growth cone development.

In newborn neurons, locating the target during the extension of neurites is mediated by growth cones, the actin filament-rich structures at the tip of neurites which mediate targeting of growing neurites (Lowery and Van Vactor, 2009). In order to examine the phenotypic changes of growth cone in neuronal βPix isoform KO neurons, we fixed cultured hippocampal neurons at DIV4 and stained growth cone with F-actin and β3-Tubulin antibodies (Figure 24A). Average growth cone area was significantly larger in neuronal βPix isoform KO neurons than WT neurons (Figure 24B). The distribution graph showed that the area of growth cone ranged from 0-20 μm^2 was more and that ranged from 30-50, 60-70, 80-90, 100-110 and 120-160 μm^2 was less in neuronal βPix isoform KO neurons than WT neurons (Figure 24C), indicating that larger average growth cone area in neuronal βPix isoform KO neurons at DIV4 arose from significantly higher percentage of large growth cones and significantly lower percentage of small growth cones in neuronal βPix isoform KO neurons, compared with WT neurons. Furthermore, when classifying by growth cone shape, collapsed and filopodial growth cone were less, and lamellipodial, mainly filopdial, mainly lamellipodial growth cone were more in neuronal βPix isoform KO

Figure 23. Neuronal βPix isoform KO mice have increased GluN2B expression level in PSD fractions of hippocampal tissue.

(A) Expression of GluN2B proteins in subcellular fractions of whole brain from 5- and 12 weeks WT and neuronal βPix isoform KO mice. P2, crude synaptosomes; P3, light membrane fraction; PSD fractions, extracted with Triton X-100 once (PSD-1T) or twice (PSD-2T); An equal amount of 8 μg per each fraction was loaded in immunoblot experiments. PSD-95 and synaptophysin were used as controls. GluN2B proteins in PSD-1T and 2T fractions of 5 weeks neuronal βPix isoform KO mice were increased, but not in those of 12 weeks neuronal βPix isoform KO mice. (B) Expression of GluN2B proteins in PSD fractions of 5 weeks hippocampus. GluN2B protein was more enriched in neuronal βPix isoform KO mice than in WT mice. Data are representative of 3 independent experiments.

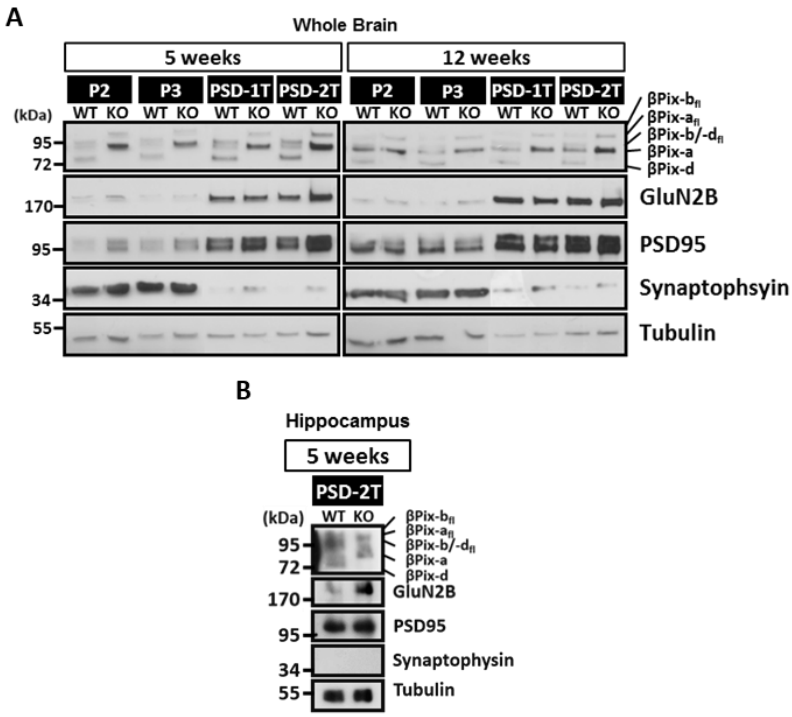
A
Whole Brain
5 weeks
12 weeks
P2
P3
PSD-1T
PSD-2T
WT KO
(kDa)
95
72
170
34
55
βPix-bfl
βPix-afl
βPix-b/-dfl
βPix-a
βPix-d
GluN2B
PSD95
Synaptophsyin
Tubulin
B
Hippocampus
5 weeks
PSD-2T
WT KO
(kDa)
95
72
170
95
34
55
βPix-bfl
βPix-afl
βPix-b/-dfl
βPix-a
βPix-d
GluN2B
PSD95
Synaptophysin
Tubulin

Figure 24. Neuronal βPix isoform KO mice have decreased proportion of the collapsed growth cone in hippocampal neurons *in vitro*.

(A) Representative images of hippocampal neurons stained with β3-Tubulin (green), F-actin (red) and DAPI (blue) at DIV4. Quantification in (B)-(D). (B) In neuronal βPix isoform KO neurons, average growth cone area was significantly larger than in WT neurons at DIV4. (C) In distribution graph, the area range of 0-20 μm^2 was less and that of 30-160 μm^2 was more in neuronal βPix isoform KO neurons than in WT neurons. (D) Collapsed and filopodial growth cone had significantly decreased and lamellipodial, mainly filopodial and mainly lamellipodial growth cone were significantly increased in neuronal βPix isoform KO neurons, compared with WT neurons. 476 growth cones of WT neurons and 524 growth cones of neuronal βPix isoform KO neurons were analyzed from 3 independent cultures.

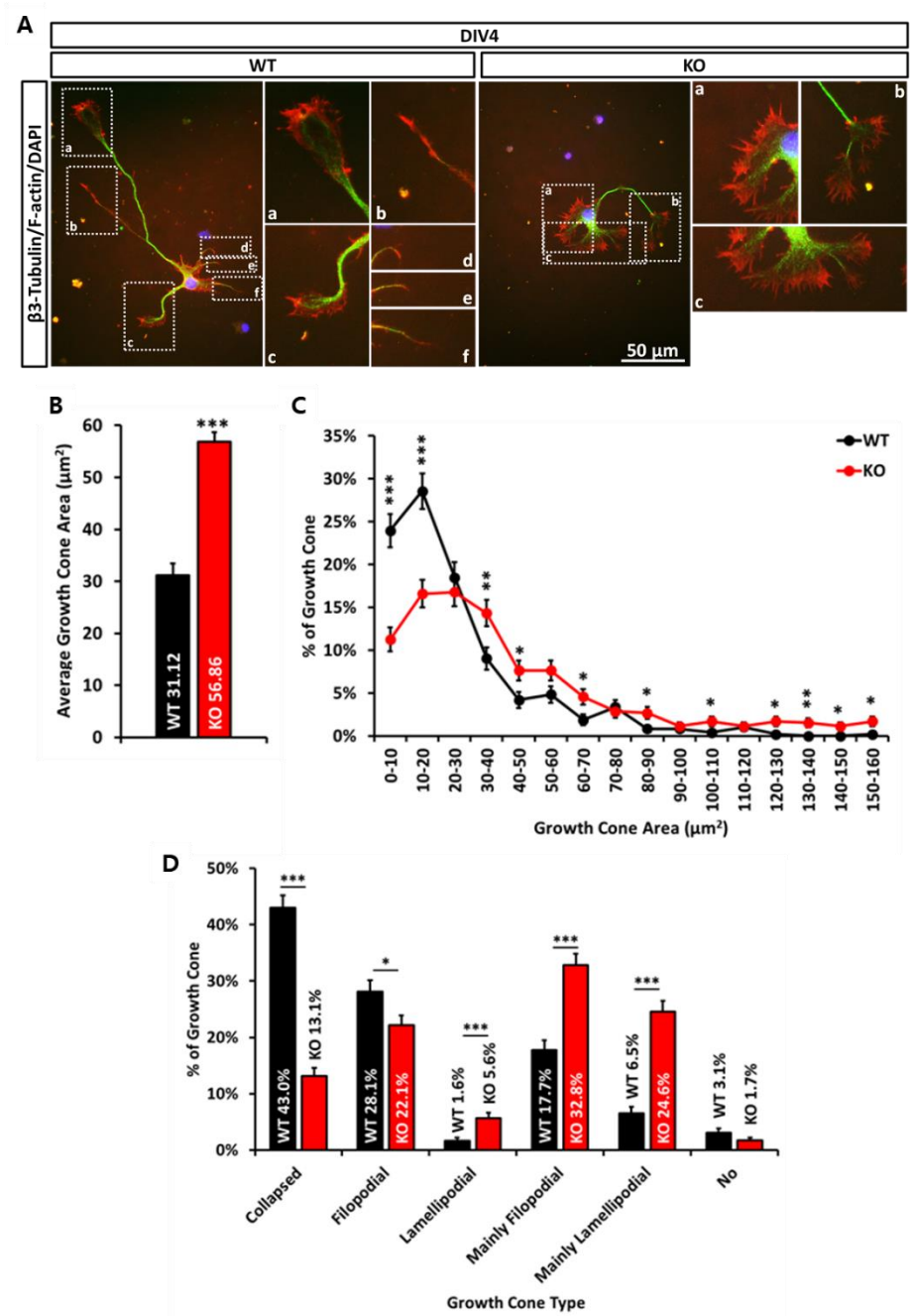
A
DIV4
WT
KO
β3-Tubulin/F-actin/DAPI
50 μm
B
Average Growth Cone Area (μm²)
WT 31.12
KO 56.86
***
C
% of Growth Cone
WT
KO
Growth Cone Area (μm²)
0-10
10-20
20-30
30-40
40-50
50-60
60-70
70-80
80-90
90-100
100-110
110-120
120-130
130-140
140-150
150-160
D
% of Growth Cone
WT 43.0%
KO 13.1%
WT 28.1%
KO 22.1%
WT 1.6%
KO 5.6%
WT 17.7%
KO 32.8%
WT 6.5%
KO 24.6%
WT 3.1%
KO 1.7%
Collapsed
Filopodial
Lamellipodial
Mainly Filopodial
Mainly Lamellipodial
No
Growth Cone Type

neurons, compared with WT neurons (Figure 24D), suggesting altered growth cone development in neuronal βPix isoform KO neurons.

To examine the role of neuronal βPix isoforms in growth cone morphogenesis in early development, we transfected cultured hippocampal neurons from neuronal βPix isoform KO neurons transfected with enhanced green fluorescent protein (EGFP) tagged βPix-b or βPix-d at DIV3 and analyzed the growth cone morphology of those neurons at DIV4. The increased area of growth cone shown in neuronal βPix isoform KO neurons, compared with WT neurons was recovered by expression of βPix-b or βPix-d (Figure 25A). Furthermore, neuronal βPix isoform KO neurons had defects in collapsed, mainly filopodial and mainly lamellipodial growth cone, and those defective phenotypes of growth cone were rescued by βPix-b or βPix-d (Figure 25B). Altogether, these results indicate that neuronal βPix isoforms are required for growth cone development.

2.6. βPix-b and βPix-d are required for neurite development.

In parallel, we evaluated the roles of neuronal βPix isoforms and neurite development *in vitro* to quantify neurite morphology at single-cell resolution. Cultured hippocampal neurons exhibit typical axonal and dendritic structures and are commonly used to analyze single-neuron morphology (Beaudoin et al., 2012). Hippocampal neurons from P0-1 mice were cultured and imaged at DIV3, DIV5, DIV14 and DIV21 in order to observe the neuronal morphogenesis from early development to late development. Those neurons are stained with β3-Tubulin to visualize the overall shape of the neurons. Immunostaining showed that loss of neuronal βPix isoforms abolished normal neuronal development (Figure 26A).

Figure 25. βPix-b and βPix-d are required for growth cone development.

(A) Average growth cone area was decreased in neuronal βPix isoform KO neurons, compared with WT neurons, and expression of βPix-b and βPix-d in neuronal βPix isoform KO neurons were recovered in the average growth cone area. (B) Collapse growth cone was decreased in neuronal βPix isoform KO neurons, compared with WT neurons, and the recovery of the decreased collapsed growth cone in neuronal βPix isoform KO neurons were shown in expression of βPix-b and βPix-d. Lamellipodial, mainly filopodial and mainly lamellipodial growth cone were receoverd by βPix-b, and filopdial, lamellipodial, mainly filopodial and mainly lamellipodial growth cone were recovered by βPix-d and in neuronal βPix isoform KO neurons. 279-289 growth cones were analyzed in each group from 3 independent experiments.

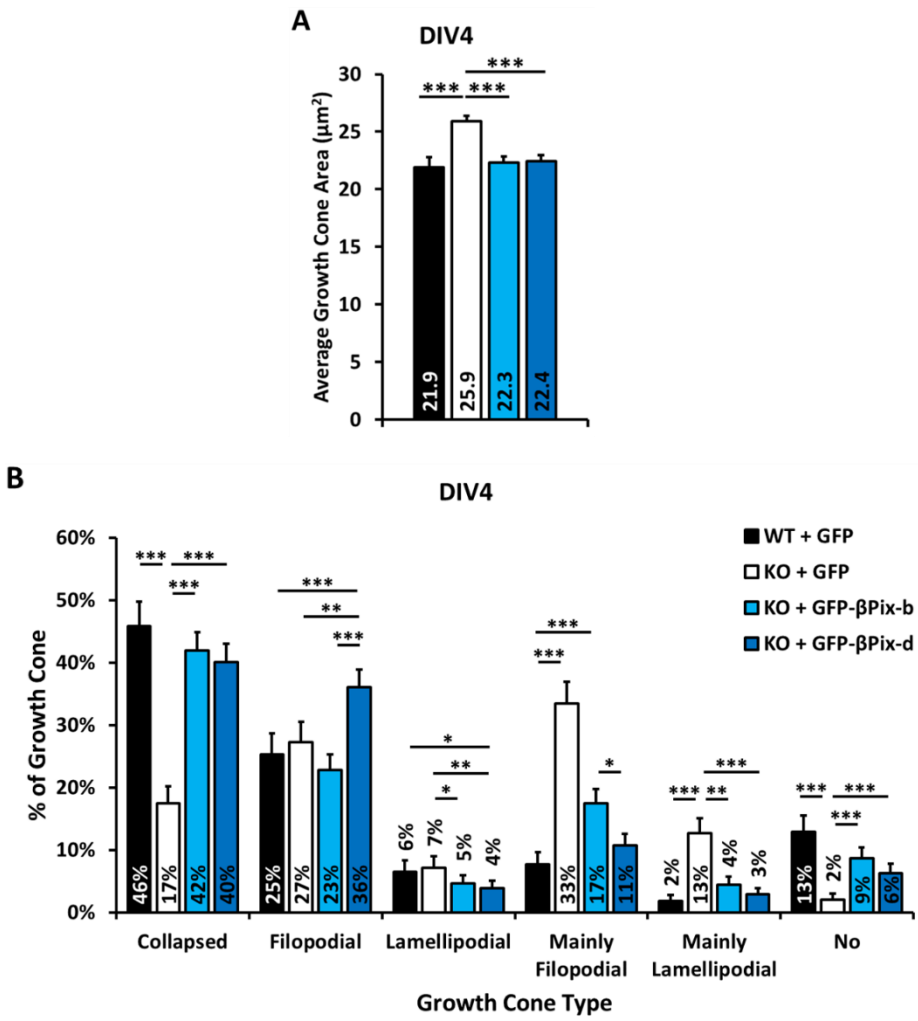
A
DIV4
Average Growth Cone Area (µm²)
30
25
20
15
10
5
0
***
***
***
21.9
25.9
22.3
22.4
B
DIV4
% of Growth Cone
60%
50%
40%
30%
20%
10%
0%
WT + GFP
KO + GFP
KO + GFP-βPix-b
KO + GFP-βPix-d
46%
17%
42%
40%
25%
27%
23%
36%
6%
7%
5%
4%
33%
17%
11%
2%
13%
4%
3%
13%
2%
9%
6%
Collapsed
Filopodial
Lamellipodial
Mainly Filopodial
Mainly Lamellipodial
No
Growth Cone Type

Figure 26. Neuronal βPix isoform KO mice have defects in neurite morphology in hippocampal neurons *in vitro*.

(A) Representative images of cultured hippocampal neurons from WT and neuronal βPix isoform KO mice fixed at DIV3, DIV5, DIV14 and DIV21. (B) Average primary neurite length was significantly shorter in neuronal βPix isoform KO mice than in WT mice at DIV3 and DIV5. (C) Total neurite length was significantly shorter in neuronal βPix isoform KO mice than in WT mice at DIV3, DIV5, DIV14 and DIV21. (D) Sholl analysis revealed simplified dendritic arborizations of neuronal βPix isoform KO mice, compared to WT mice at DIV3, DIV5, DIV14 and DIV21. 96-100 neurons at DIV3, 77-81 neurons at DIV5, 62-66 neurons at DIV14 and 50-51 neurons were analyzed in each group from 3 independent cultures.

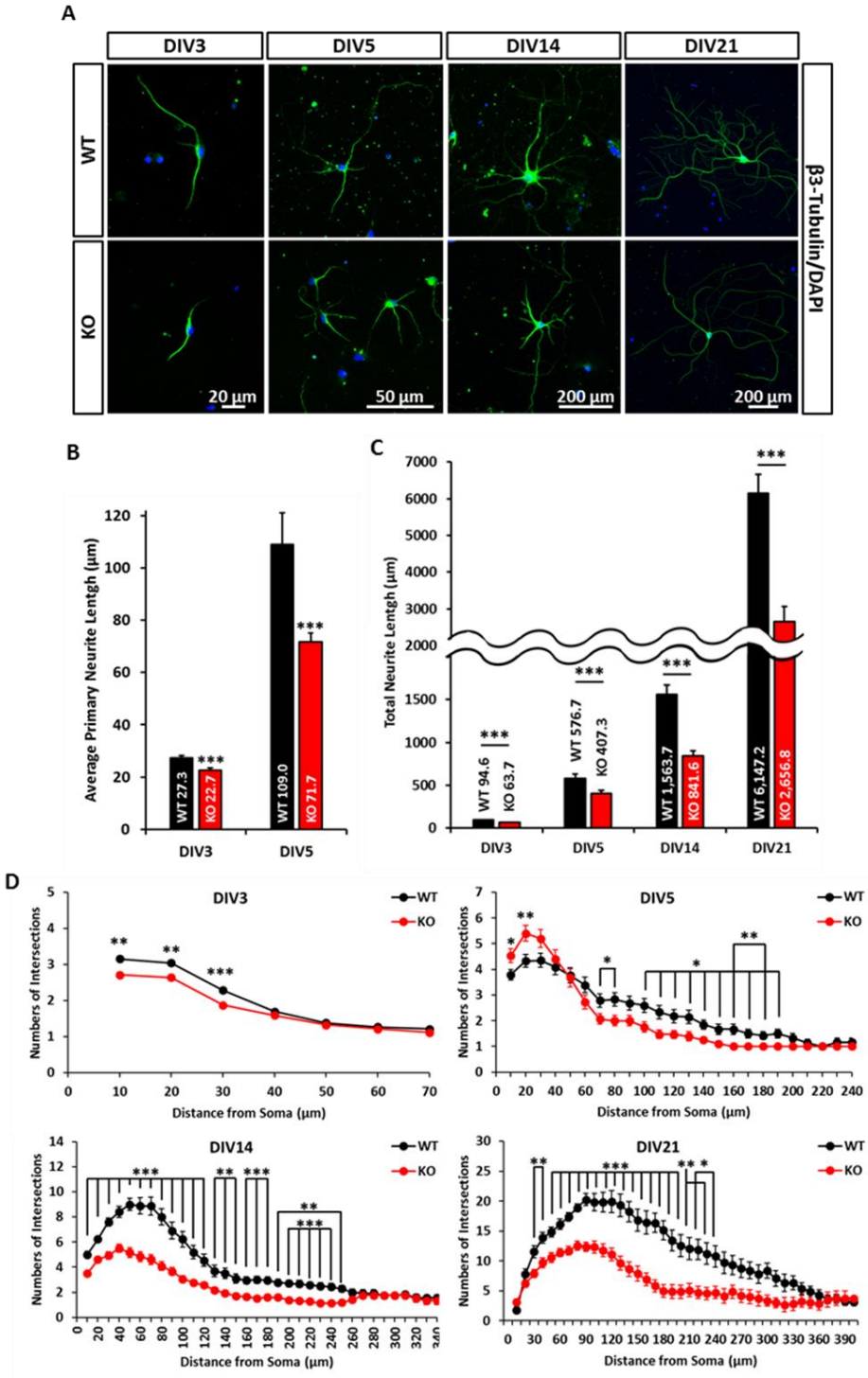
A
DIV3
DIV5
DIV14
DIV21
WT
KO
β3-Tubulin/DAPI
20 μm
50 μm
200 μm
200 μm
B
Average Primary Neurite Lentgh (μm)
WT 27.3
KO 22.7
WT 109.0
KO 71.7
DIV3
DIV5
C
Total Neurite Lentgh (μm)
WT 94.6
KO 63.7
WT 576.7
KO 407.3
WT 1,563.7
KO 841.6
WT 6,147.2
KO 2,656.8
DIV3
DIV5
DIV14
DIV21
D
DIV3
DIV5
DIV14
DIV21
WT
KO
Numbers of Intersections
Distance from Soma (μm)

Quantitative data showed that average primary neurite length has 17% decrease at DIV3 and 34% decrease at DIV5 in neuronal βPix isoform KO neurons (Figure 26B). In addition, total neurite length has 33% decrease at DIV3, 29% decrease at DIV5, 46% decrease at DIV14 and 57% decrease at DIV21 in neuronal βPix isoform KO neurons (Figure 26C). Consistent with the *in vivo* results (Figure 20), Sholl analysis revealed decreased neuronal complexity in neuronal βPix isoform KO neurons during neuronal development (Figure 26D), suggesting that loss of neuronal βPix isoforms perturbs neurite development.

To assess the involvement of neuronal βPix isoforms in neurite development, P0-1 dissociated hippocampal neurons from KO mice were co-transfected with βPix-b or βPix-d in combination with EGFP expression vector and DsRed at DIV7. Neurons were fixed and imaged 7 days after transfection (Figure 27A). Immunostaining showed that neuronal βPix isoform KO neurons expressing βPix-d exhibited a marked increase in primary neurite numbers compared to control-transfected neurons (Figure 27B). Total neurite length, branching numbers and neuronal complexity are significantly increased in neuronal βPix isoform KO neurons introducing βPix-b or βPix-d (Figure 27C-27E). Specifically, the level of those phenotypes by βPix-d is much higher than that by βPix-b, suggesting that different neuronal βPix isoforms display different ability to control neurite morphogenesis. Taken together, these results indicate that neuronal βPix isoforms are essential to regulate neurite formation, elongation and branching in hippocampal neurons.

2.7. βPix-b and βPix-d are required for dendritic spine development.

To further examine the role of neuronal βPix isoforms in dendritic spine

Figure 27. βPix-b and βPix-d are required for neurite morphogenesis.

(A) Representative images of hippocampal neurons from neuronal βPix isoform KO mice co-transfected with GFP, GFP-βPix-b or GFP-βPix-d and DsRed at DIV7 and analyzed by double immunofluorescence with antibodies to GFP and β3-Tubulin at DIV14. (B) Primary neurite numbers were significantly increased in expression of βPix-d, compared to control vector in neuronal βPix isoform KO neurons. (C) Total neurite length was significantly longer in expression of βPix-b or βPix-d than control vector in neuronal βPix isoform KO neurons. (D) Branching numbers were significantly increased in expression of βPix-b or βPix-d than control vector in neuronal βPix isoform KO neurons. (E) Sholl analysis revealed more complex dendritic arborizations in expression of βPix-b or βPix-d than control vector in neuronal βPix isoform KO neurons. 45-60 neurons were analyzed in each group from 3 independent cultures. *P* values (*$P < 0.05$, **$P < 0.01$ and ***$P < 0.001$) are derived from two-tailed student's t-test between GFP and GFP-βPix-b, and *P* values (# $P < 0.05$, ## $P < 0.01$ and ### $P < 0.001$) between GFP and GFP-βPix-d.

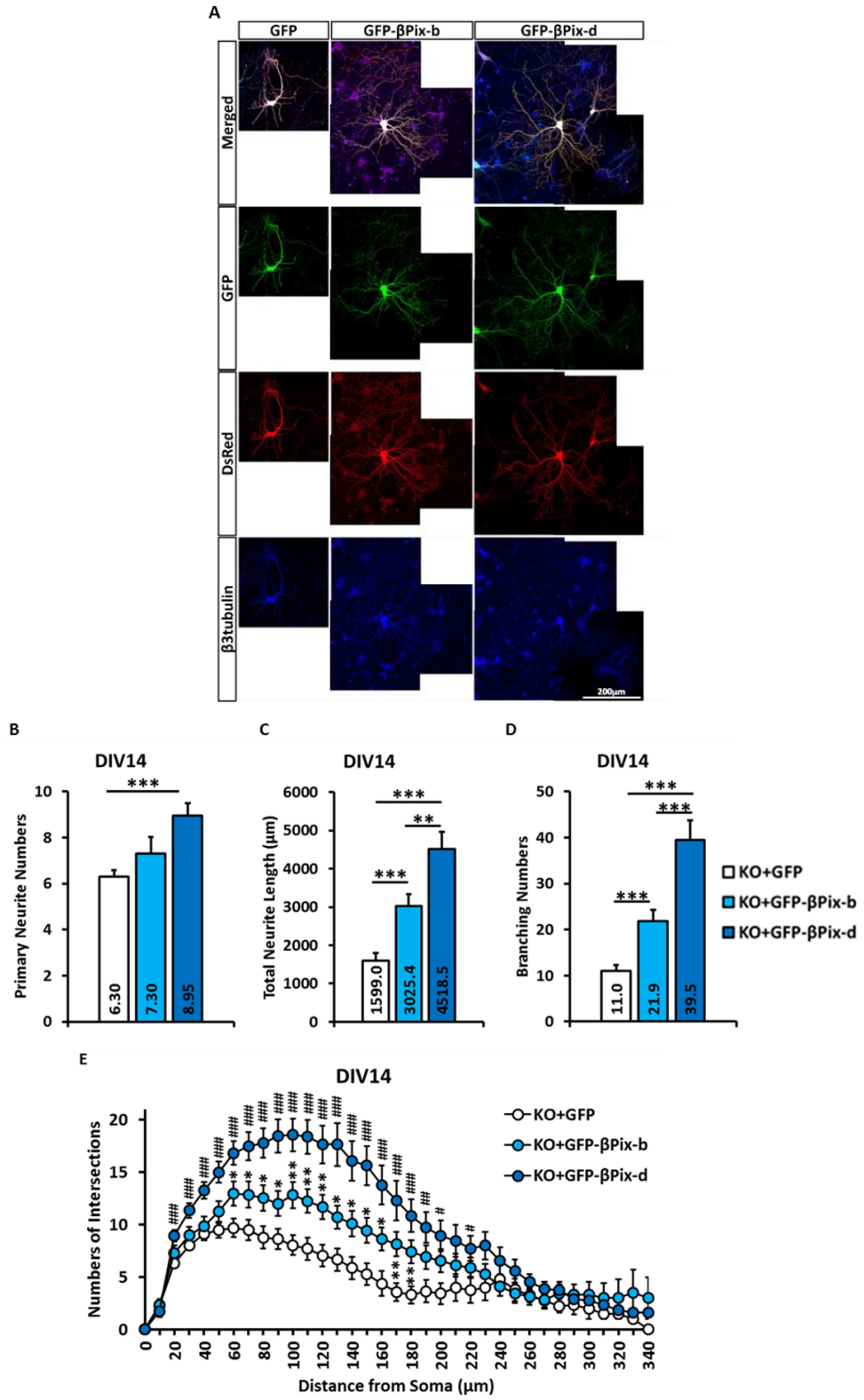
A
GFP
GFP-βPix-b
GFP-βPix-d
Merged
GFP
DsRed
β3tubulin
200μm
B
DIV14
Primary Neurite Numbers
6.30
7.30
8.95
C
DIV14
Total Neurite Length (μm)
1599.0
3025.4
4518.5
D
DIV14
Branching Numbers
11.0
21.9
39.5
KO+GFP
KO+GFP-βPix-b
KO+GFP-βPix-d
E
DIV14
Numbers of Intersections
Distance from Soma (μm)
KO+GFP
KO+GFP-βPix-b
KO+GFP-βPix-d

development, we asked whether the differences in dendritic spine density seen in the βPix KO mice *in vivo* could be reproduced *in vitro*. Dissociated hippocampal neurons prepared from P0-1 WT and neuronal βPix isoform KO littermates were transfected with EGFP at DIV7 to visualize the cellular morphology of transfected neurons and fixed at DIV14 for analysis of dendritic spine morphology (Figure 28A). We first analyzed the morphology of dendritic protrusions. We found a significant increase in length and a decrease in width of dendritic protrusions in neuronal βPix isoform KO neurons relative to those in WT neurons, suggesting a high level of immature filopodia among dendritic protrusions in neuronal βPix isoform KO neurons (Figure 28B and 28C). Indeed, we found that the percentage of filopodia in neuronal βPix isoform KO neurons is elevated by two–folds, compared to that in WT neurons (Figure 28D). We detected a significant decrease in dendritic spine density of neuronal βPix isoform KO neurons (Figure 28E), similar to that observed by Golgi stained hippocampal tissue.

We next asked whether the deficit in dendritic spines observed in neuronal βPix isoform KO neurons could be repaired by introduction of exogenous βPix-b or βPix-d. DIV7 hippocampal neurons from neuronal βPix isoform KO mice were co-transfected with an EGFP expression vector encoding βPix-b or βPix-d and DsRed to visualize the cellular morphology of transfected neurons (Figure 29A). For both βPix-b and βPix-d, expression of the individual isoform significantly decreased protrusion length and increased protrusion width at DIV14, compared with the GFP only control (Figure 29B and 29C). We also found that each neuronal βPix isoform significantly reduced the percentage of filopodia and increased dendritic spine density (Figure 29D and 29E), indicating that the neuronal βPix isoforms contribute

Figure 28. Neuronal βPix isoform KO mice have defects in dendritic spine morphology in hippocampal neurons *in vitro*.

(A) Representative images of cultured hippocampal neurons from WT and neuronal βPix isoform KO mice transfected with GFP at DIV7 and fixed at DIV14. Arrows point to dendritic protrusions with head and asterisk point to those with no head. Quantification in (B)-(E). (B) The length of protrusions was significantly longer in neuronal βPix isoform KO neurons than in WT neurons. (C) The width of protrusions was significantly thinner in neuronal βPix isoform KO neurons than in WT neurons. (D) Percentage of filopodia and spine on the dendrites of cultured hippocampal neurons from WT and neuronal βPix isoform KO mice. Filopodia percentage of neuronal βPix isoform KO neurons was significantly higher than that of WT neurons. (E) Dendritic spine density was significantly decreased in neuronal βPix isoform KO neurons than in WT neurons. 683-708 protrusions were analyzed in each group from 3 independent cultures.

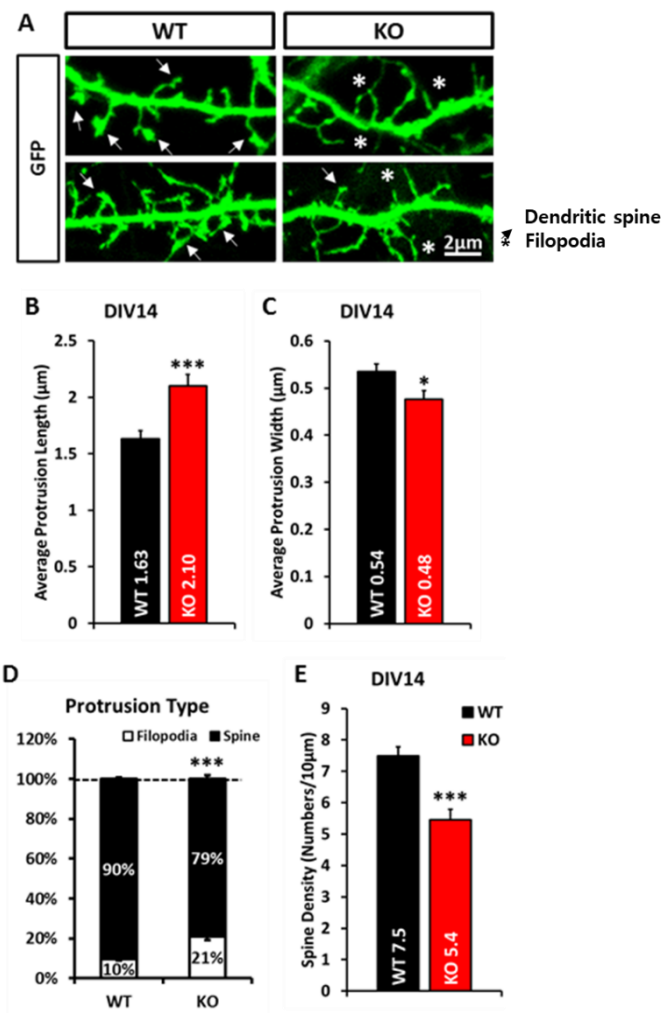
A
WT
KO
GFP
2μm
Dendritic spine
Filopodia
B
DIV14
Average Protrusion Length (μm)
2.5
2
1.5
1
0.5
0
***
WT 1.63
KO 2.10
C
DIV14
Average Protrusion Width (μm)
0.6
0.5
0.4
0.3
0.2
0.1
0
*
WT 0.54
KO 0.48
D
Protrusion Type
Filopodia
Spine
120%
100%
80%
60%
40%
20%
0%
***
90%
10%
79%
21%
WT
KO
E
DIV14
WT
KO
Spine Density (Numbers/10μm)
9
8
7
6
5
4
3
2
1
0
***
WT 7.5
KO 5.4

Figure 29. βPix-b and βPix-d are required for dendritic spine morphogenesis.

(A) Representative images of neuronal βPix isoform KO hippocampal neurons co-transfected with GFP, GFP-βPix-b or GFP-βPix-d and DsRed at DIV7 and analyzed by Image J software at DIV14. Quantification in (B)-(E). (B) The length of protrusions was significantly shorter in expression of βPix-b or βPix-d than control vector in neuronal βPix isoform KO neurons. (C) The width of protrusions was significantly thicker in expression of βPix-b or βPix-d than control vector in neuronal βPix isoform KO neurons. (D) Percentage of filopodia and spine on the dendrites in neuronal βPix isoform KO neurons by βPix-b or βPix-d expression. Filopodia percentage was significantly lower in expression of βPix-b or βPix-d than control vector in neuronal βPix isoform KO neurons. (E) Dendritic spine density was significantly increased in expression of βPix-b or βPix-d than control vector in neuronal βPix isoform KO neurons. 600-627 protrusions were analyzed in each group from 3 independent cultures.

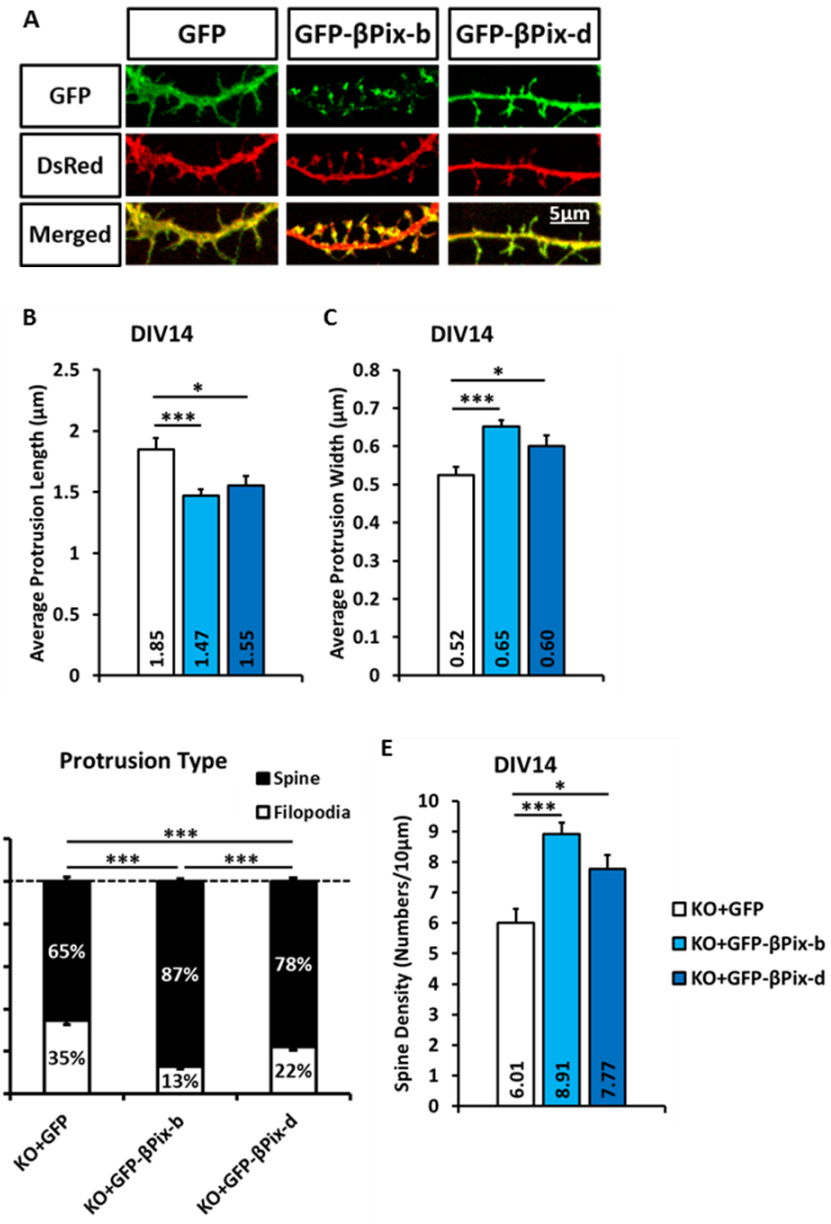
A
GFP
GFP-βPix-b
GFP-βPix-d
GFP
DsRed
Merged
5μm
B
DIV14
Average Protrusion Length (μm)
2.5
2
1.5
1
0.5
0
*
***
1.85
1.47
1.55
C
DIV14
Average Protrusion Width (μm)
0.8
0.7
0.6
0.5
0.4
0.3
0.2
0.1
0
*
***
0.52
0.65
0.60
D
Protrusion Type
Spine
Filopodia
120%
100%
80%
60%
40%
20%
0%
***
***
***
65%
35%
87%
13%
78%
22%
KO+GFP
KO+GFP-βPix-b
KO+GFP-βPix-d
E
DIV14
Spine Density (Numbers/10μm)
10
9
8
7
6
5
4
3
2
1
0
*
***
6.01
8.91
7.77
KO+GFP
KO+GFP-βPix-b
KO+GFP-βPix-d

to the maturation of dendritic spines. Moreover, βPix-b rescued the defects in dendritic spine maturation and the spine density in neuronal βPix isoform KO neurons more effectively than βPix-d, suggesting that βPix-b is the major βPix isoform regulating dendritic spine formation. These data are highly consistent with previous findings that βPix-b stimulates actin dynamics via the interaction between with N-WASP (Park et al., 2012) and KCC2 (Llano et al., 2015) in dendritic spines. Therefore, our findings demonstrate that the neuronal βPix isoforms play critical roles in dendritic spine development.

2.8. βPix-b and βPix-d are required for synaptic development.

To determine whether abnormal dendritic spine development caused by loss of βPix-b and βPix-d affects synapse development, we examined excitatory and inhibitory synapse density. The hippocampal neurons isolated from P0-1 WT and neuronal βPix isoform KO mice littermates were cultured for DIV14 and then stained for PSD-95 (postsynaptic marker) and VGLUT1 (presynaptic marker) to visualize excitatory synapses (Figure 30A), and Gephyrin (postsynaptic marker) and VGAT (presynaptic marker) to visualize inhibitory synapses (Figure 30B). Synapses were defined by immunofluorescent puncta that are positive for both presynaptic and postsynaptic markers. The neuronal βPix isoform KO neurons displayed significant reduction in both excitatory synaptic density and inhibitory synaptic density (Figure 30C). The puncta size immunostained by individual synaptic markers, PSD-95, VGLUT1, Gephyrin and VGAT, also markedly decreased in the KO neurons (Figure 30D).

We next investigated whether the neuronal βPix isoforms promote synapse

Figure 30. Neuronal βPix isoform KO mice have defects in synapse development in hippocampal neurons *in vitro*.

(A) Representative images of hippocampal neurons stained with VGLUT1, the excitatory presynaptic marker and PSD95, the excitatory postsynaptic marker at DIV14. Arrowheads point to the VGLUT1-positive PSD-95 indicating excitatory synapse. Quantification in (C) and (D). (B) Representative images of hippocampal neurons stained with VGAT, the inhibitory presynaptic marker and Gephyrin, the inhibitory postsynaptic marker at DIV14. Arrowheads point to the VGAT-positive Gephyrin indicating inhibitory synapse. Quantification in (C) and (D). (C) VGLUT1-positive PSD-95 and VGAT-positive Gephyrin puncta densities were decreased in cultured hippocampal neurons from neuronal βPix isoform KO mice at DIV14. (D) PSD-95 at synapse (VGLUT1-positive PSD-95), VGLUT1 at synapse (PSD-95-positive VGLUT1), gephyrin at synapse (VGAT-positive gephyrin), and VGAT at synapse (gephyrin-positive VGAT) had reduced puncta area in cultured hippocampal neurons from neuronal βPix isoform KO mice at DIV14. 62-80 neurons were analyzed in each group from 3 independent cultures.

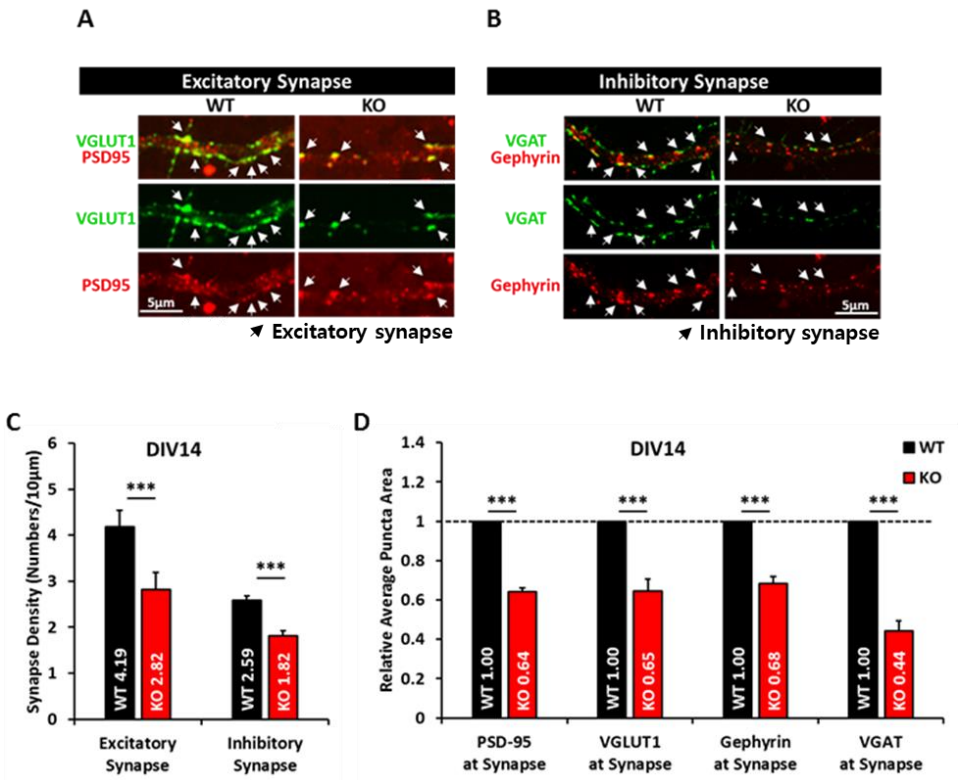
A
Excitatory Synapse
WT
KO
VGLUT1
PSD95
VGLUT1
PSD95
5μm
Excitatory synapse
B
Inhibitory Synapse
WT
KO
VGAT
Gephyrin
VGAT
Gephyrin
5μm
Inhibitory synapse
C
DIV14
Synapse Density (Numbers/10μm)
***
***
WT 4.19
KO 2.82
WT 2.59
KO 1.82
Excitatory Synapse
Inhibitory Synapse
D
DIV14
WT
KO
Relative Average Puncta Area
***
***
***
***
WT 1.00
KO 0.64
WT 1.00
KO 0.65
WT 1.00
KO 0.68
WT 1.00
KO 0.44
PSD-95 at Synapse
VGLUT1 at Synapse
Gephyrin at Synapse
VGAT at Synapse

formation and maturation by restoring each isoform in neuronal βPix isoform KO hippocampal neurons. We co-transfected neuronal βPix isoform KO neurons with GFP vector, GFP-βPix-b or GFP-βPix-d and DsRed at DIV7, and immunostained the neurons for VGLUT1 (Figure 31A) or VGAT (Figure 32A) at DIV14. Excitatory or inhibitory synaptic density was determined by quantifying the number of VGLUT1 or VGAT puncta, respectively, in the DsRed-positive transfected neurons. We found that each of βPix-b and βPix-d significantly increased both excitatory and inhibitory synapse density (Figure 31B and 32B), a finding reminiscent of previous observation that βPix is involved in excitatory (Zhang et al., 2005) and inhibitory synapse formation (Smith et al., 2014). Moreover, at a synapse, total VGLUT1 and VGAT puncta area per 10 μm are significantly increased by expression of βPix-b or βPix-d in neuronal βPix isoform KO neurons, compared to the GFP control (Figure 31C and 32D). More importantly, expression of βPix-b restored the deficits in excitatory synapse density in neuronal βPix isoform KO neurons more effectively than expression of βPix-d (Figure 31B), indicating that βPix-b isoform plays a major role in dendritic spine and excitatory synapse maturation. In contrast, expression of βPix-d appears more effective in rescuing the deficits in inhibitory synapse density in neuronal βPix isoform KO neurons than expression of βPix-b (Figure 32B). Investigation of subcellular localization of exogenous βPix-b or βPix-d in neuronal βPix isoform KO neurons, visualized by βPix-b or βPix-d fused with EGFP, showed that EGFP-βPix-b was mainly present in the head of dendritic spine, whereas EGFP-βPix-d was present in dendritic shaft and spine neck (Figure 33). Furthermore, we found that endogenous βPix-d stained with 11 a.a. antibody existed in linear patterns in the neurites at DIV14 (Figure 34) and WT hippocampal neurons co-staining with

Figure 31. βPix-b and βPix-d are required for excitatory synapse development. (A) Representative images of neuronal βPix isoform KO hippocampal neurons co-transfected with GFP, GFP-βPix-b or GFP-βPix-d and DsRed at DIV7 and analyzed by double immunofluorescence with antibodies to GFP and VGLUT1 at DIV14. Quantification in (B) and (C). (B) Average VGLUT1 puncta intensity was increased in expression of βPix-b in neuronal βPix isoform KO neurons. (C) Excitatory synapse density was increased in expression of βPix-b and βPix-d in neuronal βPix isoform KO neurons. 61-62 neurons were analyzed in each group from 3 independent cultures.

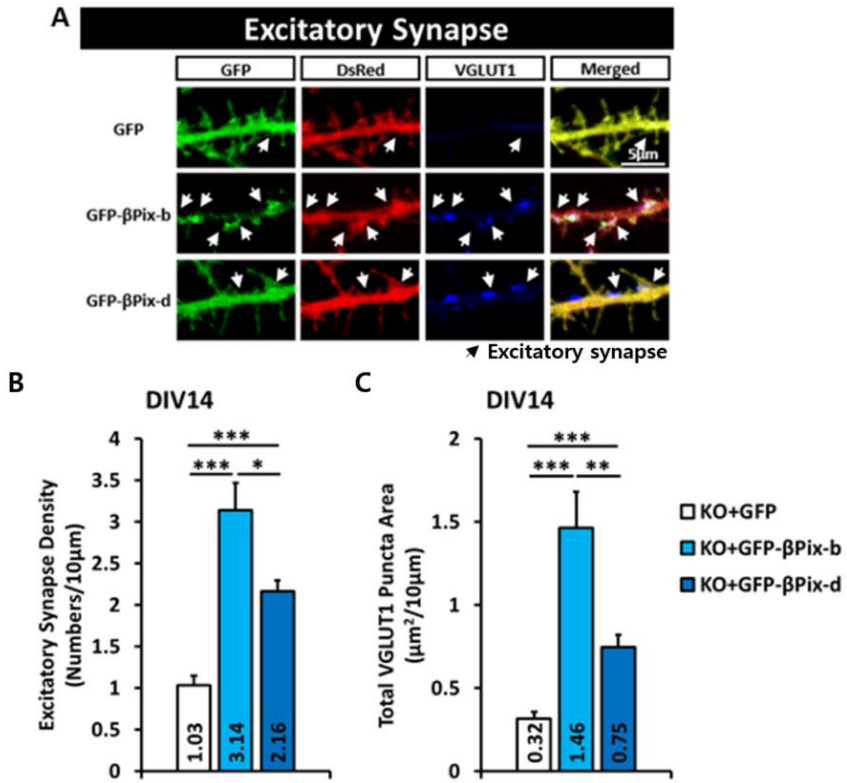
A
Excitatory Synapse
GFP
DsRed
VGLUT1
Merged
GFP
GFP-βPix-b
GFP-βPix-d
5μm
Excitatory synapse
B
DIV14
Excitatory Synapse Density (Numbers/10μm)
***
***
*
1.03
3.14
2.16
C
DIV14
Total VGLUT1 Puncta Area (μm²/10μm)
***
***
**
0.32
1.46
0.75
KO+GFP
KO+GFP-βPix-b
KO+GFP-βPix-d

Figure 32. βPix-b and βPix-d are required for inhibitory synapse development. (A) Representative images of hippocampal neurons co-transfected with GFP, GFP-βPix-b or GFP-βPix-d and DsRed at DIV7 and analyzed by double immunofluorescence with antibodies to GFP and VGAT at DIV14. Quantification in (B) and (C). (B) Expression of βPix-b or βPix-d in neuronal βPix isoform KO neurons did not show significant difference in average VGAT puncta intensity compared to expression of control vector in neuronal βPix isoform KO neurons. (C) Inhibitory synapse density was increased in expression of βPix-b or βPix-d in neuronal βPix isoform KO neurons. 24 neurons were analyzed in each group from 3 independent cultures.

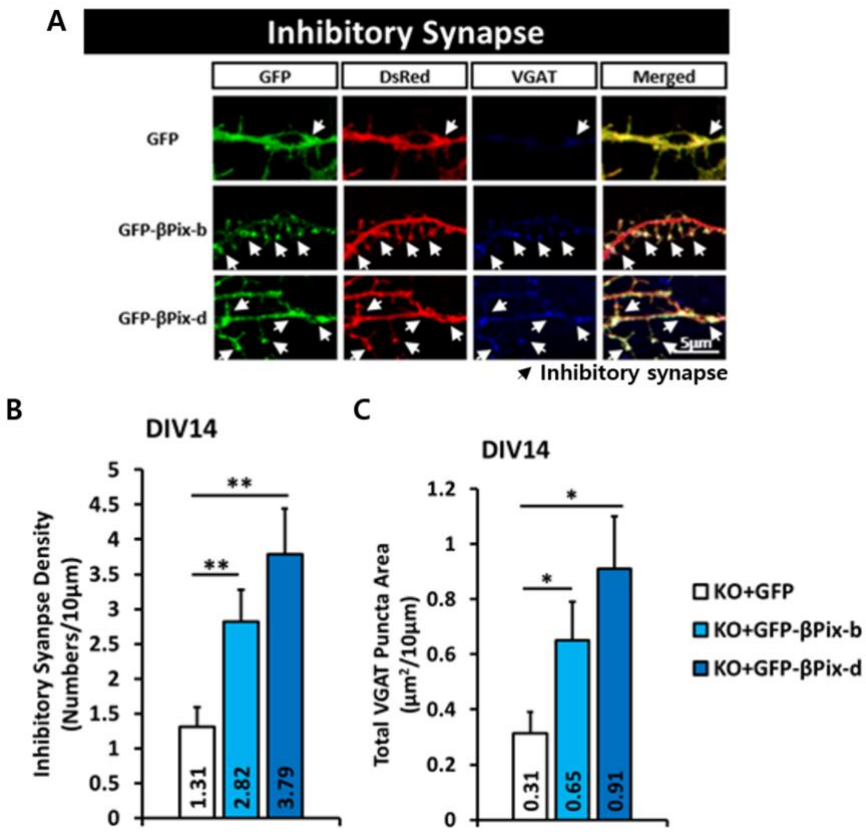
A
Inhibitory Synapse
GFP
DsRed
VGAT
Merged
GFP
GFP-βPix-b
GFP-βPix-d
5μm
Inhibitory synapse
B
DIV14
Inhibitory Syanpse Density (Numbers/10μm)
1.31
2.82
3.79
C
DIV14
Total VGAT Puncta Area (μm²/10μm)
0.31
0.65
0.91
KO+GFP
KO+GFP-βPix-b
KO+GFP-βPix-d

Figure 33. βPix-b is localized in dendritic spine, and βPix-d is localized in dendritic shaft and spine.

Representative images of neuronal βPix isoform KO hippocampal neurons co-transfected with GFP, GFP-βPix-b or GFP-βPix-d and DsRed at DIV7 and fixed DIV14. Higher magnification of each white line box is located at the top of each panel. Data are representative of 3 independent experiments.

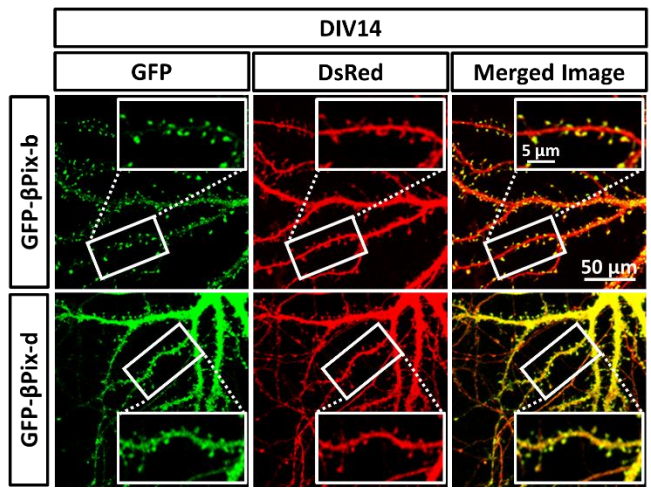
DIV14
GFP
DsRed
Merged Image
GFP-βPix-b
GFP-βPix-d
5 μm
50 μm

Figure 34. Endogenous βPix-d exists in linear patterns in the neurites.

Representative images of WT neurons fixed at DIV14 and stained with INS antibody or 11 a.a. antibody (red) and SH3 antibody (green). Higher magnification of each white line box is located at the top of each panel. Data are representative of 3 independent experiments.

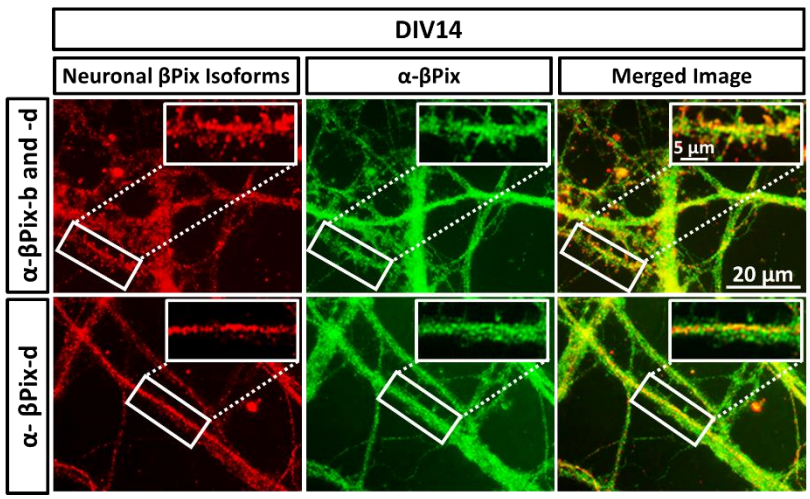
DIV14
Neuronal βPix Isoforms
α-βPix
Merged Image
α-βPix-b and -d
α- βPix-d
5 µm
20 µm

INS antibody and 11 a.a. antibody showed that βPix-d among neuronal βPix isoforms was not co-localized with F-actin (Figure 35), suggesting that βPix-d correlates with microtubules. Overall, the results highlight that βPix-b and βPix-d are differentially localized in the neurons and regulate the formation of the different types of synapses in an isoform-dependent manner.

2.9. Neuronal βPix isoform KO mice have reduced LTP at hippocampal Schaffer collateral-CA1 synapses.

Given that spine morphology is intimately related to synaptic function (Carlisle and Kennedy, 2005), the mechanisms that determine the morphological development of dendrites and dendritic spines have a significant impact on the function of synapses, and in turn, neuronal circuits. Given the reduction in spine density observed in the hippocampal neurons of neuronal βPix isoform KO mice, we examined whether neurotransmission is also altered in the hippocampus of neuronal βPix isoform KO mice. We performed electrophysiological recordings of hippocampal Schaffer collateral-CA1 (SC-CA1) synapses from acute slice preparations of juvenile mice to elucidate the functional consequences of deleting expression of neuronal βPix isoforms. Basal excitatory transmission shown in input-output curve and paired–pulse ratio was unchanged in neuronal βPix isoform KO mice (Figure 36A and 36B). To assess synaptic plasticity, fEPSPs were examined before and after applying a Schaffer collateral stimulation. LTP induced by thetaburst stimulation (TBS) was severely decreased in neuronal βPix isoform KO mice (Figure 36C). A significant reduction between the two groups was shown at a later stage of LTP, indicating impaired maintenance of LTP in neuronal βPix isoform KO mice (Figure 36D). We

Figure 35. βPix-d is not co-localized with F-actin.

Representative images of WT neurons fixed at DIV14 and stained with INS antibody (green), 11 a.a. antibody (blue) and Phalloidin (red). The lower panels showed higher magnifications of white dotted boxes in the upper panels. White regions shown in co-localization analysis indicated the localization of βPix-d. In a, b and c panels, yellow arrow heads indicated that βPix-b among neuronal βPix isoforms localized to F-actin. Data are representative of 3 independent experiments.

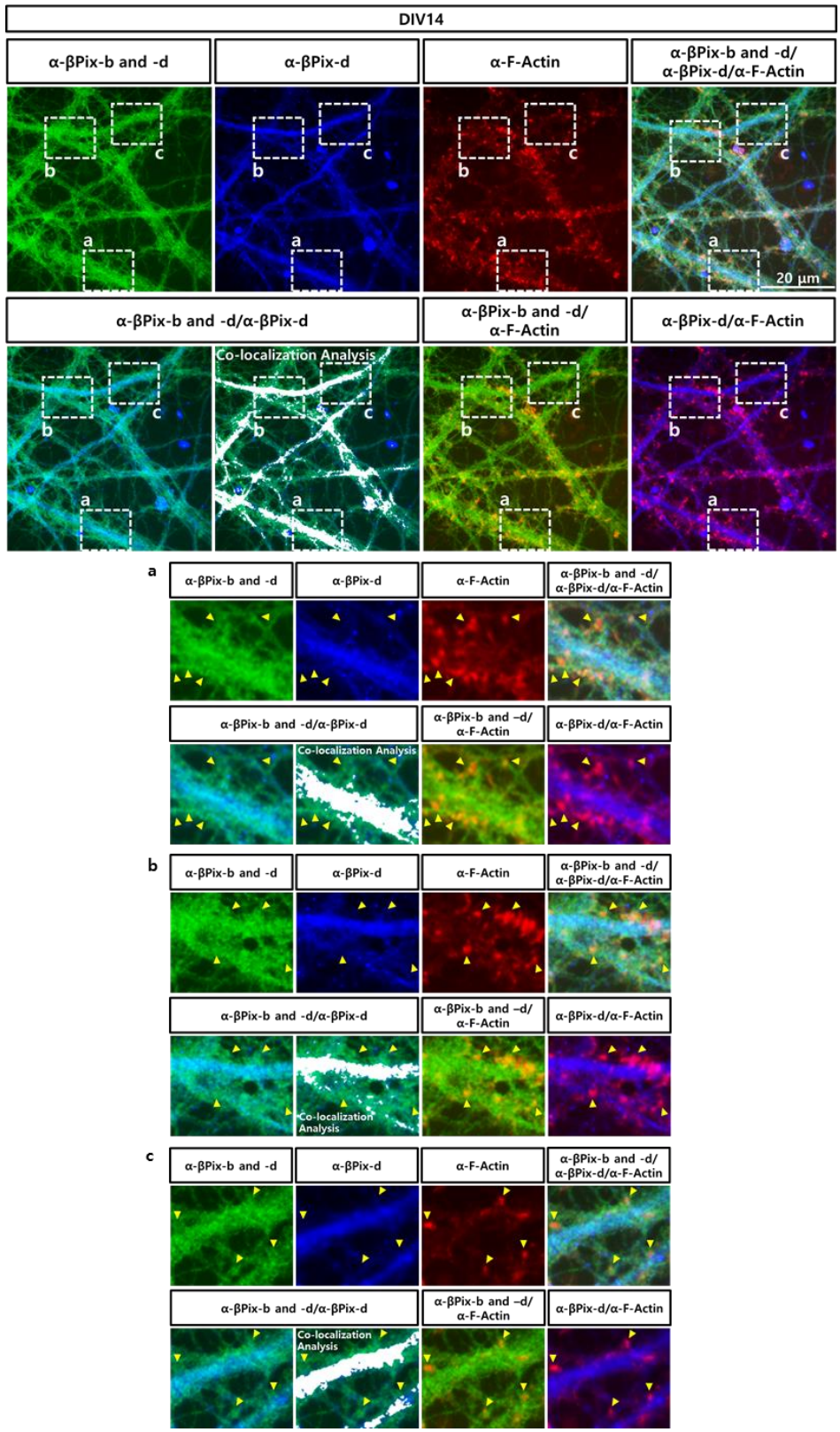
DIV14
α-βPix-b and -d
α-βPix-d
α-F-Actin
α-βPix-b and -d/
α-βPix-d/α-F-Actin
20 μm
α-βPix-b and -d/α-βPix-d
Co-localization Analysis
α-βPix-b and -d/
α-F-Actin
α-βPix-d/α-F-Actin
a
b
c

Figure 36. Schaffer collateral-CA1 LTP is decreased in neuronal βPix isoform KO mice.

(A) Synaptic input/output (I/O) relationship at Schaffer collateral-CA1 synapses showed normal in neuronal βPix isoform KO mice. (B) Paired pulse facilitation ratio of evoked EPSP at Schaffer collateral-CA1 synapses showed normal in neuronal βPix isoform KO mice. (C) LTP induced by TBS in CA1 region in acute hippocampal slices was significantly impaired in slices taken from 6-7 weeks neuronal βPix isoform KO mice in comparison with littermate WT mice. (D) Quantification of (C). Late LTP was significantly decreased in neuronal βPix isoform KO mice. (E) Long-term depression at Schaffer collateral-CA1 synapses was normal in 4-5 weeks neuronal βPix isoform KO brain slice. TBS to induce LTP and SP-LFS to induce LTD were applied to the Schaffer collateral. fEPSP slope were expressed as percentage of the mean of baseline values in the last 20 min before stimulation. Experiments were performed in laboratory of Prof. Se-Young Choi (Seoul National University).

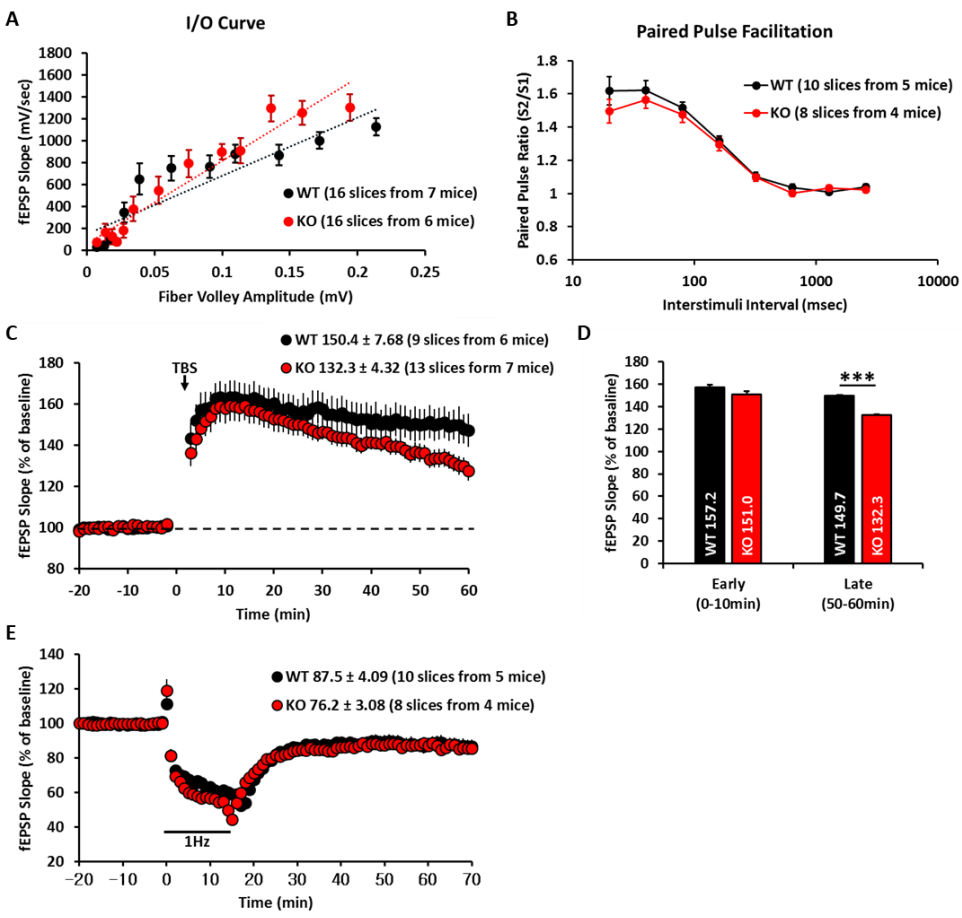
A
I/O Curve
fEPSP Slope (mV/sec)
Fiber Volley Amplitude (mV)
WT (16 slices from 7 mice)
KO (16 slices from 6 mice)
B
Paired Pulse Facilitation
Paired Pulse Ratio (S2/S1)
Interstimuli Interval (msec)
WT (10 slices from 5 mice)
KO (8 slices from 4 mice)
C
WT 150.4 ± 7.68 (9 slices from 6 mice)
KO 132.3 ± 4.32 (13 slices form 7 mice)
TBS
fEPSP Slope (% of baseline)
Time (min)
D
fEPSP Slope (% of basaline)
WT 157.2
KO 151.0
WT 149.7
KO 132.3
***
Early
(0-10min)
Late
(50-60min)
E
WT 87.5 ± 4.09 (10 slices from 5 mice)
KO 76.2 ± 3.08 (8 slices from 4 mice)
fEPSP Slope (% of baseline)
1Hz
Time (min)

then evaluated the effect of neuronal βPix isoform deficiency on long-term depression (LTD) induced by low-frequency stimulation (LFS). LTD was not different across genotypes (Figure 36E). Our findings indicate that LTP was impaired in neuronal βPix isoform KO mutants, demonstrating that neuronal βPix isoforms are necessary for hippocampal synaptic function, and suggest that the synaptic defects may be accompanied by behavioral changes.

2.10. Neuronal βPix isoform KO mice show impaired recognition memory and startle response, and low anxiety levels.

Dendrite and dendritic spine morphogenesis is required for establishing normal cognitive functions, and deficits in cognitive functions, especially in working memory, are associated with certain neurological disorders in humans, such as schizophrenia, ADHD and Alzheimer's disease (Barch, 2005; Doyle, 2006; Germano and Kinsella, 2005). As described above, our molecular and electrophysiological studies of neuronal βPix isoform KO mice indicated hippocampal synaptic defects. Given the apparent deficits in synaptic connectivity in neuronal βPix isoform KO mice, we performed hippocampus-dependent behavior test to determine whether the absence of neuronal βPix isoforms affects cognitive functions. In neuronal βPix isoform KO mice, cognitive abilities assessed by Morris water maze test were generally intact for learning the localization of a hidden platform (Figure 38A) and trace fear conditioned memory were also normal (Figure 39B). In contrast, performance in novel object recognition test was largely impaired in neuronal βPix isoform KO mice in the test session conducted 24 hours after training (Figure 37A).

Figure 37. Neuronal βPix isoform KO mice show impaired recognition memory and startle response, and low anxiety level.

(A) Neuronal βPix isoform KO mice spent less time to explore a novel object than WT mice. Shown in recognition index, A represents the amount of time spent interacting with a familiar object and B with a novel object. (B) Neuronal βPix isoform KO mice spent less time in closed arms and more time in open arms on elevated plus maze test compared to WT mice. (C) Neuronal βPix isoform KO mice displayed impaired acoustic startle response. (D) Neuronal βPix isoform KO mice showed a significantly reduced prepulse inhibition response relative to WT mice. 12 10-12 weeks mice for WT and 10 10-12 weeks mice for neuronal βPix isoform KO mice were analyzed for data. Experiments were performed in laboratory of Prof. June-Seek Choi (Korea University).

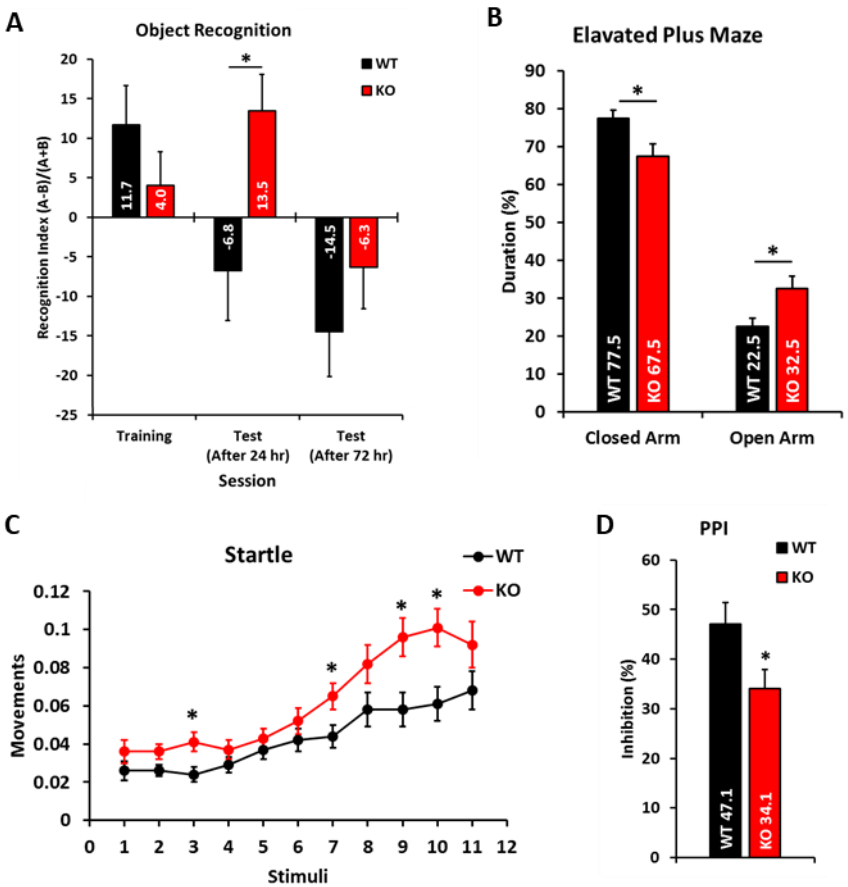
A
Object Recognition
WT
KO
Recognition Index (A-B)/(A+B)
11.7
4.0
-6.8
13.5
-14.5
-6.3
Training
Test (After 24 hr)
Test (After 72 hr)
Session
B
Elavated Plus Maze
Duration (%)
WT 77.5
KO 67.5
WT 22.5
KO 32.5
Closed Arm
Open Arm
C
Startle
WT
KO
Movements
Stimuli
D
PPI
WT
KO
Inhibition (%)
WT 47.1
KO 34.1

Figure 38. Spatial learning and open field activity are normal in WT and neuronal βPix isoform KO mice.

(A) Spatial learning in the Morris water maze test was normal in KO mice. (B) No genotype differences were found in total moved distance on open field test. 12 10-12 weeks male mice for WT and 10 10-12 weeks male mice for neuronal βPix isoform KO mice were analyzed for data. *P* values (* $P < 0.05$) are derived from two-tailed student's t-test. Experiments were performed in laboratory of June-Seek Choi (Korea University).

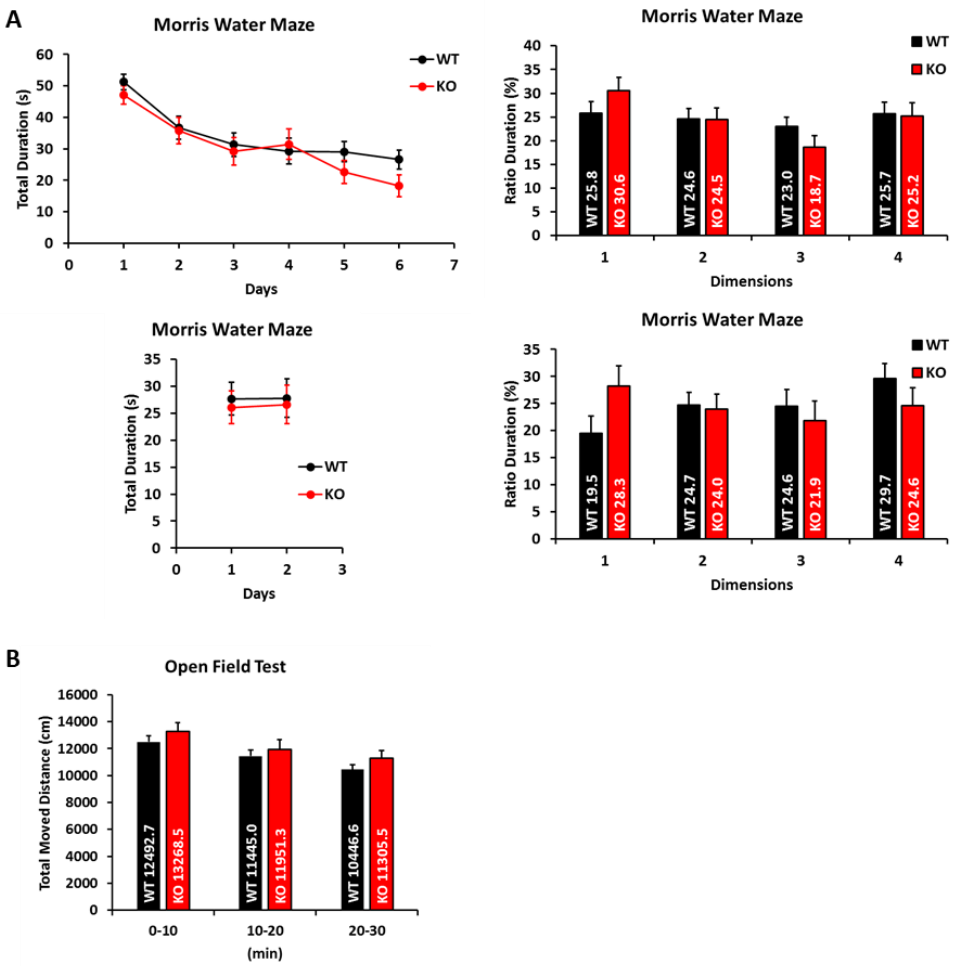
A
Morris Water Maze
Total Duration (s)
Days
WT
KO
Morris Water Maze
Ratio Duration (%)
Dimensions
WT 25.8
KO 30.6
WT 24.6
KO 24.5
WT 23.0
KO 18.7
WT 25.7
KO 25.2
Morris Water Maze
Total Duration (s)
Days
Morris Water Maze
Ratio Duration (%)
Dimensions
WT 19.5
KO 28.3
WT 24.7
KO 24.0
WT 24.6
KO 21.9
WT 29.7
KO 24.6
B
Open Field Test
Total Moved Distance (cm)
WT 12492.7
KO 13268.5
WT 11445.0
KO 11951.3
WT 10446.6
KO 11305.5
0-10
10-20
20-30
(min)

Figure 39. Neuronal βPix isoform KO mice have low freezing levels during conditioning on trace fear conditioning test.

(A) During conditioning, neuronal βPix isoform KO mice displayed lower levels of freezing behavior compared with WT mice. (B) During testing, no genotype differences were found in trace fear conditioning. 10-12 weeks male for WT mice and 10 10-12 weeks male for neuronal βPix isoform KO mice were analyzed for data. Experiments were performed in laboratory of Prof. June-Seek Choi (Korea University).

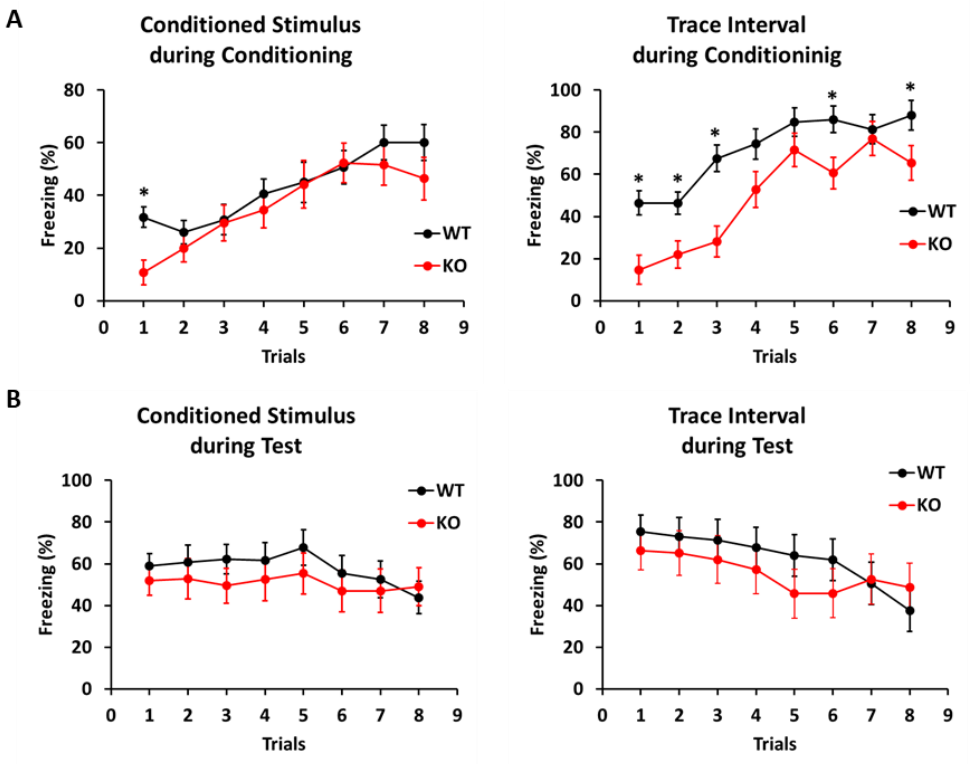
A
Conditioned Stimulus
during Conditioning
Freezing (%)
Trials
WT
KO
Trace Interval
during Conditioninig
Freezing (%)
Trials
WT
KO
B
Conditioned Stimulus
during Test
Freezing (%)
Trials
WT
KO
Trace Interval
during Test
Freezing (%)
Trials
WT
KO

WT mice spent more time to explore the novel object than the familiar object, but neuronal βPix isoform KO mice spent more time to explore the familiar one than the novel one. No significant genotype differences were found in the test conducted 72 hours after training, indicating that neuronal βPix isoform KO mice take more time to recognize a novel object than WT mice. Novel object recognition is a form of declarative memory, dependent on intact CA1 hippocampal function (Hammond et al., 2004; Rampon and Tsien, 2000). Therefore, these data suggest that the LTP impairment in the hippocampus of neuronal βPix isoform KO mice could contribute to their deficits in recognition memory for novelty.

We next set out to determine whether the behavioral deficits in neuronal βPix isoform KO mice are limited to hippocampus-associated behavioral phenotypes. First, baseline anxiety-like behavior was assessed in WT and neuronal βPix isoform KO mice by using an elevated plus maze test. When compared with WT mice, neuronal βPix isoform KO mice spent significantly longer in the open arms of the elevated plus maze (Figure 37B), indicating that neuronal βPix isoform KO mice have low levels of anxiety. These data are consistent with our results that neuronal βPix isoform KO mice showed a significant decrease in freezing during conditioning in the trace fear conditioning test (Figure 39A), whereas freezing levels during testing were not altered (Figure 39B). Neuronal βPix isoform KO mice have no problems in memory for trace fear conditioning, but anxiety levels appear to be lower than in WT mice during conditioning. No significant genotype differences were found in total distance traveled during open-field test, indicating that motor abilities were normal in neuronal βPix isoform KO mice on open-field locomotion (Figure 38B). Taken together, given the greater time spent in the open arms and the more

decreased freezing levels in neuronal βPix isoform KO mice in comparison to the WT mice, it is apparent that neuronal βPix isoform KO mice have significantly decreased levels of anxiety-like behavior at baseline.

Sensory-motor gating deficits are common in mice with genetically induced NMDARs hypofunction (Duncan et al., 2004; Fradley et al., 2005). Acoustic startle response and pre-pulse inhibition (PPI) tests are frequently used to assess anxiety levels and sensory-motor gating both in patients and animal models (Geyer et al., 2002). We found that neuronal βPix isoform KO mice show profound defects in acoustic startle response and PPI (Figure 37C and 37D), demonstrating that the neuronal βPix isoforms are required for the anxiety-like behavior and sensorimotor gating. Taken together, these data show that loss of neuronal βPix isoforms causes defective neuronal morphogenesis, which accompanies the electrophysiological deficits and behavioral impairments. Therefore, these results demonstrate that the neuronal βPix isoforms play essential roles for neural circuit formation and function.

Discussion

Given that the neuronal phenotypes caused by loss of βPix *in vivo* have not yet been identified, we generated βPix deficient mice. We found that the deletion of βPix resulted in embryonic lethality at E9.5. Before the embryonic death, βPix null embryos exhibited impairment of axial rotation, neural tube closure and allantois-chorion fusion. Therefore, we observed the phenotypes in their neuronal morphology in βPix heterozygous mice and neuronal βPix isoform KO mice. Firstly, in βPix heterozygous mice, the hippocampal neurons have simplified dendritic arbors and reduced dendritic spine density both *in vitro* and *in vivo*. Interestingly, the cultured hippocampal neurons of βPix heterozygous mice had decrease in both excitatory and inhibitory synapse densities, and in hippocampus from βPix heterozygous mice, the expression levels of NMDA and AMPA receptor subunits and Git1 protein were reduced. Next, neuronal βPix isoform KO mice have decreased activity of Rac1 and Cdc42 in hippocampus, and morphology of neurite and dendritic spine have defects in hippocampal neurons from neuronal βPix isoform KO mice *in vivo*. Interestingly, in 5 weeks, hippocampus from neuronal βPix isoform KO mice have increased expression level of NMDA receptor subunit and CaMKIIα proteins. Cultured hippocampal neurons from neuronal βPix isoform KO mice have impairments in development of neurite, dendritic spine and synapse, and those defects were recovered by expression βPix-b or βPix-d.

βPix heterozygous mice have defects in neuronal structures and functions.

In this study, we investigated the phenotypes in neuronal morphology and social

behavior of βPix heterozygous mice. βPix plays important roles in neurite development and synapse formation *in vivo* (Figure 13 and 14) as well as *in vitro* (Figure 10-12). These findings are the first report showing that βPix regulates neuronal development *in vivo*. βPix has been reported to work together with Git1 to regulate spine morphogenesis and synapse formation (Zhang et al., 2005). Our present study showed that adult βPix heterozygous mice have reduced expression level of Git1 protein (Figure 15A and 15C) that might lead to weakening a signaling complex consisting of βPix and Git1, and in turn cause impairment of dendritic spine and synapse formation. In line with our data, Git1 KO mice shows reduced amounts of βPix in the brain lysates (Won et al., 2011) and decreased dendritic spine numbers in the hippocampus (Hong and Mah, 2015). Our biochemical study also showed that hippocampus from adult βPix heterozygous mice expressed decreased amounts of glutamate receptor subunits (Figure 15A and 15C). There is a well-established correlation between dendritic spine morphology and synaptic function. Specifically, a previous study demonstrated that dendritic spine morphology is critical for AMPA receptor expression in hippocampal CA1 pyramidal neurons (Matsuzaki et al., 2001). The integrity of actin cytoskeleton is critical for membrane delivery and stability of NMDA and AMPA receptors (Gu et al., 2010; Wyszynski et al., 1997). βPix, a key regulator of actin dynamics, regulates activity-dependent localization of GluN3A, one of NMDA receptor subunits (Fiuza et al., 2013), and activity-dependent Ca^{2+} influx through the NMDA receptor induces CaMKI-mediated phosphorylation of S516 in βPix with resultant activation of its GEF activity (Saneyoshi et al., 2008), suggesting the tight association between βPix and NMDA receptor. These relationships support our hypothesis that the reduced spine density caused by βPix

deficiency in the neuron results in reduced protein levels of glutamate receptor subunits that are located in dendritic spine.

Behaviorally, βPix heterozygous mice displayed impaired social preference (Figure 16). Defects in social preference are found in several neuropsychiatric disorders such as autism spectrum disorder, attention deficit hyperactivity disorder, and schizophrenia (Cross-Disorder Group of the Psychiatric Genomics et al., 2013). Although the exact mechanism by which the reduced expression of βPix affect psychiatric-like behavior is still unknown, our present study showed potential roles of βPix in pathogenesis of certain neuropsychiatric disorders. In conclusion, our present study further advanced the previous researches that focused on the βPix function in neuronal morphogenesis and synapse formation shown in *in vitro* models. We found that βPix heterozygous mice had defects in neuronal structures and synapse that could be severe enough to affect social behaviors. Although it is difficult for βPix heterozygous mice to directly associate abnormal behavior with certain patient symptoms, our study on structural and behavioral defects resulting from βPix deficiency suggest some evidences of a relationship between βPix and neurological diseases. Thus, additional behavioral and electrophysiological analysis for βPix heterozygous mice will help to gain an exact understanding of βPix function in brain, and relationship with certain neuropsychiatric diseases such as autism spectrum disorder.

Neuronal βPix isoform KO mice have defects in neuronal structures and functions.

Neuronal βPix isoform KO mice show decreased levels of hippocampal neurite

complexity and dendritic spine density (Figure 20 and 21), accompanied by lower levels of active Rac1 and Cdc42 in the hippocampus (Figure 19), compared to the WT mice *in vivo*. Also, in cultured hippocampal neurons from the neuronal βPix isoform KO mice, neurite length and complexity, and dendritic spine density were decreased, compared to the WT neurons (Figure 26 and 28). Rho family of GTPases and related molecules play important roles in various aspects of neuronal development, including neurite outgrowth and differentiation, axon pathfinding, and dendritic spine formation and maintenance (Govek et al., 2005). Therefore, the loss of neuronal βPix isoforms affects dendritic complexity and spine density likely due to impaired Rac1 and Cdc42 signaling. Consistently, βPix-a was reported to work together with Rac, Pak and Git to regulate spine morphogenesis and synapse formation in rat primary hippocampal neurons (Zhang et al., 2005) and in *Drosophila* (Parnas et al., 2001). Other Rho family GEFs, including Tiam1 and Kalirin, have also been shown to affect neuronal morphology through Rac1 and Cdc42 (Cahill et al., 2009; Tolias et al., 2005; Yan et al., 2015). In the current study, we provide the first evidence that βPix-b and βPix-d play essential roles in neuronal development through activation of Rac1 and Cdc42 in hippocampus.

The neuronal βPix isoform KO mice exhibit increased expression levels of βPix-a while βPix-b and βPix-d are completely eliminated. Hence, we complemented βPix-b or βPix-d in the hippocampal neurons cultured from neuronal βPix isoform KO mice to determine whether the defects in neuronal morphology shown in neuronal βPix isoform KO mice resulted from either loss of βPix-b and βPix-d or overexpression of βPix-a (Figure 27 and 29). Interestingly, expression of neuronal βPix isoforms alleviated the abnormal neuronal phenotypes of neuronal βPix isoform

KO neurons with βPix-d being more effective than βPix-b in neurite morphology and βPix-b than βPix-d in dendritic spine morphology. Likewise, we observed that expression of βPix-b promotes development of the excitatory synapses more effectively than βPix-d does (Figure 31). Taken together, these results suggest that βPix-d is essential for neurite development and βPix-b is essential for the formation of excitatory synapses that develops on dendritic spines.

Previously, CaMKs that are related to NMDARs has been reported to promote phosphorylation at Ser516 of βPix in Git1/βPix complex; this phosphorylation stimulates the GEF activity to induce Rac1 activation, promoting the formation and stabilization of mature dendritic spines (Saneyoshi et al., 2008). We found that both neuronal βPix isoforms and GluN2B were enriched in the same PSD fraction that are extracted after two consecutive treatments of Triton X-100 (Figure 23). Furthermore, expression levels of GluN2B, one of the NMDAR subunits, and CaMKIIα were increased in the neuronal βPix isoform KO hippocampi (Figure 22), indicating that βPix is specifically involved in NMDAR signaling, as previously suggested by Fiuza *et al* (Fiuza et al., 2013). Interestingly, a previous report has shown that mice lacking GluN2B in pyramidal neurons of cortex and hippocampal CA1 region also exhibited decreased dendritic spine density in CA1 hippocampal neurons compared with controls (Brigman et al., 2010). Our study, showing increased GluN2B in the neuronal βPix isoform KO mice leading to decreased spine formation, can be interpreted in two ways. One is presynaptic effect; previous studies have shown that βPix-mediated actin polymerization at synapses regulates vesicle localization in presynaptic terminals (Momboisse et al., 2009; Shirafuji et al., 2014; Sun and Bamji, 2011). Furthermore, our present study shows that presynaptic puncta

sizes in synapses are smaller in the neuronal βPix isoform KO neurons than in the WT neurons (Figure 30D). Although distinguishable functions of neuronal βPix isoforms in presynaptic terminal are unknown, it is likely that the loss of neuronal βPix isoforms disrupts presynaptic functions and, in turn, leads to more expression of GluN2B and CaMKIIα as a homeostatic mechanism. The other possibility is postsynaptic effect; previous study on synaptic localization of GluN3A through Git1/βPix complex supports that the neuronal βPix isoforms regulate the synaptic localization of GluN2B (Fiuza et al., 2013). Although all βPix isoforms have GBD (Figure 1), we speculate that the distinct neuronal correlation of βPix-b and βPix-d with Git1 could affect expression and localization of GluN2B in synapse. Our present study also indicates that those expression patterns were caused by the compensatory effects of decreased dendritic complexity and spine density in the hippocampus of 5weeks neuronal βPix isoform KO mice (Figure 20B and 21B). 12 weeks neuronal βPix isoform KO mice showed decreased dendritic complexity and dendritic spine density (Figure 20C and 21B), but no changes in those expression levels, leading to hypofunction of glutamatergic signaling that induces impaired synaptic transmission and behavior during adolescent development (Duncan et al., 2004; Fradley et al., 2005; Luscher and Malenka, 2012). Indeed, we observed defects in LTP maintenance in 6-7 weeks neuronal βPix isoform KO mice (Figure 36) and PPI and acoustic startle response in 12 weeks neuronal βPix isoform KO mice (Figure 37C and 37D).

Given the established role of dendritic spines in memory formation and the aberrant spine morphology seen in mental retardation (Benarroch, 2007), it is not surprising that the neuronal βPix isoform KO mice exhibit learning deficits (Figure 37A). The

process of learning is often linked to attention (Eldar et al., 2013) and learning disabilities have been found to occur in about 20-30 % of children with ADHD (Cantwell and Baker, 1991). The neuronal βPix isoform KO mice showed reduced levels in PPI and hypersensitivity in startle response (Figure 37C and 37D), which both have been linked to abnormalities in sensorimotor gating and attention (Kedzior and Martin-Iverson, 2006). In addition, during trace fear conditioning test, conditioning that requires attention was mildly disrupted in the neuronal βPix isoform KO mice (Figure 39A). Hence, these results suggest that the various behavioral phenotypes seen in the neuronal βPix isoform KO mice might be associated with attention deficiency. We found that the neuronal βPix isoform KO mice have problems in specific type of memory; spatial memory and learning ability for fear conditioning test were intact (Figure 38A and 39B), whereas novel object recognition was impaired (Figure 37A). Although the hippocampus is a common region involved in multiple aspects of memory (Antunes and Biala, 2012; Ramos, 2000), there are specific areas and circuits of brain associated with each memory type. Our finding is consistent with the hypothesis that specific synapses or molecular pathways underlie different forms of hippocampal memory, which was previously raised (Bach et al., 1995), but has not been investigated extensively.

In our study, the decreased density of dendritic spine and excitatory synapse and reduced VGLUT1 puncta size in the neuronal βPix isoform KO neurons are rescued more effectively by transfection with GFP-βPix-b than GFP-βPix-d (Figure 29 and 31). On the other hand, the inhibitory synapse density and VGAT puncta size reduced in neuronal βPix isoform KO neurons are recovered better by transfection with GFP-βPix-d than GFP-βPix-b (Figure 32). Therefore, our data demonstrate that different

βPix isoforms have differential functions. Although the precise mechanism for βPix-b and βPix-d governing synaptic development remains obscure, we suggest that βPix-b and βPix-d serve as regulators of excitatory or inhibitory synapses and they are placed center stage for the control of excitatory-inhibitory balance, which is critical for neuronal function (Liu, 2004). In line with the notion, we observed that βPix-b and βPix-d are differentially localized in dendrites. βPix-b is primarily localized in dendritic spine head, and βPix-d is localized in both dendritic shaft and spine (Figure 33), indicating that the difference in distributions of βPix isoforms highly correlates with their roles in the formation of specific synapse types. We speculate that each neuronal βPix isoform is associated with unique molecules in specific regions of dendrites or well-known interactors to regulate compartmental mechanism depending on their specific distribution, leading to formation and maturation of either excitatory or inhibitory synapses. As studied for another Rho family GEF, Tiam1 (Zhang and Macara, 2006), our present study indicates that the functions of neuronal βPix isoforms must be spatially regulated to control synaptogenesis. Furthermore, because misregulation of excitation-inhibition balance is frequently associated with a number of nervous system disorders, such as epilepsy, mental retardation and autism, our study gains influence in both basic and clinical research (Eichler and Meier, 2008).

Symptoms that appear in high percentages of individuals with various neurological disorders include cognitive disabilities, anxiety, hypersensitivity and hyposensitivity to sensory stimuli and motor impairments. WT and neuronal βPix isoform KO littermate mice scored similarly on the measures of body and brain weight (Figure 18A and 18B), motor functions shown in open field test (Figure 38B) and spatial and

trace fear memory (Figure 38A and 39B). However, the neuronal βPix isoform KO mice showed low anxiety levels on elevated plus-maze (Figure 37B) and for fear response during conditioning on trace fear conditioning test (Figure 39A). The response and prepulse inhibition to acoustic sensory stimuli were also impaired in the neuronal βPix isoform KO mice (Figure 37C and 37D). Moreover, they have impairments in LTP maintenance (Figure 36) and novel object recognition memory (Figure 37A). Our studies indicate potential roles of βPix signaling for pathogenesis of neurological disorders. There has been no reported occurrence of neurological disorder genetically linked to βPix. Meanwhile, patients with deletions of chromosome bands 13q33-34 have mental retardation, microcephaly, and distinct facial features and molecular cytogenetic definition of a common deleted region in all patients suggests *ARHGEF7* gene as a candidate gene causing mental retardation and microcephaly (Walczak-Sztulpa et al., 2008). In addition, βPix was found to interact with neurological disorder risk factors including the postsynaptic protein Shank (Park et al., 2003) that is a representatively ASD and schizophrenia risk factor (Zhou et al., 2016), Git (Bagrodia et al., 1998) that is associated with ADHD in humans and mice (Won et al., 2011), and LRRK2 (Haebig et al., 2010) that is a common cause of familial and sporadic Parkinson's disease (Zimprich et al., 2004). Genetic studies have also described association of other Rac/Cdc42 GEF genes in neuropsychiatric disorders: *ARHGEF6* gene identified in patients with X-linked mental retardation (Ramakers et al., 2012), *KALRN* gene associated with adult ADHD and schizophrenia (Kushima et al., 2012; Youn et al., 2007), and *Tiam1* gene involved in Alzheimer's disease pathology by activating and recruiting amyloid beta peptide (Aβ) (Ma et al., 2008; Mendoza-Naranjo et al., 2007). Therefore, performing

additional behavioral experiments, including olfaction, stereotypes, social interaction and vocalization, will further highlight the notion that synaptic signaling cascades of neuronal βPix isoforms are involved in pathophysiological mechanisms underlying specific neuropsychiatric diseases.

There is a point in dispute that βPix, Kalirin-7 and Tiam1, the well-known Rho-family GEFs, share some similarities for their roles in synaptic transmission in the hippocampus (Blanco-Suarez et al., 2014; Xie et al., 2011). βPix has several unique features that may explain why these other Rac-GEFs are unable to fully compensate for loss of neuronal βPix isoforms. Particularly, βPix interacts with Pak and Git and thereby constitutes putative positive feedback loop. This feature suggests temporally explosive all-or-none activation of its GEF activity as well as tight spatial regulation of βPix-dependent signaling (Tolias et al., 2011). However, these ideas cannot fully account for how βPix differs from the other GEFs. Future studies on the circuit formation, behavioral characterization and neurochemical mapping using each Rho-family GEF KO mouse line will help clarify both shared and distinct roles of the GEFs in synaptic signaling pathways.

In conclusion, our present study further advanced the previous researches that focused on the βPix function in neuronal structures and synapse formation shown *in vitro* models. We found that βPix heterozygous mice had defects in neuronal structures and synapse, and were severe enough to affect social behaviors. Although it is difficult for βPix heterozygous mice to directly associate abnormal behavior with certain patient symptoms, our study on structural and behavioral defects resulting from βPix deficiency suggest convincing evidences of a relationship between βPix and neurological diseases. Thus, additional behavioral and electrophysiological

analysis for βPix heterozygous mice will help to gain an exact understanding of synaptic development and function, further suggesting βPix as a potential treatment target for future neuropsychiatric studies. Furthermore, we examined the structural, functional and behavioral consequences resulting from the loss of neuronal βPix isoforms and characterized their roles in hippocampus. Our results provide, for the first time, neurobiological insights on how loss of neuronal βPix isoforms leads to morphological and synaptic defects, and relevant behavior abnormalities. The neuronal βPix isoform KO mouse line will serve as a valuable model for understanding synaptic malfunctions and human psychiatric disorders. An in-depth study of neural circuits in various brain regions that have the complete absence of βPix-b and βPix-d will shed light on the detailed molecular mechanisms of synapse development for βPix-b and βPix-d, and could unveil the pathophysiological mechanisms by which their dysfunctions contribute to the behavioral and cognitive deficits in related neuropsychiatric conditions.

CHAPTER II

Studies on the role of βPix-d in microtubule stabilization and neurite outgrowth

Abstract

Microtubules are one of the major cytoskeletal components of neurites including axons and dendrites. The regulation of microtubule stability is important for appropriate neurite morphogenesis during neuronal development, which in turn is critical for establishment of functional neuronal connections. βPix is a GEF for Rac1 and Cdc42 small GTPases that play a role in diverse cellular functions by modulating organizations of actin filaments and microtubules. By alternative splicing, βPix has a ubiquitous isoform, βPix-a, and neuronal isoforms, βPix-b and βPix-d. In neurons, βPix-b plays a role in dendritic spine morphogenesis that mainly involves reorganizations of actin filaments, but the neuronal role of βPix-d has not been revealed. In addition, the role of neuronal βPix isoforms during neurite outgrowth is not well understood. Here, we unveil a novel mechanism for βPix-d to regulate microtubule stabilization and neurite outgrowth. At DIV4, hippocampal neurons cultured from neuronal βPix isoform KO mice show defects in neurite length and complexity, and microtubule stability. Treatment of taxol that stabilizes microtubules alleviates the impairment of neurite morphology and microtubule stability in the neuronal βPix isoform KO neurons. Neuronal βPix isoforms increase microtubule stability and βPix-d stabilizes microtubules more than βPix-b. We also find the localization of βPix-d on microtubules. In addition, the neuronal βPix isoform KO neurons have a deficit in phosphorylation level of Stathmin1, a microtubule severing protein, at Ser16. Neuronal βPix isoforms recover the impairments of neurite morphology and phosphorylation level in Stathmin1 shown in the neuronal βPix isoform KO neurons and the levels of those recoveries are greater in expression of

βPix-d than βPix-b. Furthermore, those recoveries by βPix-d in the neuronal βPix isoform KO neurons are not observed by inhibition of PAK1 activity that phosphorylates Stathmin1 at Ser16. Taken together, our present study show that βPix-d stabilizes microtubules and phosphorylates Stathmin1 at Ser16 with PAK1 more than βPix-b, and is consequently involved in neurite morphogenesis.

Introduction

Nervous system development requires proper neuronal morphogenesis. During the neuronal morphogenesis, the formation and outgrowth of neurites require coordinated and dynamic reorganization of actin filaments and microtubules (Poulain and Sobel, 2010). Microtubules are one of the major cytoskeletal components of neurites (Kapitein and Hoogenraad, 2015) and can be both stable and dynamic, controlled by numerous regulators (Baas et al., 2016; Poulain and Sobel, 2010). Microtubule stability is required for neuronal structure and vary in different regions of a neuron during the neuronal morphogenesis (Song and Brady, 2015). Furthermore, impairments of microtubule stability are observed in diverse neurological disease. Reduced microtubule stability has been observed in several neurodegenerative diseases such as AD, Parkinson's disease and amyotrophic lateral sclerosis whereas hyperstable microtubules has been observed in hereditary spastic paraplegia (Dubey et al., 2015).

One of the major factors regulating microtubule stability, Stathmin is a cytosolic phosphoprotein that has been identified as a microtubule-destabilizing factor. Stathmin destabilizes the microtubule in two distinct ways, by sequestering α- and β-Tubulin heterodimers and by promoting microtubule catastrophe (Cassimeris, 2002; Grenningloh et al., 2004). The microtubule-destabilizing activity of Stathmin is suppressed by phosphorylation on four serine (Ser) sites (Ser16, Ser25, Ser38 and Ser63). When Stathmin is phosphorylated, it releases tubulin dimers leading to microtubule assembly (Di Paolo et al., 1997; Larsson et al., 1997). PAK1, which is well known as a βPix interactor (Manser et al., 1998), phosphorylates Stathmin at

Ser16 (Daub et al., 2001). Although phosphorylation of Stathmin at all Ser residues are important for inactivation of its depolymerization activity (Lawler, 1998; Melander Gradin et al., 1997), phosphorylation of Ser16 or Ser63 appears to be more critical than phosphorylation of Ser25 and Ser38 for the ability of Stathmin to bind to soluble tubulin and to inhibit microtubule assembly *in vitro* (Di Paolo et al., 1997; Larsson et al., 1997; Manna et al., 2009). In neurons, Stathmin mediates the developments of axons (Watabe-Uchida et al., 2006) and dendrites (Ohkawa et al., 2007) by phosphorylation at Ser16.

βPix acts as a GEF that specifically activates Rho family GTPases, Rac1 and Cdc42 (Bagrodia et al., 1998; Koh et al., 2001) and binds to PAK1, an effector kinase of Rac1 and Cdc42 (Manser et al., 1994; Manser et al., 1998). In neurons, Rac1 and Cdc42 are involved in the neuronal morphogenesis regulating actin and microtubule dynamics (Luo, 2000) and several studies showed that βPix acts as an important regulator of dendritic spine and synapse morphogenesis (Park et al., 2003; Saneyoshi et al., 2008; Zhang et al., 2005). We previously identified alternatively spliced βPix isoforms, βPix-a, βPix-b and βPix-d (Kim and Park, 2001), and also found that βPix-b and βPix-d are expressed specifically in neurons (Kim et al., 2000). Most of the studies on the role of βPix in spine morphogenesis had focused on the ubiquitous βPix-a isoform, but recent reports from our group and others showed that βPix-b, which is one of the neuronal βPix isoforms, plays a role in dendritic spine morphogenesis (Llano et al., 2015; Shin et al., 2019). It is necessary to unveil the neuronal role of βPix-d that has not been identified so far and the involvement of neuronal βPix isoforms in neurite outgrowth.

Here, we demonstrate that βPix-d is involved in neurite outgrowth by increase in

microtubule stability. At DIV4, loss of neuronal βPix isoforms in cultured hippocampal cells results in reduced neurite length and complexity, and impaired microtubule stability. Treating the neuronal βPix KO cultures with paclitaxel (taxol) suppresses the defects in neuronal morphology and microtubule stability. Rescuing expression of neuronal βPix isoforms in the neuronal βPix isoform KO cultures recovers microtubule stability and neurite outgrowth, and the recovery level of βPix-d is greater than βPix-b. We also find the localization of βPix-d in microtubules. Phosphorylation of Stathmin1 at Ser16 is impaired in the neuronal βPix isoform KO neurons and the phosphorylation level is recovered by complementing expression of neuronal βPix isoforms. The expression of βPix-d recovered it more than that of βPix-b. When PAK inhibitory domain (PID) is expressed simultaneously with βPix-d, such recovery is not observed, supporting the requirement of PAK activity in the βPix-d-mediated Stathmin1 phosphorylation and regulation of neurite morphogenesis. Taken together, our data demonstrate that βPix-d is required for neurite outgrowth via microtubule stabilization and PAK1-induced phosphorylation of Stathmin1 at Ser16.

Results

1. Neurite length and branching are decreased in hippocampal neurons from neuronal βPix isoform KO mice at DIV4.

Neurite elongation and branching are key events during neuronal development, and Rac1 and Cdc42 small GTPases that are activated by βPix play an essential role in the neurite morphogenesis (Govek et al., 2005). To investigate the neurite morphology at the stage when the axonal and dendritic outgrowth proceeds, we cultured and analyzed morphology of hippocampal neurons from neuronal βPix isoform KO mice at DIV4, compared to WT mice. For analysis of the neurite morphology, we merged each of image stained with Tau antibody, an axonal marker and MAP2 antibody, a dendritic marker (Figure 40A). As a result of analysis, the neuronal βPix isoform KO neurons showed a decrease in the longest neurite length (Figure 40B) and total neurite length per neuron (Figure 40C), compared to the WT neurons. For neuronal complexity, total branching number in the neuronal βPix isoform KO neurons was less than in the WT neurons (Figure 40D). By Sholl analysis, neurite complexity in the neuronal βPix isoform KO neurons appeared significantly simplified in 50-80 μm range and at 110 μm away from soma, compared to that in the WT neurons (Figure 40E). Specifically, axons, which are more enriched with long-lived stable microtubules compared to the dendrites (Yogev and Shen, 2017), were shorter in the neuronal βPix isoform KO neurons than in the WT neurons (Figure 41A). In the neuronal βPix isoform KO neurons, the ratio of axons shorter than 100 μm in length was higher and the ratio of those longer than 200 μm was lower than in the WT neurons (Figure 41B). The number of branching points in axons

Figure 40. Length and branching of neurites are decreased in hippocampal neurons from neuronal βPix isoform KO mice.

(A) Representative images of hippocampal neurons from WT and neuronal βPix isoform KO mice fixed at DIV4 and stained with Tau (green), MAP2 (red) and DAPI (blue). (B) The longest neurite length had 19% decrease in neuronal βPix isoform KO neurons, compared to WT neurons. (C) Total neurite length had 21% decrease in neuronal βPix isoform KO neurons, compared to WT neurons. (D) Total branching number had 25% decrease in neuronal βPix isoform KO neurons, compared to WT neurons. (E) Sholl analysis revealed simplified dendritic arborizations of neuronal βPix isoform KO neurons, compared to WT neurons. 53-58 neurons were analyzed in each group from 3 independent cultures.

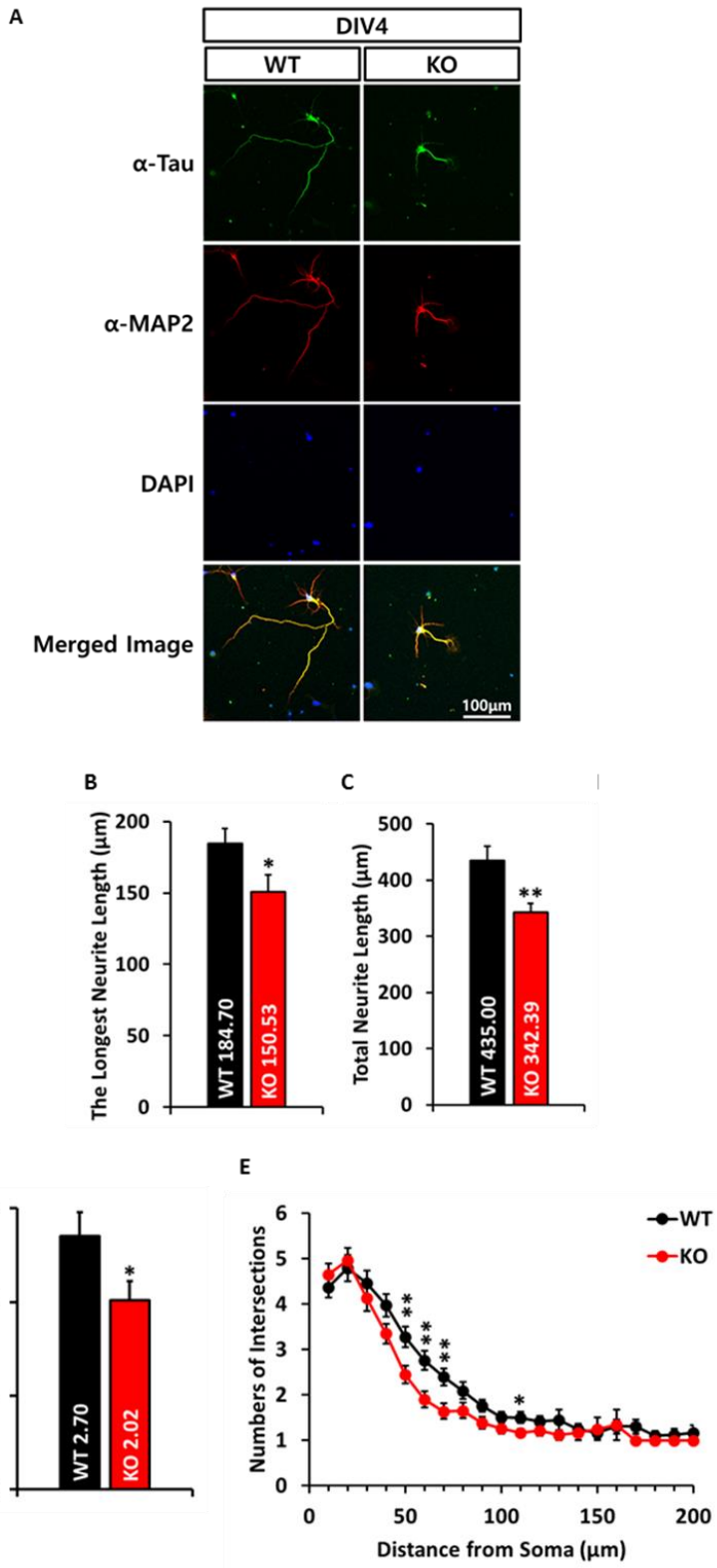
A
DIV4
WT
KO
α-Tau
α-MAP2
DAPI
Merged Image
100μm
B
The Longest Neurite Length (μm)
200
150
100
50
0
WT 184.70
KO 150.53
*
C
Total Neurite Length (μm)
500
400
300
200
100
0
WT 435.00
KO 342.39
**
D
Total Branching Number
3
2
1
0
WT 2.70
KO 2.02
*
E
Numbers of Intersections
6
5
4
3
2
1
0
WT
KO
**
**
**
*
0
50
100
150
200
Distance from Soma (μm)

Figure 41. Length and branching of axons are decreased in hippocampal neurons from neuronal βPix isoform KO mice.

(A) Average axon length per neuron had 31% decrease in neuronal βPix isoform KO neurons, compared to WT neurons. (B) Hippocampal neurons from neuronal βPix isoform KO mice had more axons with a length of 100 μm or less and fewer axons with a length of above 200 μm than those from WT mice. (C) Number of branching points in axon had 41% decrease in neuronal βPix isoform KO neurons, compared to WT neurons. (D) There are no changes in axon number of hippocampal neurons from WT and neuronal βPix isoform KO mice. 162-195 axons were analyzed in each group from 3 independent cultures.

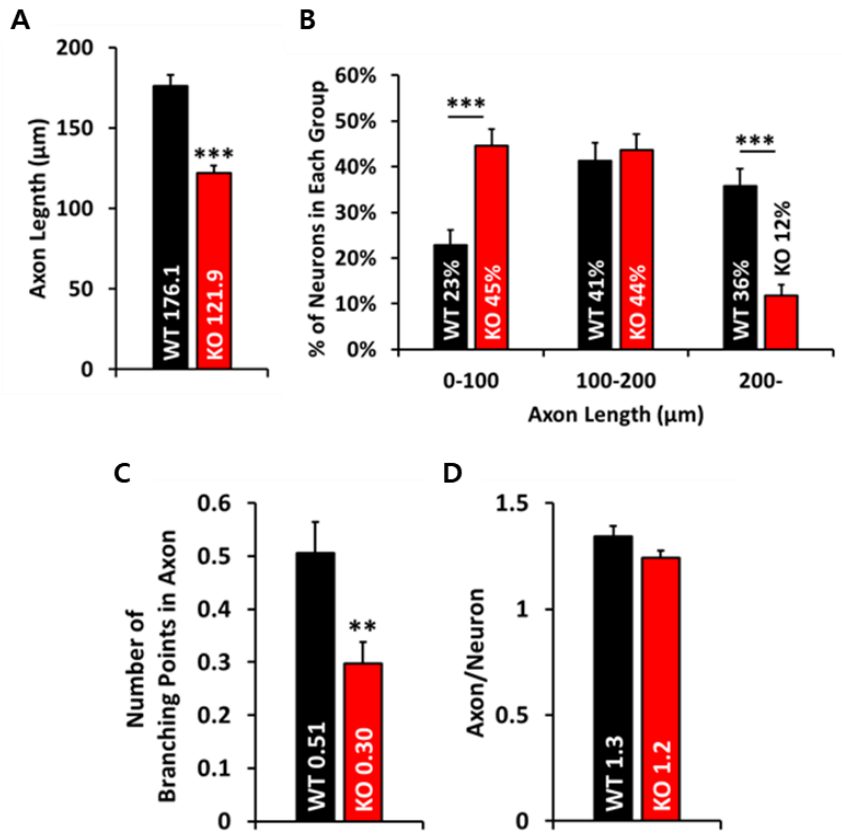
A
Axon Legnth (μm)
200
150
100
50
0
WT 176.1
KO 121.9
***
B
% of Neurons in Each Group
60%
50%
40%
30%
20%
10%
0%
WT 23%
KO 45%
WT 41%
KO 44%
WT 36%
KO 12%
***
***
0-100
100-200
200-
Axon Length (μm)
C
Number of Branching Points in Axon
0.6
0.5
0.4
0.3
0.2
0.1
0
WT 0.51
KO 0.30
**
D
Axon/Neuron
1.5
1
0.5
0
WT 1.3
KO 1.2

extending from the neuronal βPix isoform KO neurons was less than the WT neurons (Figure 41C). But, there was no change in axon number between the neurons from WT and neuronal βPix isoform KO mice (Figure 41D). Our data showed that the neurite morphology in the neuronal βPix isoform KO neurons have defects during the stage where outgrowth of axons and dendrites is prominent.

2. Microtubule stability is decreased in the longest neurite extending from hippocampal neurons from neuronal βPix isoform KO mice.

In the developing neurites, microtubules coalesce together to form bundles which construct the core of neurite and are more stable, with stability increasing as neurons grow and become polarized (Flynn, 2013). To examine the stability of microtubules in neurites extending from hippocampal neurons from WT and neuronal βPix isoform KO mice, we stained the neurons at DIV4 with acetylated α-Tubulin (Acet. Tub.) antibody for stable microtubule and tyrosinated α-Tubulin (Tyr. Tub.) antibody for dynamic microtubule (Figure 42A). We straightened the microscopic image of the longest neurite and analyzed the distribution of fluorescence intensity in it (Figure 42B). Along the longest neurite, the average ratio of Acet. Tub. to Tyr. Tub. (Acet. Tub./Tyr. Tub.) was lower in the neuronal βPix isoform KO neurons than in the WT neurons (Figure 42C). We found that the Acet. Tub./Tyr. Tub. ratio in the neuronal βPix isoform KO neurons was significantly reduced along the neurite (significant regions of $P < 0.01$ highlighted in yellow in Figure 42D). The mean level of Acet. Tub. in the longest neurite from the neuronal βPix isoform KO neurons was decreased, compared to the WT neurons (Figure 42E). Significant reduction in Acet. Tub. level was also found along the longest neurite (significant regions of $P < 0.01$

Figure 42. Microtubule stabilization is decreased in the longest neurite of hippocampal neurons from neuronal βPix isoform KO mice.

(A) Representative images of hippocampal neurons from WT and neuronal βPix isoform KO mice fixed at DIV4 and stained with Acet. Tub. (red) and Tyr. Tub. (green). White dashed lines indicated the longest neurite of the neuron in each group and are straightened in (B). (B) The longest neurite of hippocampal neurons from WT and neuronal βPix isoform KO mice shown in (A) were straightened by ImageJ software. (C) In the longest neurite, ratio of Acet. Tub. to Tyr. Tub. had 72% decrease in hippocampal neurons from neuronal βPix isoform KO mice, compared to those from WT mice. (D) The distribution graph showed that the ratio of Acet. Tub. to Tyr. Tub. had decrease along the longest neurite extending from neuronal βPix isoform KO neurons, compared to that from WT neurons. (E) In the longest neurite, Acet. Tub. had 68% decrease in hippocampal neurons from neuronal βPix isoform KO mice, compared to those from WT mice. (F) The distribution graph showed that Acet. Tub. had decrease along the longest neurite extending from neuronal βPix isoform KO neurons, compared to that from WT neurons. (G) In the longest neurite, Tyr. Tub. Had 1.1-fold increase in hippocampal neurons from neuronal βPix isoform KO mice, compared to those from WT mice. (H) The distribution graph showed that Tyr. Tub. had partial increase along the longest neurite extending from neuronal βPix isoform KO neurons, compared to that from WT neurons. 23-39 neurons were analyzed in each group from 3 independent cultures.

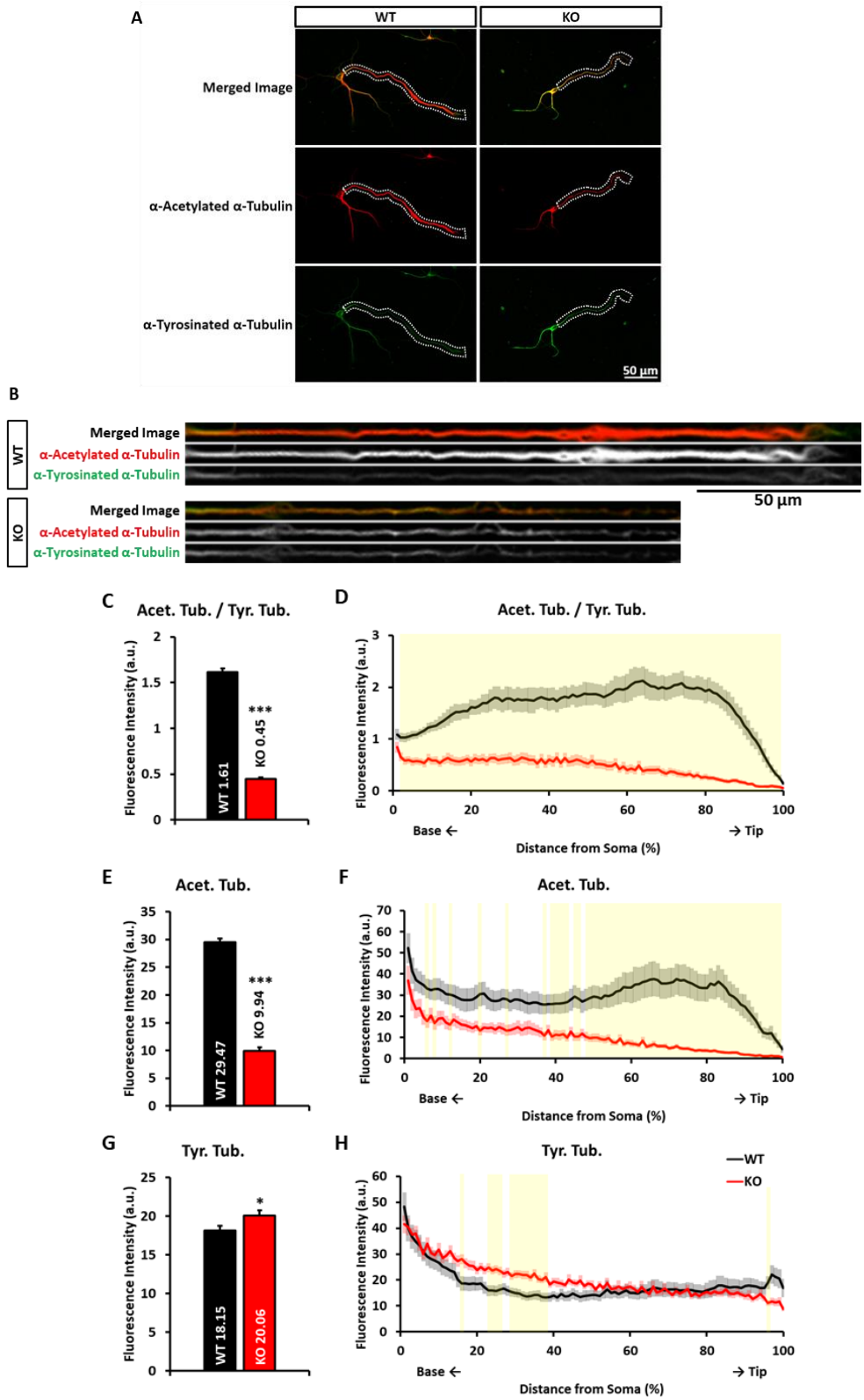
A
WT
KO
Merged Image
α-Acetylated α-Tubulin
α-Tyrosinated α-Tubulin
50 µm
B
WT
KO
Merged Image
α-Acetylated α-Tubulin
α-Tyrosinated α-Tubulin
50 µm
C
Acet. Tub. / Tyr. Tub.
Fluorescence Intensity (a.u.)
WT 1.61
KO 0.45
***
D
Acet. Tub. / Tyr. Tub.
Fluorescence Intensity (a.u.)
Base ←
→ Tip
Distance from Soma (%)
E
Acet. Tub.
Fluorescence Intensity (a.u.)
WT 29.47
KO 9.94
***
F
Acet. Tub.
Fluorescence Intensity (a.u.)
Base ←
→ Tip
Distance from Soma (%)
G
Tyr. Tub.
Fluorescence Intensity (a.u.)
WT 18.15
KO 20.06
*
H
Tyr. Tub.
WT
KO
Fluorescence Intensity (a.u.)
Base ←
→ Tip
Distance from Soma (%)

highlighted in yellow in Figure 42F). On the other hand, the mean level of Tyr. Tub. in the longest neurite from the neuronal βPix isoform KO neurons was increased, compared to the WT neurons (Figure 42G). Partially, significant increment in Tyr. Tub. level was found along the neurite (significant regions of $P < 0.01$ highlighted in yellow in Figure 42H). Hence, our data showed that neuronal βPix isoform KO neurons had decrease in microtubule stabilization, indicating that neuronal βPix isoforms are required for microtubule stability in hippocampal neurons.

3. Recovery of microtubule stability by taxol rescues the impaired neurite morphology in hippocampal neurons from neuronal βPix isoform KO mice.

Defects in neurite outgrowth are often accompanied by dysregulation of microtubule stability, indicating that the precise regulation of microtubule stability is essential for neurite development (Baas et al., 2016). We hypothesized that the neuronal morphology defects observed in the neuronal βPix isoform KO neurons were caused by impaired microtubule stability. To test this hypothesis, we treated WT and neuronal βPix isoform KO hippocampal cultures with a microtubule-stabilizing reagent, taxol at DIV1 and incubated for 72 hours (Figure 43A). With taxol treatment, Acet. Tub. was increased in the longest neurite extending from both the WT and the neuronal βPix isoform KO neurons (Figure 43B and 43C), indicating that taxol was effective enough to promote the microtubule stability. When we assessed the neuronal morphology, we observed no change in neurite morphology of the WT neurons by taxol (Figure 43D-43G), but the changes in neuronal morphology occurred only in the neuronal βPix isoform KO neurons. The defects in the longest neurite length and total neurite length observed in the neuronal βPix isoform KO

Figure 43. Impaired neurite morphology in hippocampal neurons from neuronal βPix isoform KO mice is recovered by microtubule stabilization.

(A) Representative images of hippocampal neurons from WT and neuronal βPix isoform KO mice treated with 0.2% DMSO or 4 nM Taxol at DIV1, fixed at DIV4 and stained with Acet. Tub. (red), Tyr. Tub. (green) and DAPI (blue). (B) Taxol recovered Acet. Tub. in the longest neurite extending from WT and neuronal βPix isoform KO neurons. (C) The distribution graph showed that Acet. Tub. was recovered by taxol along the longest neurite extending from WT and neuronal βPix isoform KO neurons. (D) The recovery in the longest neurite length by taxol was shown in neuronal βPix isoform KO neurons, not in WT neurons. (E) The recovery in total neurite length by taxol was shown in neuronal βPix isoform KO neurons, not in WT neurons. (F) Taxol does not recover total branching number in WT and neuronal βPix isoform KO neurons. (G) By Sholl analysis, taxol recovers neurite complexity of neuronal βPix isoform KO neurons, not that of WT neurons. 27-33 neurons were analyzed in each group from 3 independent cultures. In (B) and (D)-(F), * $P < 0.05$ and *** $P < 0.001$, and in (G), * $P < 0.05$ for a comparison of WT+DMSO and KO+DMSO, # $P < 0.05$ and ## $P < 0.01$ for a comparison of KO+DMSO and KO+Taxol and + $P < 0.05$ and ++ $P < 0.01$ for a comparison of WT+Taxol and KO+Taxol by student's t-test.

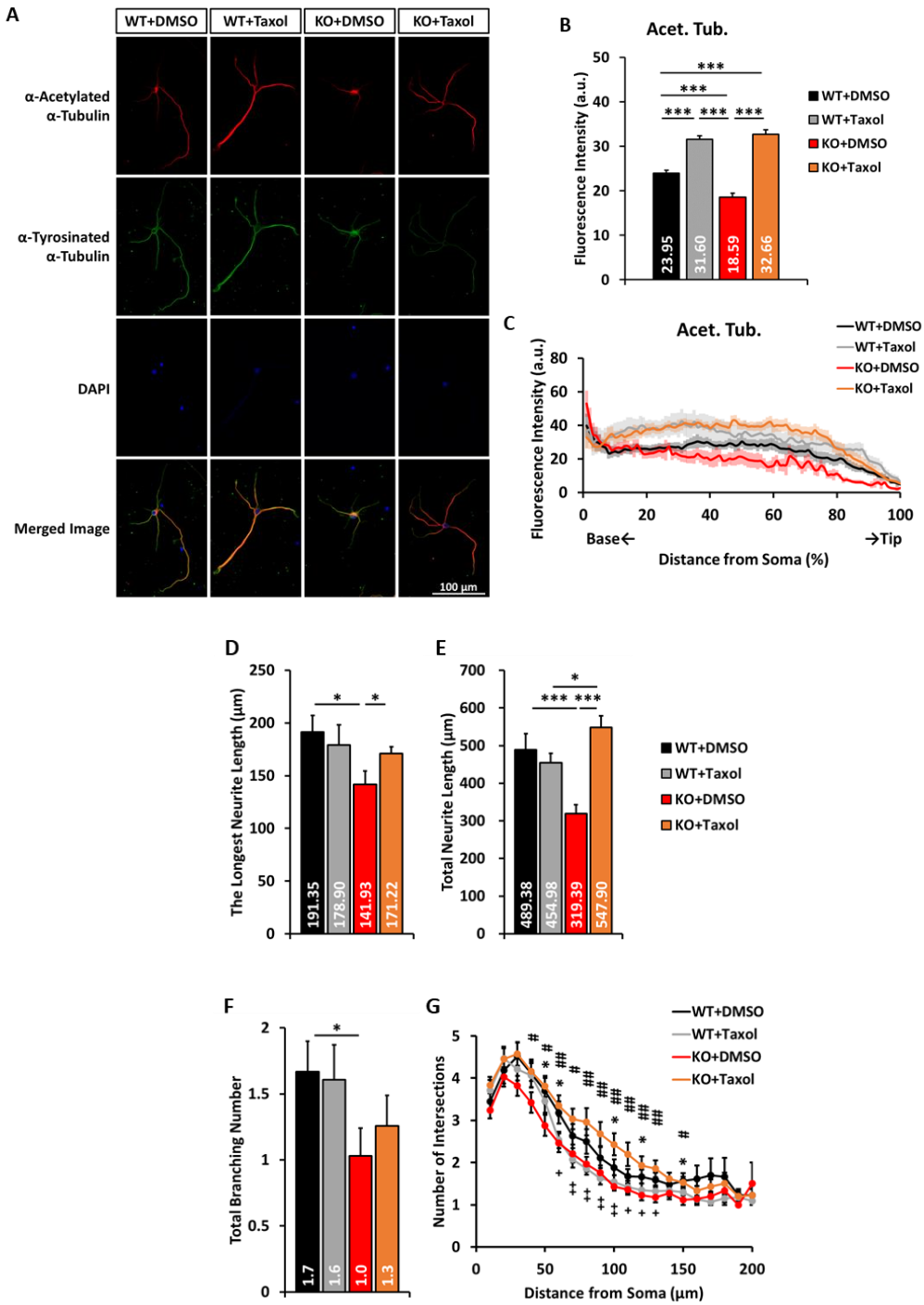
A
WT+DMSO
WT+Taxol
KO+DMSO
KO+Taxol
α-Acetylated α-Tubulin
α-Tyrosinated α-Tubulin
DAPI
Merged Image
100 μm
B
Acet. Tub.
Fluorescence Intensity (a.u.)
***
23.95
31.60
18.59
32.66
C
Acet. Tub.
Fluorescence Intensity (a.u.)
Base←
→Tip
Distance from Soma (%)
D
The Longest Neurite Length (μm)
191.35
178.90
141.93
171.22
E
Total Neurite Length (μm)
489.38
454.98
319.39
547.90
F
Total Branching Number
1.7
1.6
1.0
1.3
G
Number of Intersections
Distance from Soma (μm)

neurons were completely rescued by the taxol treatment (Figure 43D and 43E). The defects in total branching number observed in the neuronal βPix isoform KO neurons was not affected by the taxol (Figure 43F), but the impaired neuronal complexity by Sholl analysis was recovered (Figure 43G). We suggest that microtubule stability in the WT neurons was enough to develop normal neurite outgrowth, resulting in taxol increased microtubule stability but did not cause neurite outgrowth in the WT neurons. On the other hand, in case of the neuronal βPix isoform KO neurons, decrease in microtubule stability caused defects in neurite outgrowth, so recovery of defect in microtubule stability by taxol rescued abnormal neurite outgrowth. Taken together, we suggest that the defects in neuronal morphology observed in the neuronal βPix isoform KO neurons result from decreased microtubule stabilization and neuronal βPix isoforms are essential for microtubule stabilization.

4. βPix-d is required for microtubule stabilization.

To identify the relationship between βPix isoforms and microtubule stabilization, we transfected hippocampal neurons from neuronal βPix isoform KO mice at DIV3 with GFP, GFP-βPix-a, GFP-βPix-b or GFP-βPix-d, and performed Western blotting at DIV4 (Figure 44A). Quantitatively, expression of GFP-βPix-a did not affect the level of Acet. Tub., but expression of GFP-βPix-b or GFP-βPix-d caused increase in the level of Acet. Tub. (Figure 44B). Specifically, the increase by GFP-βPix-d was significantly greater than by GFP-βPix-b (Figure 44B). There was no difference in the level of Tyr. Tub. by transfection with GFP-βPix-a, GFP-βPix-b or GFP-βPix-d, compared with control vector (Figure 44C). To ensure the role of βPix-b or βPix-d in microtubule stabilization, we transfected the neuronal βPix isoform KO neurons

Figure 44. βPix-b and βPix-d increase tubulin acetylation.

(A) Representative blots for the level of Acet. Tub. and Tyr. Tub. in hippocampal neurons from neuronal βPix isoform KO mice transfected with GFP, GFP-βPix-a, GFP-βPix-b or GFP-βPix-d at DIV3 and identified at DIV4. (B) Quantification of relative expression levels for (A) as normalized to α-Tubulin expression. GFP-βPix-b or GFP-βPix-d significantly increased the level of Acet. Tub. and GFP-βPix-d more increased it than GFP-βPix-b. (C) Quantification of relative expression levels for (A) as normalized to α-Tubulin expression. There was no significant difference in the level of Tyr. Tub. among expression of GFP-βPix-a, GFP-βPix-b or GFP-βPix-d in neuronal βPix isoform KO neurons. Data are representative of 5 independent experiments.

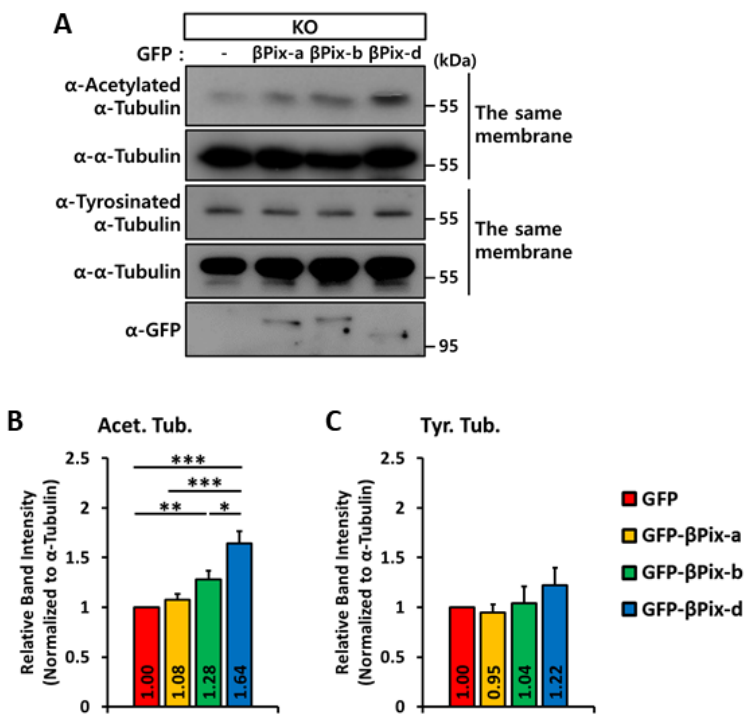
A
KO
GFP : - βPix-a βPix-b βPix-d
(kDa)
α-Acetylated α-Tubulin
55
The same membrane
α-α-Tubulin
55
α-Tyrosinated α-Tubulin
55
The same membrane
α-α-Tubulin
55
α-GFP
95
B
Acet. Tub.
Relative Band Intensity (Normalized to α-Tubulin)
2.5
2
1.5
1
0.5
0
***
***
**
*
1.00
1.08
1.28
1.64
C
Tyr. Tub.
Relative Band Intensity (Normalized to α-Tubulin)
2.5
2
1.5
1
0.5
0
1.00
0.95
1.04
1.22
GFP
GFP-βPix-a
GFP-βPix-b
GFP-βPix-d

at DIV3 with GFP, GFP-βPix-b or GFP-βPix-d and stained with Acet. Tub. antibody and Tyr. Tub. antibody at DIV4 (Figure 45A). We straightened the microscopic image of the longest neurite and analyzed the distribution of fluorescence intensity (Figure 45B). In the neuronal βPix isoform KO neurons transfected with GFP-βPix-b or GFP-βPix-d, the mean level of Acet. Tub./Tyr. Tub. ratio was increased, compared with GFP (Figure 45C). In the distribution graph, we observed the higher ratio along the longest neurite from the neuronal βPix isoform KO neurons transfected with GFP-βPix-b or GFP-βPix-d than with GFP (significant regions of $P < 0.01$ highlighted in pink and yellow in Figure 45D). Intriguingly, for the Acet. Tub./Tyr. Tub. ratio, significant change is observed in 5% section of the longest neurite length between GFP and GFP-βPix-b, and 71% section of the longest neurite length between GFP and GFP-βPix-d, suggesting that the effect of βPix-d was greater than βPix-b. Like the results from Western blotting, the mean level of Acet. Tub. was increased by GFP-βPix-b or GFP-βPix-d in the neuronal βPix isoform KO neurons, compared to GFP, and GFP-βPix-d affected more the level of Acet. Tub. than GFP-βPix-b (Figure 45E). The same result was found in the distribution graph for the level of Acet. Tub. along the longest neurite. Of the longest neurite, significant change is 16% section for a comparison of GFP and GFP-βPix-b and 81% section for a comparison of GFP and GFP-βPix-d (significant regions of $P < 0.01$ highlighted in pink and yellow in Figure 45F). GFP-βPix-b or GFP-βPix-d increased the mean level of Tyr. Tub in the neuronal βPix isoform KO neurons (Figure 45G), but in the distribution graph, significant change was not observed in the longest neurite of the neuronal βPix isoform KO neurons expressed GFP-βPix-b, compared to GFP (Figure 45H). In GFP-βPix-d expression, there is a significant change in 10% section of the

Figure 45. βPix-b and βPix-d are required for microtubule stabilization in the longest neurite.

(A) Representative images of hippocampal neurons from βPix isoform KO mice transfected with GFP, GFP-βPix-b or GFP-βPix-d at DIV3, fixed at DIV4 and stained with Acet. Tub. (red) and Tyr. Tub. (blue). White dashed lines indicated the longest neurite of the neuron in each group and were straightened in (B). (B) The longest neurite of the neuronal βPix isoform KO neurons transfected with GFP, GFP-βPix-b or GFP-βPix-d shown in Fig. 4D was straightened by ImageJ software. (C) In the longest neurite, ratio of Acet. Tub. to Tyr. Tub. had 1.2-fold increase by GFP-βPix-b and 1.5-fold increase by GFP-βPix-d in neuronal βPix isoform KO neurons, compared to those transfected with GFP. (D) The distribution graph showed that ratio of Acet. Tub. to Tyr. Tub. had increase by GFP-βPix-b or GFP-βPix-d along the longest neurite extending from neuronal βPix isoform KO neurons, compared to those transfected with GFP. (E) In the longest neurite, Acet. Tub. had 1.3-fold increase by GFP-βPix-b and 1.9-fold increase by GFP-βPix-d in neuronal βPix isoform KO neurons, compared to those transfected with GFP. (F) The distribution graph showed that Acet. Tub. had increase by GFP-βPix-b and GFP-βPix-d along the longest neurite extending from the neuronal βPix isoform KO neurons, compared to those transfected with GFP. (G) In the longest neurite, Tyr. Tub. had 1.1-fold increase by GFP-βPix-b and 1.3-fold increase by GFP-βPix-d in neuronal βPix isoform KO neurons, compared to those transfected with GFP. (H) The distribution graph showed that there had no significant change by GFP-βPix-b or GFP-βPix-d along the longest neurite extending from neuronal βPix isoform KO neurons, compared to those transfected with GFP. 61-82 neurons were analyzed in each group

from 3 independent cultures for (C)-(H). For a comparison among hippocampal neurons from neuronal βPix isoform KO mice transfected with GFP, GFP-βPix-b and GFP-βPix-d by student's t-test, * $P < 0.05$, ** $P < 0.01$ and *** $P < 0.001$ for (C), (E) and (G). Pink boxes in (D) and (F) indicate $P < 0.01$ for a comparison of GFP and GFP-βPix-b and Yellow boxes in (D), (F) and (H) indicated $P < 0.01$ for a comparison of GFP and GFP-βPix-d.

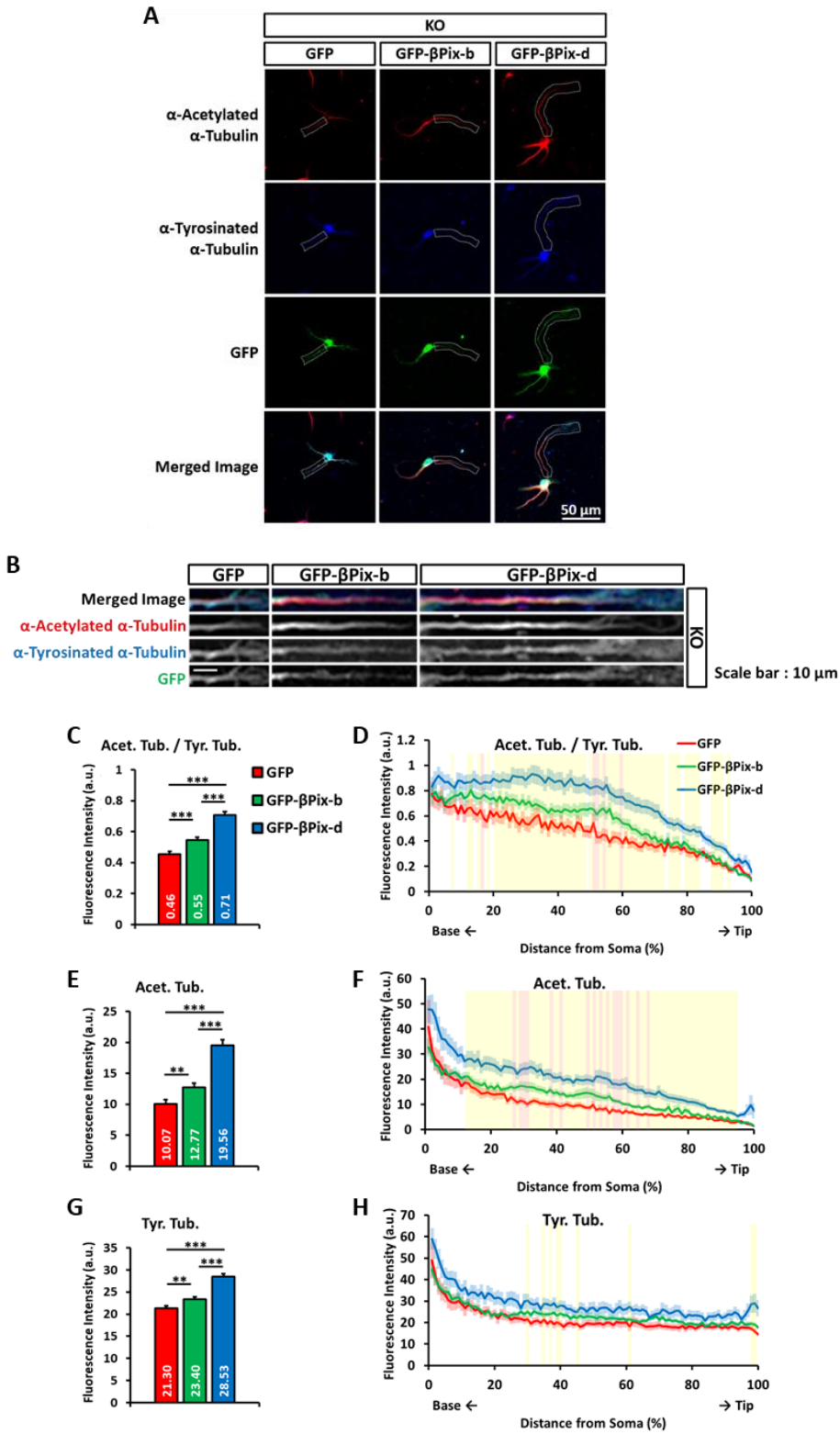
A
KO
GFP
GFP-βPix-b
GFP-βPix-d
α-Acetylated α-Tubulin
α-Tyrosinated α-Tubulin
GFP
Merged Image
50 μm
B
GFP
GFP-βPix-b
GFP-βPix-d
Merged Image
α-Acetylated α-Tubulin
α-Tyrosinated α-Tubulin
GFP
KO
Scale bar : 10 μm
C
Acet. Tub. / Tyr. Tub.
Fluorescence Intensity (a.u.)
GFP
GFP-βPix-b
GFP-βPix-d
0.46
0.55
0.71
D
Acet. Tub. / Tyr. Tub.
Fluorescence Intensity (a.u.)
Base ←
→ Tip
Distance from Soma (%)
E
Acet. Tub.
10.07
12.77
19.56
F
Acet. Tub.
G
Tyr. Tub.
21.30
23.40
28.53
H
Tyr. Tub.

longest neurite, compared with GFP expression (significant regions of $P < 0.01$ highlighted in yellow in Figure 45H). Taken together, these data indicate that neuronal βPix isoforms enhance microtubule stability and furthermore βPix-d more stabilizes microtubules than βPix-b.

5. βPix-d is co-localized with microtubule.

Our previous study showed that βPix-b is localized in dendritic spine that are enriched in F-actin (Shin et al., 2019) and the localization of βPix-d in neurons has not been revealed. As performed in our previous study (Shin et al., 2019), we co-transfected with GFP-βPix-b or GFP-βPix-d and DsRed in hippocampal neurons from neuronal βPix isoform KO mice at DIV7 and identified the localization of GFP-βPix-b or GFP-βPix-d in overall neuronal structure at DIV14 when dendritic spines are observed (Figure 33). In line with our previous study, GFP-βPix-b was localized in dendritic spine, but GFP-βPix-d was localized in not only dendritic spine but also dendritic shaft. F-actin was rich at the dendritic spine, whereas microtubules were distributed throughout the dendritic shaft. Furthermore, we found that endogenous βPix-d stained with 11 a.a. antibody existed in linear patterns in the neurites at DIV14 (Figure 34), suggesting that βPix-d correlates with microtubules.

We next set out to test whether βPix-d co-localizes with cytoskeleton including microtubules or F-actin. We labeled F-actin and neuronal microtubules in hippocampal neurons from WT mice with phalloidin and β3-Tubulin antibody, respectively, and compared their localization patterns with βPix-d (Figure 46A). As mentioned above, we straightened and analyzed the fluorescence intensities along the longest neurite extending from the WT neurons (Figure 46B). Growth cones are

Figure 46. βPix-d is co-localized with microtubules at DIV4.

(A) Representative images of hippocampal neurons from WT mice fixed at DIV4 and stained with 11 a.a. antibody (green), β3-Tubulin (blue) and Phalloidin (red). White dashed lines indicated the longest neurite of the WT neurons and were straightened in (B). (B) The longest neurite extending from WT neurons shown in (A) was straightened by ImageJ software. (C) The distribution graph showed that βPix-d was co-localized with microtubule and not with F-actin. 21 neurons were analyzed from 3 independent cultures.

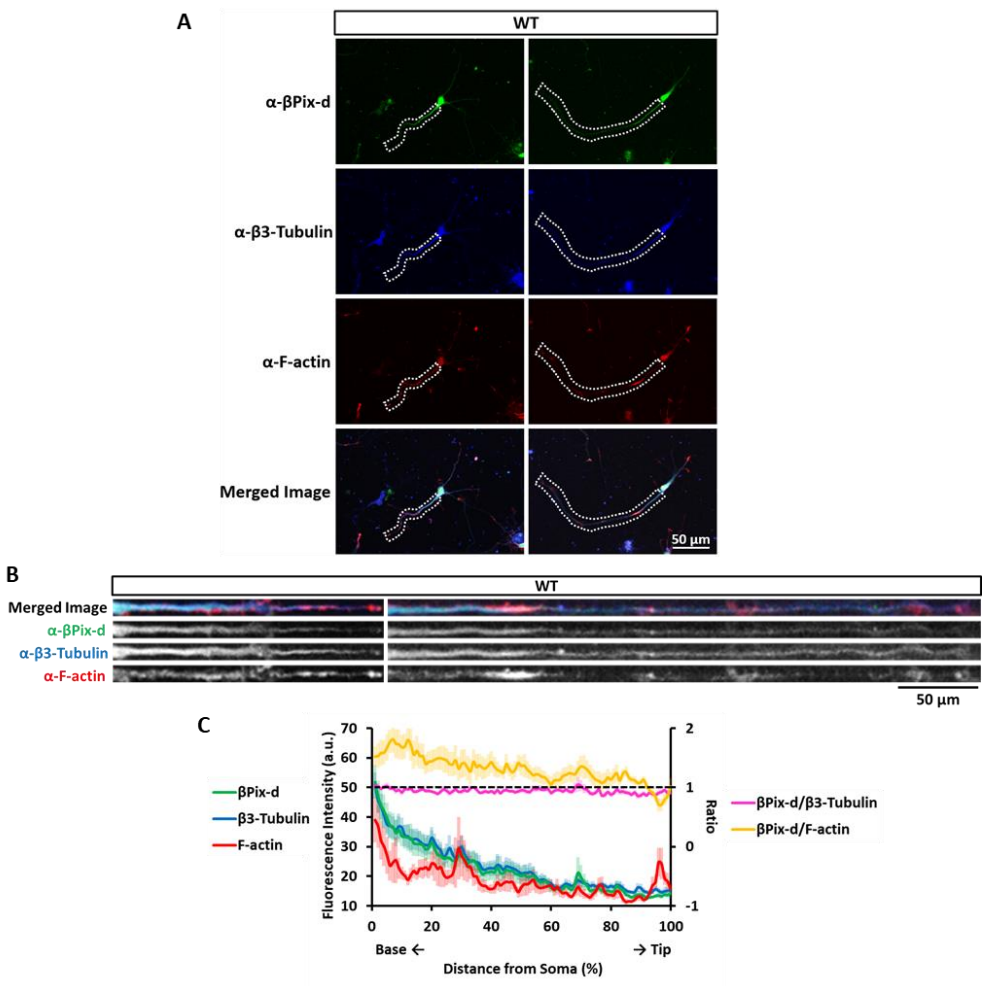
A
WT
α-βPix-d
α-β3-Tubulin
α-F-actin
Merged Image
50 μm
B
WT
Merged Image
α-βPix-d
α-β3-Tubulin
α-F-actin
50 μm
C
βPix-d
β3-Tubulin
F-actin
Fluorescence Intensity (a.u.)
70
60
50
40
30
20
10
0
20
40
60
80
100
Base ←
→ Tip
Distance from Soma (%)
2
1
0
-1
Ratio
βPix-d/β3-Tubulin
βPix-d/F-actin

motile structures at the tip of neurite and actin-rich compartments, and neurites are microtubule-rich compartments in neurons. Specifically, one of the major events of branched neurite formation is the initiation of actin filament based protrusion from the shaft of neurite (Lowery and Van Vactor, 2009). We found that F-actin was rich at the tip and the partial shaft of neurite whereas microtubules were distributed throughout the neurite (Figure 46C). Interestingly, distribution of βPix-d was similar to that of microtubules, not that of F-actin (Figure 46C). In addition, we identified the quantitative distribution of βPix-d in β3-Tubulin or F-actin through line graphs that showed the ratio of βPix-d to β3-Tubulin (βPix-d/β3-Tubulin) and βPix-d to F-actin (βPix-d/F-actin) along the longest neurite extending from the WT neurons (Figure 46C). The line graph for βPix-d/β3-Tubulin ratio remained constant at one, but the line graph showed fluctuation in the βPix-d/F-actin ratio, ensuring that βPix-d was co-localized in microtubules not in F-actin. During neuronal development, βPix-d was co-localized with β3-Tubulin (Figure 47) and *in vivo* data also showed that βPix-d was co-localized with β3-Tubulin (Figure 48). Taken together, we exhibited that βPix-d is associated with microtubules.

Furthermore, to identify whether βPix-d is associated with stable or dynamic microtubules, we co-stained WT neurons with 11 a.a. antibody and Tyr. Tub. or Acet. Tub., and analyzed those fluorescence intensities in the same way as mentioned above (Figure 49A and 49D). The distribution of βPix-d in the longest neurite was entirely consistent with that of Acet. Tub. (Figure 49B and 49C). In contrast, βPix-d was not co-localized with Tyr. Tub. that was rich in the section about 25% off the tip of the longest neurite (Figure 49E and 49F). Taken together, we suggest that βPix-d is closely related to stable microtubules.

Figure 47. βPix-d is co-localized with microtubules during neuronal development.

Representative images of hippocampal neurons from WT mice fixed at DIV3, DIV5 and DIV14 and stained with 11 a.a. antibody (green) and β3-Tubulin (blue). In all stages observed, βPix-d was co-localized with β3-Tubulin.

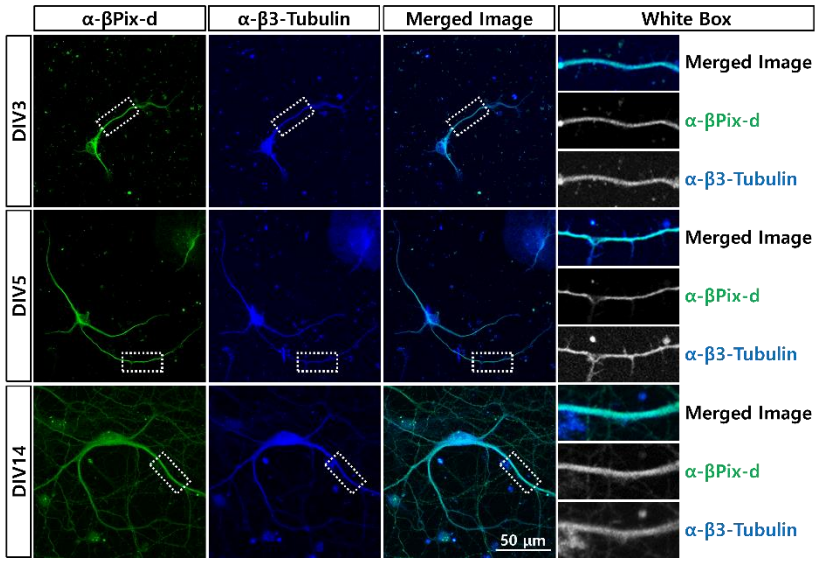
α-βPix-d
α-β3-Tubulin
Merged Image
White Box
DIV3
DIV5
DIV14
Merged Image
α-βPix-d
α-β3-Tubulin
Merged Image
α-βPix-d
α-β3-Tubulin
Merged Image
α-βPix-d
α-β3-Tubulin
50 μm

Figure 48. βPix-d is co-localized with microtubules *in vivo*.

Representative images of WT hippocampal CA1 region in 5 weeks mice stained with 11 a.a. antibody (red), β3-Tubulin (green) and DAPI (blue). The right panels showed higher magnifications of white dotted boxes in the left panels. White regions shown in co-localization analysis indicated the co-localization of βPix-d with β3-Tubulin.

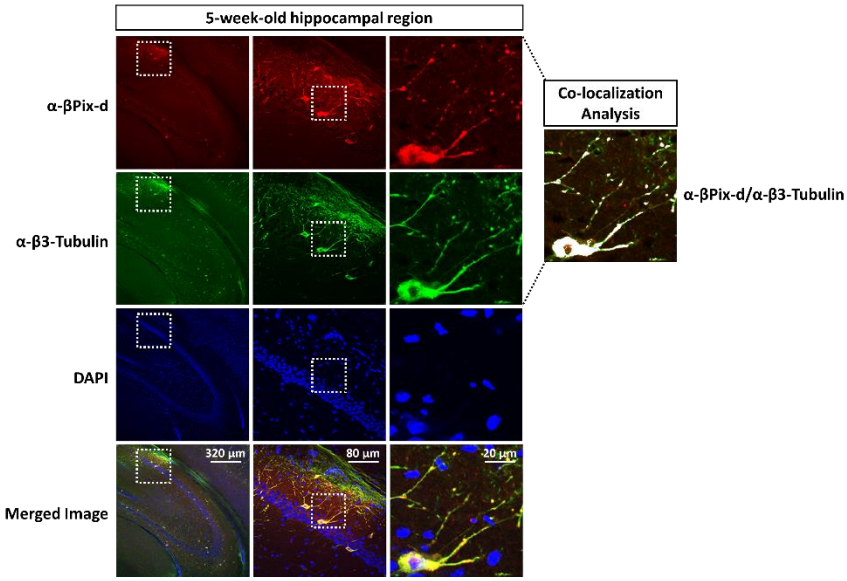
5-week-old hippocampal region
α-βPix-d
α-β3-Tubulin
DAPI
Merged Image
320 μm
80 μm
20 μm
Co-localization Analysis
α-βPix-d/α-β3-Tubulin

Figure 49. βPix-d is co-localized with stable microtubules.

(A) Representative images of hippocampal neurons from WT mice fixed at DIV4 and stained with 11 a.a. antibody (blue) and Acet. Tub. (green). The right panels showed higher magnifications of yellow dotted box in the left panels. The white dashed lines in the left panels indicated the longest neurite of WT neuron and were straightened in (B). The white dashed lines in the right panels were for 25% of the longest neurite length from the tip and distributions of fluorescence intensities in that region was shown in (C). (B) Straightened image for the white dashed lines in the left panels of (A). βPix-d was co-localized with Acet. Tub.. (C) βPix-d was co-localized with Acet. Tub. in 25% of the longest neurite length from the tip. (D) Representative images of hippocampal neurons from WT mice fixed at DIV4 and stained with 11 a.a. antibody (blue) and Tyr. Tub. (green). The right panels showed higher magnifications of yellow dotted box in the left panels. The white dashed lines in the left panels indicated the longest neurite of the neuron and were straightened in (E). The white dashed lines in the right panels were for 25% of the longest neurite length from the tip and distributions of fluorescence intensities in that region was shown in (F). (E) Straightened image for the white dashed lines in the left panels of (D). βPix-d was partially co-localized with Tyr. Tub.. (F) βPix-d was not co-localized with Tyr. Tub. in 25% of the longest neurite length from the tip.

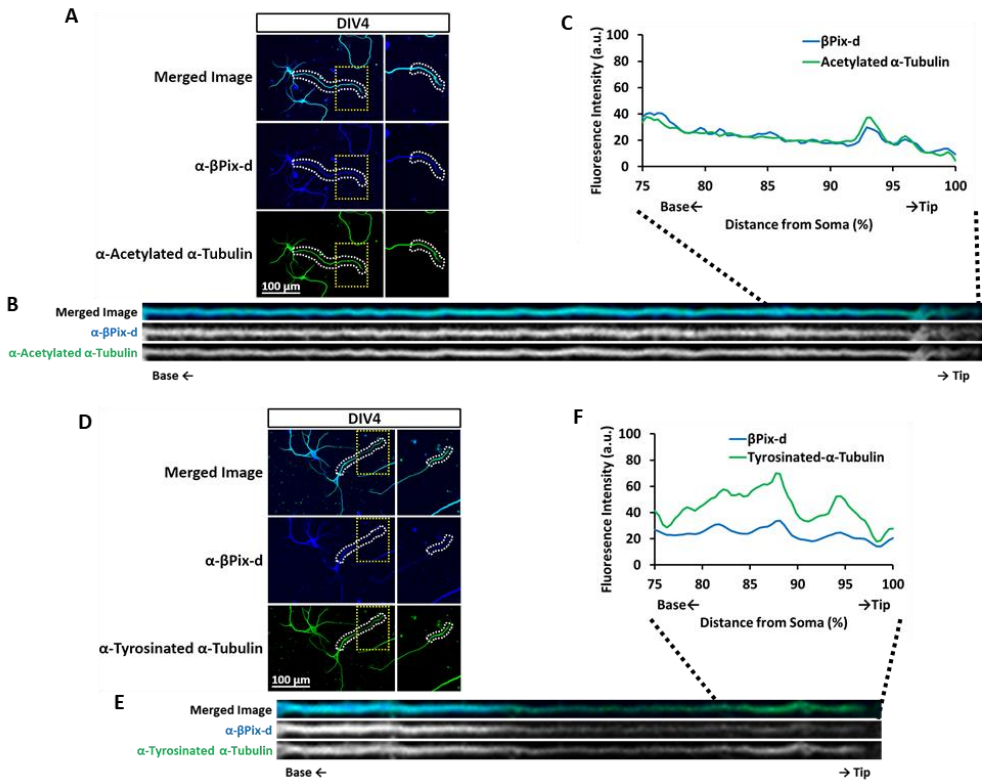
A
DIV4
Merged Image
α-βPix-d
α-Acetylated α-Tubulin
100 μm
B
Merged Image
α-βPix-d
α-Acetylated α-Tubulin
Base ←
→ Tip
C
βPix-d
Acetylated α-Tubulin
Fluoresence Intensity (a.u.)
100
80
60
40
20
0
75
80
85
90
95
100
Base←
→Tip
Distance from Soma (%)
D
DIV4
Merged Image
α-βPix-d
α-Tyrosinated α-Tubulin
100 μm
E
Merged Image
α-βPix-d
α-Tyrosinated α-Tubulin
Base ←
→ Tip
F
βPix-d
Tyrosinated-α-Tubulin
Fluoresence Intensity (a.u.)
100
80
60
40
20
0
75
80
85
90
95
100
Base←
→Tip
Distance from Soma (%)

6. βPix-d is required for phosphorylation of Stathmin1 at Ser16 and neurite outgrowth.

We found that βPix-d promoted microtubule stabilization and was localized to microtubules in neurites. Firstly, to identify the role of βPix-d in neurite outgrowth, we expressed GFP-βPix-d in hippocampal neurons from neuronal βPix isoform KO mice at DIV3 and tested whether the expression of βPix-d restores the reduced length and complexity of neurite at DIV4 (Figure 50A). As shown in Figure 43, the longest neurite length, total neurite length and total branching number had decrease in the neuronal βPix isoform KO neurons, compared with the WT neurons and those defects are recovered by transfection with βPix-d in the neuronal βPix isoform KO neurons (Figure 50B-50D). Likewise, Sholl analysis revealed simplified neuronal complexity in the neuronal βPix isoform KO neurons, compared to the WT neurons, and expression of βPix-d rescued it (Figure 50E). These data suggest that βPix-d regulates neurite morphogenesis.

Next, to find out a novel effector with βPix-d to play a role in both microtubule stabilization and neurite morphogenesis, we focused on Stathmin1. Stathmin appears as an essential regulator of neuronal differentiation at the various stages during development and plasticity of the nervous system (Chauvin and Sobel, 2015). Among four phosphorylation sites in Stathmin1, Ser16 is phosphorylated by PAK1 (Daub et al., 2001) that directly associated with βPix (Manser et al., 1998). By immunocytochemistry (Figure 51A), the longest neurite from the neuronal βPix isoform KO neurons had decreased level of phosphorylation in Stathmin1 at Ser16, compared to that from the WT neurons, and expression of βPix-d in the neuronal βPix isoform KO neurons recovered those decreased level (Figure 51B). The

Figure 50. βPix-d is required for neurite outgrowth.

(A) Representative images of hippocampal neurons from WT mice transfected with GFP and neuronal βPix isoform KO mice transfected with GFP or GFP-βPix-d at DIV3, fixed at DIV4 and stained with p-Stathmin1 (S16) (red) and β3-Tubulin (blue). (B) The longest neurite length had 60% decrease in neuronal βPix isoform KO neurons compared to WT neurons transfected with GFP. Expression of GFP-βPix-d in neuronal βPix isoform KO neurons rescues the length. (C) Total neurite length had 62% decrease in neuronal βPix isoform KO neurons compared to WT neurons transfected with GFP. Expression of GFP-βPix-d in neuronal βPix isoform KO neurons rescued the length. (D) Total branching number had 73% decrease in neuronal βPix isoform KO neurons compared to WT neurons transfected with GFP. Expression of GFP-βPix-d in neuronal βPix isoform KO neurons rescued the number. (E) By Sholl analysis, neurite complexity had significant decrease in neuronal βPix isoform KO neurons compared to WT neurons transfected with GFP. Expression of GFP-βPix-d in neuronal βPix isoform KO neurons rescued the complexity. 30-35 neurons were analyzed in each group from 3 independent cultures for (B)-(E). In (B)-(D), * $P < 0.05$, ** $P < 0.01$ and *** $P < 0.001$ by student's t-test, and in (E), ** $P < 0.01$ for a comparison of WT+GFP and KO+GFP and # $P < 0.05$, ## $P < 0.01$ and ### $P < 0.001$ for a comparison of KO+GFP and KO+GFP-βPix-d by student's t-test.

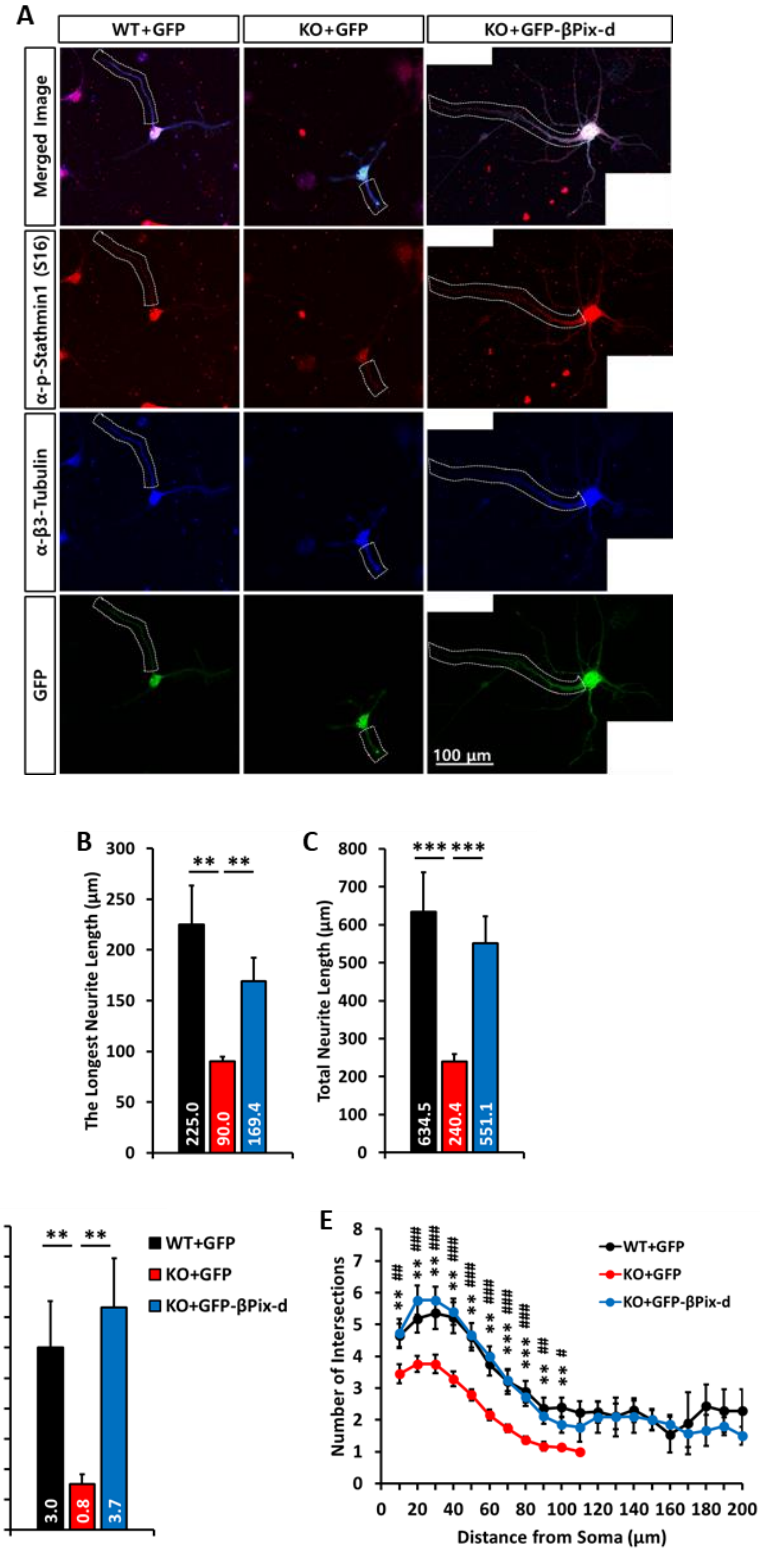
A
WT+GFP
KO+GFP
KO+GFP-βPix-d
Merged Image
α-p-Stathmin1 (S16)
α-β3-Tubulin
GFP
100 μm
B
The Longest Neurite Length (μm)
225.0
90.0
169.4
C
Total Neurite Length (μm)
634.5
240.4
551.1
D
Total Branching Number
3.0
0.8
3.7
WT+GFP
KO+GFP
KO+GFP-βPix-d
E
Number of Intersections
Distance from Soma (μm)

Figure 51. βPix-d is required for phosphorylation of Stathmin1 at Ser16.

(A) In the longest neurite, phosphorylation level of Stathmin1 at Ser16 that was normalized to β3-Tubulin had 20% decrease in neuronal βPix isoform KO neurons compared to the WT neurons transfected with GFP. Expression of GFP-βPix-d in neuronal βPix isoform KO neurons rescued the phosphorylation level of Stathmin1 at Ser16. (B) In the longest neurite, the distribution graph showed that the phosphorylation of Stathmin1 at Ser16 was significantly decreased in neuronal βPix isoform KO neurons, compared to WT neurons transfected with GFP and recovered by expression of GFP-βPix-d in neuronal βPix isoform KO neurons. (C) Representative blots for the level of phosphorylation of Stathmin1 at Ser16 in hippocampal neurons from WT mice transfected with GFP and neuronal βPix isoform KO mice transfected with GFP or GFP-βPix-d at DIV3 and identified at DIV4. (D) Quantification of relative expression levels for (H) as normalized to α-Tubulin expression. Compared to WT neurons transfected with GFP, neuronal βPix isoform KO neurons transfected with GFP had 41% decrease in ratio of p-Stathmin1 at Ser16 to Stathmin1 and the ratio was recovered by expression of GFP-βPix-d in neuronal βPix isoform KO neurons. 30-35 neurons were analyzed in each group from 3 independent cultures for (A) and (B) and 6 independent cultures were performed for (C) and (D).

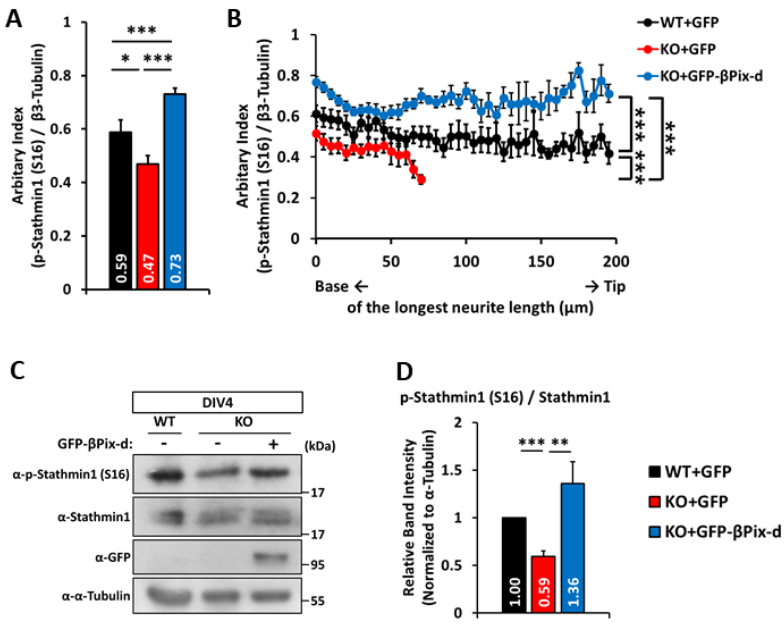
A
Arbitary Index
(p-Stathmin1 (S16) / β3-Tubulin)
0.59
0.47
0.73
B
WT+GFP
KO+GFP
KO+GFP-βPix-d
Base ←
→ Tip
of the longest neurite length (μm)
C
DIV4
WT
KO
GFP-βPix-d:
(kDa)
α-p-Stathmin1 (S16)
α-Stathmin1
α-GFP
α-α-Tubulin
D
p-Stathmin1 (S16) / Stathmin1
Relative Band Intensity
(Normalized to α-Tubulin)
1.00
0.59
1.36

distribution graph also showed significant decrease in the phosphorylation level along the longest neurite from the neuronal βPix isoform KO neurons, compared with the WT neurons, and βPix-d recovered it in the neuronal βPix isoform KO neurons (Figure 51C). When we performed Western blotting, we also observed the consistent result (Figure 51D). Quantitatively, compared with the WT neurons, the neuronal βPix isoform KO neurons had 41% decrease in the phosphorylation level of Stathmin1 at Ser16 (Figure 51E). Those decreased phosphorylation level was rescued by expression of βPix-d in the neuronal βPix isoform KO neurons (Figure 51F). Taken together, we found that βPix-d is required for neurite outgrowth and phosphorylation of Stathmin1 at Ser16 that inhibits both destabilization and catastrophe of microtubules.

Previously, we identified that both βPix-b and βPix-d stabilize microtubules (Figure 44). Firstly, to examine the effect of βPix-b in neurite outgrowth and phosphorylation of Stathmin1 at Ser16, we transfected with GFP, GFP-βPix-b or GFP-βPix-d in hippocampal neurons from neuronal βPix isoform KO mice at DIV3 and analyzed those neurons in the same way as mentioned as above at DIV4 (Figure 52A). Expression of GFP-βPix-b as well as GFP-βPix-d recovered the longest neurite length, total neurite length, total branching number and neurite complexity by Sholl analysis in the neuronal βPix isoform KO neurons, compared with expression of GFP (Figure 52B-52E). Specifically, the longest neurite length was more rescued by GFP-βPix-d than GFP-βPix-b (Figure 52B). Next, to identify the recovery of phosphorylation level in Stathmin1 at Ser16 by βPix-b, we analyzed the fluorescence intensity of phosphorylation in Stathmin1 at Ser16 along the longest neurite extending from the neuronal βPix isoform KO neurons expressed GFP tagged

Figure 52. βPix-b and βPix-d are required for neurite outgrowth.

(A) Representative images of hippocampal neurons from neuronal βPix isoform KO mice transfected with GFP, GFP-βPix-b or GFP-βPix-d at DIV3, fixed at DIV4 and stained with p-Stathmin1 (S16) (red) and β3-Tubulin (blue). (B) The longest neurite length was recovered by GFP-βPix-b or GFP-βPix-d in neuronal βPix isoform KO neurons, compared to GFP. (C) Total neurite length was recovered by GFP-βPix-b or GFP-βPix-d in neuronal βPix isoform KO neurons, compared to GFP. (D) Total branching number was recovered by GFP-βPix-b or GFP-βPix-d in neuronal βPix isoform KO neurons, compared to GFP. (E) By Sholl analysis, neurite complexity was recovered by GFP-βPix-b or GFP-βPix-d in neuronal βPix isoform KO neurons, compared to GFP. 61-82 neurons were analyzed in each group from 3 independent cultures for (A)-(E) and 61-82 neurons were analyzed in each group from 3 independent cultures for (B)-(E). In (B)-(D), * $P < 0.05$, ** $P < 0.01$ and *** $P < 0.001$ by student's t-test, and in (E), * $P < 0.05$, ** $P < 0.01$ and *** $P < 0.001$ for a comparison of KO+GFP and KO+GFP-βPix-b and # $P < 0.05$, ## $P < 0.01$ and ### $P < 0.001$ for a comparison of KO+GFP and KO+GFP-βPix-d by student's t-test.

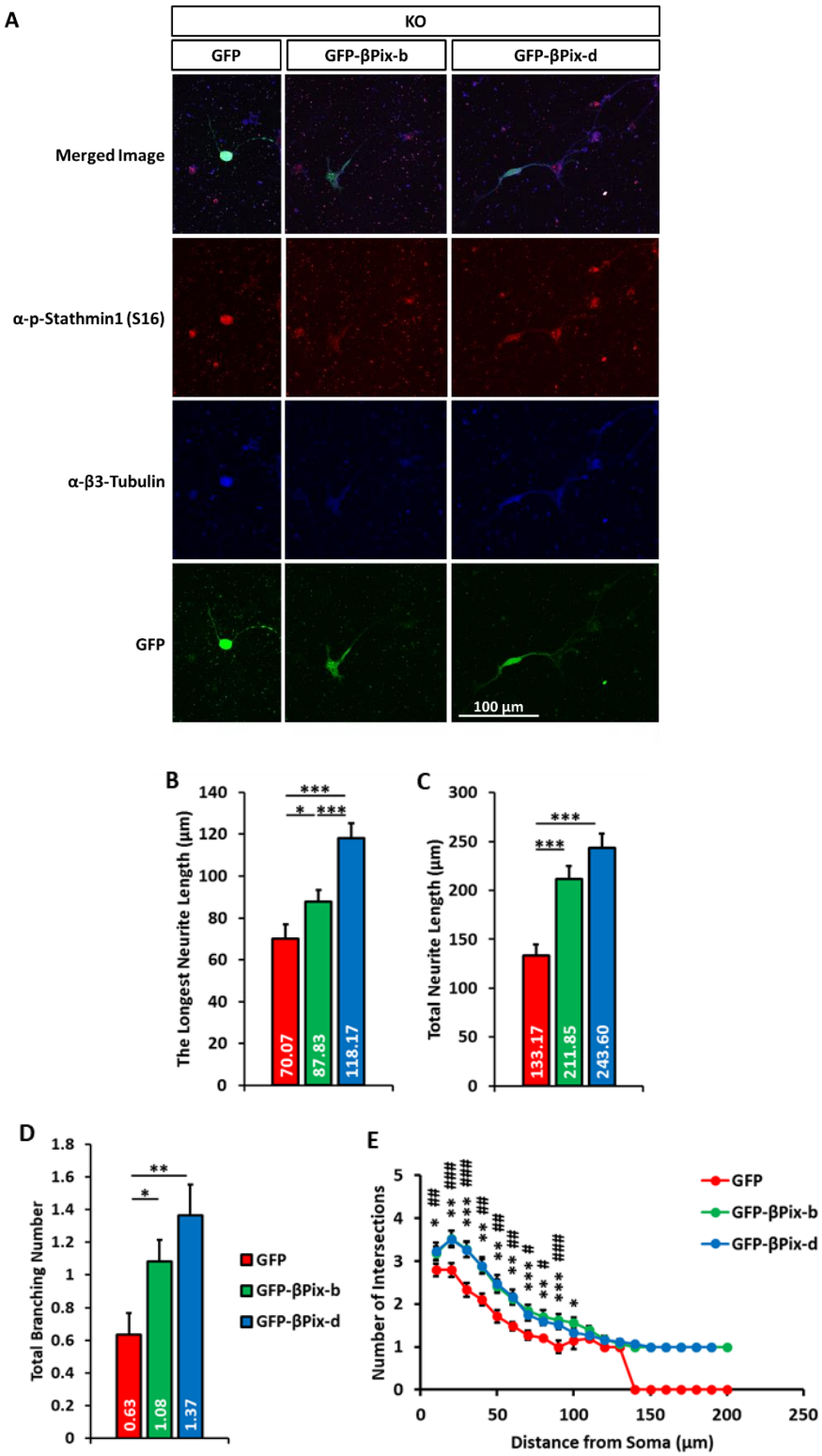
A
KO
GFP
GFP-βPix-b
GFP-βPix-d
Merged Image
α-p-Stathmin1 (S16)
α-β3-Tubulin
GFP
100 μm
B
The Longest Neurite Length (μm)
70.07
87.83
118.17
C
Total Neurite Length (μm)
133.17
211.85
243.60
D
Total Branching Number
0.63
1.08
1.37
GFP
GFP-βPix-b
GFP-βPix-d
E
Number of Intersections
Distance from Soma (μm)
GFP
GFP-βPix-b
GFP-βPix-d

neuronal βPix isoforms (Figure 52A). Both βPix-b and βPix-d recovered the phosphorylation level of Stathmin1 at Ser16 in the longest neurite from the neuronal βPix isoform KO neurons (Figure 53A and 53B). Interestingly, βPix-d more phosphorylated Stathmin1 at Ser16 than βPix-b (Figure 53A and 53B). These data showed that βPix-b controlled neurite outgrowth and phosphorylation of Stathmin1 at Ser16 like βPix-d, but for length of the longest neurite and phosphorylation of Stathmin1 at Ser16 in it, the effect of βPix-b was weaker than that of βPix-d. Altogether, among neuronal βPix isoforms, βPix-d predominantly acts on neurite outgrowth and phosphorylation of Stathmin1 at Ser16.

7. βPix-d is required for PAK1-induced phosphorylation of Stathmin1 at Ser16 and neurite outgrowth.

PAK1, a well-known βPix interactor, phosphorylates the specific site at Ser16 in Stathmin1 (Daub et al., 2001). To identify whether phosphorylation of Stathmin1 at Ser16 through βPix-d is affected by activity of PAK1, we co-transfected hippocampal neurons from neuronal βPix isoform KO mice with GFP-βPix-d and PID which leads to inactivation of PAK (Figure 54A). The neuronal βPix isoform KO neurons transfected with only GFP-βPix-d had recovery of phosphorylation in Stathmin1 at Ser16, compared to the neuronal βPix isoform KO neurons with control vectors. However, we did not observe the increased level in the neuronal βPix isoform KO neurons transfected with both GFP-βPix-d and PID (Figure 54B). Likewise, along the longest neurite extending from the neuronal βPix isoform KO neurons, the increased phosphorylation of Stathmin1 at Ser16 through GFP-βPix-d was inhibited by PID (Figure 54C). These data exhibited that βPix-d phosphorylated

Figure 53. βPix-b and βPix-d are required for phosphorylation of Stathmin1 at Ser16.

(A) Phosphorylation level of Stathmin1 at Ser16 that was normalized to β3-Tubulin was recovered by GFP-βPix-b or GFP-βPix-d in the longest neurite extending from neuronal βPix isoform KO neurons, compared to GFP. (B) The distribution graph showed that the phosphorylation of Stathmin1 at Ser16 was recovered by GFP-βPix-b or GFP-βPix-d along the longest neurite extending from neuronal βPix isoform KO neurons, compared to GFP. 61-82 neurons were analyzed in each group from 3 independent cultures.

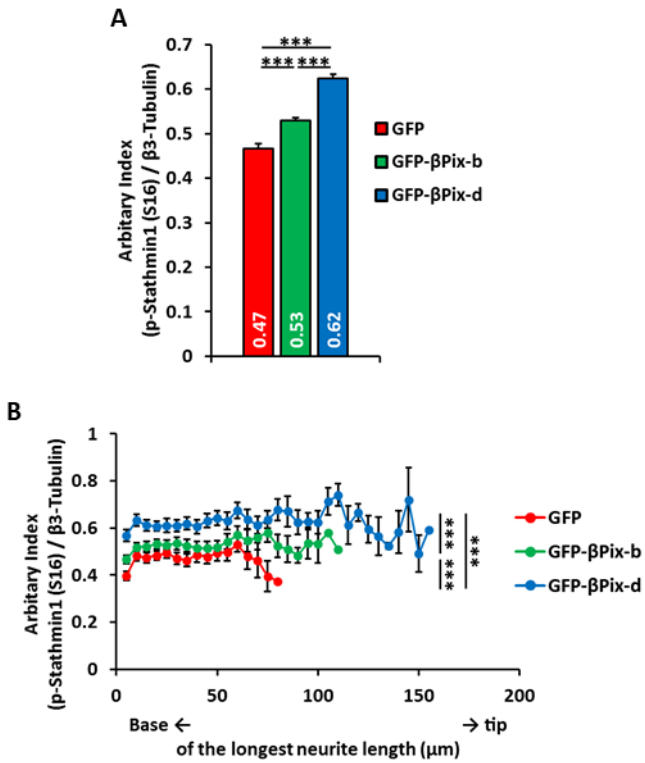
A
***
*** ***
0.7
0.6
0.5
0.4
0.3
0.2
0.1
0
Arbitary Index
(p-Stathmin1 (S16) / β3-Tubulin)
0.47
0.53
0.62
GFP
GFP-βPix-b
GFP-βPix-d
B
1
0.8
0.6
0.4
0.2
0
Arbitary Index
(p-Stathmin1 (S16) / β3-Tubulin)
0
50
100
150
200
Base ←
→ tip
of the longest neurite length (μm)
***
***
***
***
GFP
GFP-βPix-b
GFP-βPix-d

Figure 54. βPix-d is required for PAK1-induced neurite outgrowth.

(A) Representative images of hippocampal neurons from neuronal βPix isoform KO mice transfected with GFP or GFP-βPix-d and Myc or Myc-PID at DIV3, fixed at DIV4 and stained with p-Stathmin1 (S16) (blue) and Myc (red). (B) In the longest neurite extending from neuronal βPix isoform KO neurons, expression of GFP-βPix-d recovered phosphorylation level of Stathmin1 at Ser16, but co-expression of GFP-βPix-d and Myc-PID did not recover it. (C) The distribution graph showed that expression of GFP-βPix-d recovered the phosphorylation level of Stathmin1 at Ser16 along the longest neurite extending from neuronal βPix isoform KO neurons, but co-expression of GFP-βPix-d and Myc-PID did not recover it. 45-56 neurons were analyzed in each group from 3 independent cultures for (A)-(C).

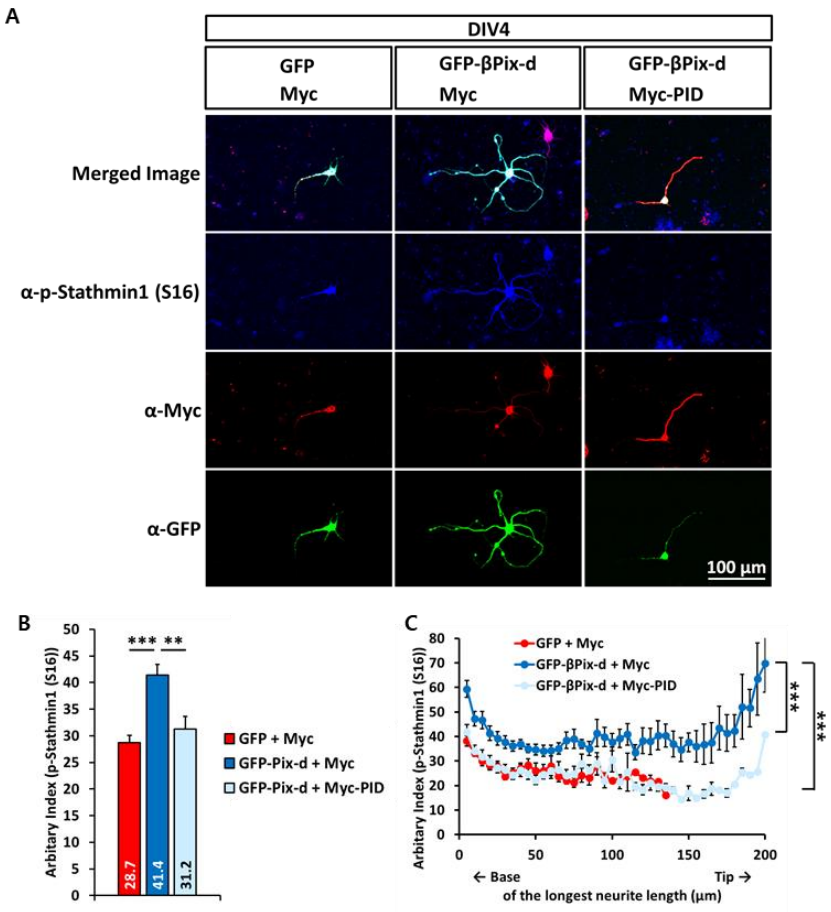
A
DIV4
GFP
Myc
GFP-βPix-d
Myc
GFP-βPix-d
Myc-PID
Merged Image
α-p-Stathmin1 (S16)
α-Myc
α-GFP
100 μm
B
Arbitary Index (p-Stathmin1 (S16))
***
**
28.7
41.4
31.2
GFP + Myc
GFP-Pix-d + Myc
GFP-Pix-d + Myc-PID
C
GFP + Myc
GFP-βPix-d + Myc
GFP-βPix-d + Myc-PID
Arbitary Index (p-Stathmin1 (S16))
***
***
← Base
Tip →
of the longest neurite length (μm)

Stathmin1 at Ser16 through PAK1 activity.

In addition, to identify whether the recovered neurite morphology in the neuronal βPix isoform KO neurons expressed βPix-d is influenced by PID, we analyzed the morphology of neurons stained with β3-Tubulin antibody at DIV4 (Figure 55A). The longest neurite length, total neurite length and total branching numbers were recovered by expression of βPix-d, but PID inhibited the recovery of βPix-d (Figure 55B-55D). By Sholl analysis, the rescued neurite complexity in the neuronal βPix isoform KO neurons transfected with GFP-βPix-d was not observed in co-transfection with PID (Fig. 55E). Altogether, our data showed that βPix-d stabilizes microtubules and promotes PAK1-mediated phosphorylation of Stathmin1 at Ser16, resulting in neurite outgrowth.

Figure 55. βPix-d is required for PAK1-induced phosphorylation of Stathmin1 at Ser16.

(A) Representative images of hippocampal neurons from neuronal βPix isoform KO mice transfected with GFP or GFP-βPix-d and Myc or Myc-PID at DIV3, fixed at DIV4 and stained with β3-Tubulin (blue) and Myc (red). (B) In neuronal βPix isoform KO neurons, recovery of the longest neurite length by GFP-βPix-d was not observed by co-expression with GFP-βPix-d and Myc-PID. (C) In neuronal βPix isoform KO neurons, recovery of total neurite length by GFP-βPix-d was not observed by co-expression with GFP-βPix-d and Myc-PID. (D) In neuronal βPix isoform KO neurons, recovery of total branching number by GFP-βPix-d was not observed by co-expression with GFP-βPix-d and Myc-PID. (E) Sholl analysis showed that recovery of neurite complexity by GFP-βPix-d was not observed by co-expression with GFP-βPix-d and Myc-PID in neuronal βPix isoform KO neurons. 67-84 neurons were analyzed in each group from 3 independent cultures for (B)-(E). In (B)-(D), ** $P < 0.01$ and *** $P < 0.001$ and in (E), * $P < 0.05$ and ** $P < 0.01$ for a comparison of GFP+Myc and GFP-βPix-d+Myc and # $P < 0.05$, ## $P < 0.01$ and ### $P < 0.001$ for a comparison of GFP-βPix-d+Myc and GFP-βPix-d+Myc-PID by student's t-test.

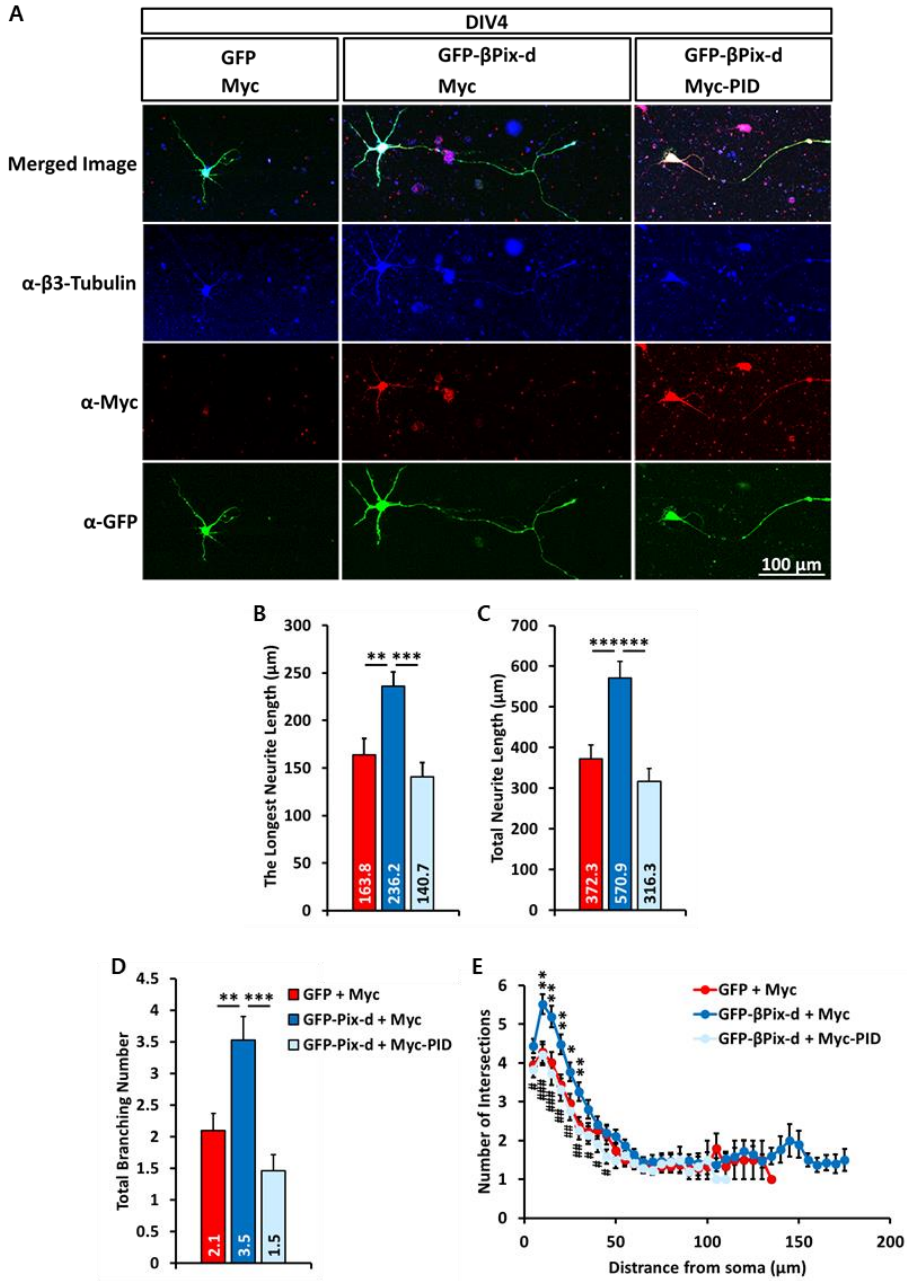
A
DIV4
GFP
Myc
GFP-βPix-d
Myc
GFP-βPix-d
Myc-PID
Merged Image
α-β3-Tubulin
α-Myc
α-GFP
100 μm
B
The Longest Neurite Length (μm)
** ***
163.8
236.2
140.7
C
Total Neurite Length (μm)
****
372.3
570.9
316.3
D
Total Branching Number
** ***
2.1
3.5
1.5
GFP + Myc
GFP-Pix-d + Myc
GFP-Pix-d + Myc-PID
E
Number of Intersections
Distrance from soma (μm)
GFP + Myc
GFP-βPix-d + Myc
GFP-βPix-d + Myc-PID

Discussion

The present study delineates a novel signaling pathway for neurite outgrowth triggered by βPix-d. Figure 56 summarizes a hypothetical model of the regulation of βPix-d for microtubule stability and neurite outgrowth with Stathmin1. We revealed the neuronal role of βPix-d for the first time. Because βPix has neuronal specific isoforms, βPix-b and βPix-d, by alternative splicing (Kim et al., 2000), it is important to identify the role of each isoform in neurons. Our recent study revealed a novel mechanism for the role of βPix-b in dendritic spine morphogenesis (Shin et al., 2019) and our present study elicits the neuronal role of βPix-d in neurite morphogenesis. We find that all of neuronal βPix isoforms are required for microtubule stabilization with phosphorylation of Stathmin1 at Ser16 and neurite outgrowth. Specifically, βPix-d is localized in microtubules and impaired neurite morphology and phosphorylated Stathmin1 at Ser16 are more recovered by βPix-d than βPix-b in neuronal βPix isoform KO hippocampal cultures. βPix is known to be essential to activate Rac1 and/or Cdc42 and in turn activate PAK1 (Bagrodia et al., 1998; Koh et al., 2001), so βPix-d on microtubules activates Pak1 and in turn active PAK1 phosphorylates Stathmin1, microtubule destabilizing protein, at Ser16, leading to inactivation of Stathmin1. The inactive Stathmin1 releases sequestered Tubulin heterodimers for microtubule polymerization and inhibits microtubule catastrophe, resulting in neurite outgrowth.

Several studies supporting that βPix is involved in neurite outgrowth have been revealed. αPix, which shares 80% of βPix polypeptide, is a specific regulator of axonal and dendritic branching hippocampal neurons (Totaro et al., 2012).

Figure 56. Model illustrating the regulation of microtubule stabilization and neurite outgrowth by βPix-d.

βPix-d localized on microtubules activates PAK1 and in turn, active PAK1 phosphorylates Stathmin1 at Ser16. Phosphorylated Stathmin1 in inactive state released α- and β-Tubulin heterodimer for microtubule polymerization and inhibited microtubule catastrophe in neurite. In summary, βPix-d is required for microtubule stabilization and neurite outgrowth.

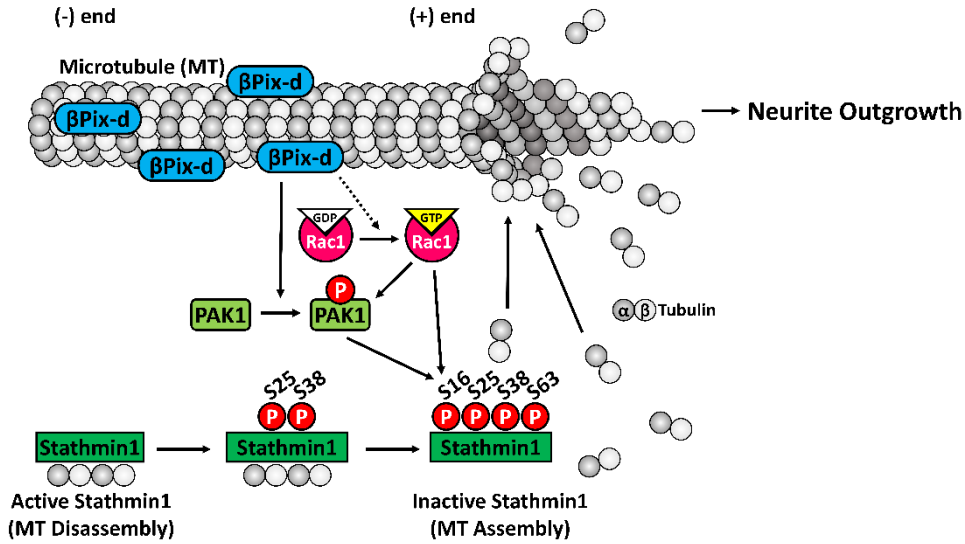
(-) end
(+) end
Microtubule (MT)
βPix-d
βPix-d
βPix-d
βPix-d
Neurite Outgrowth
GDP
Rac1
GTP
Rac1
P
PAK1
PAK1
α β Tubulin
S25 S38
P P
S16 S25 S38 S63
P P P P
Stathmin1
Stathmin1
Stathmin1
Active Stathmin1
(MT Disassembly)
Inactive Stathmin1
(MT Assembly)

βPix/Ras/ERK/PAK2 pathway is involved in fibroblast growth factor (FGF)-induced neurite outgrowth in PC12 cell (Shin et al., 2002) and βPix promotes axon formation as an upstream activator of TC10 that is closely related to Cdc42 (Lopez Tobon et al., 2018). Although the previous studies revealed the role of βPix in neurite outgrowth, those studies are for βPix-a that is ubiquitously expressed in most tissues (Oh et al., 1997) and it is necessary to investigate the role of for neuronal βPix isoforms in regulation of neurite outgrowth. As observed in our previous study (Shin et al., 2019) and present study, GFP-βPix-b is mainly localized in the head of dendritic spine, and GFP-βPix-d is localized in both shaft and spine of dendrite at DIV14 (Figure 33). Endogenous βPix-d is also localized in microtubules *in vitro* (Figure 46-47) and *in vivo* (Figure 48), suggesting that the association between βPix-d and morphogenesis of neurites that are composed of microtubules. We inferred that the GFP-βPix-d observed in dendritic spine is localized in microtubules that are invaded in dendritic spines (Merriam et al., 2013) or interacts with unknown factor in the head of dendritic spine.

We suggest that βPix-d is associated with microtubules. The GEFs, murine Lfc and its human homologue GEF-H1, and p190RhoGEF are the members of Dbl family that βPix belongs to and interact with microtubules (Glaven et al., 1999; Ren et al., 1998; van Horck et al., 2001). For the region of microtubule binding site in βPix-d, we expect Pleckstrin homology (PH) domain which associates with microtubules in Lfc proteins (Glaven et al., 1999). However, PH domain is a common domain shared by all βPix isoforms. Unlike βPix-a and βPix-b, βPix-d does not contain a PDZ binding sequence, Asp-Glu-Thr-Asn-Leu (DETNL) and coiled-coil region in the C terminal. The PDZ binding sequence of βPix interacts with PDZ domain from Shank

(Park et al., 2003) and Scribble (Audebert et al., 2004) proteins. Shank proteins are multidomain scaffold proteins of the postsynaptic density that connect synaptic proteins to the actin cytoskeleton (Naisbitt et al., 1999) and Scribble is found as a membrane protein (Humbert et al., 2003). We assume that βPix-a and βPix-b are localized in dendritic spines through the Shank and Scribble proteins. The coiled-coil region of βPix plays a key role in the localization of βPix to the cell periphery and is also responsible for βPix dimerization (Koh et al., 2001), indicating that βPix-a and βPix-b in dimeric form may mask PH and/or other domain that is the expected microtubule binding region. Taken together, we assume that βPix-a and βPix-b are localized in dendritic spine and its membrane even though they have the expected microtubule binding regions, but βPix-d that cannot form dimer is predominantly located in microtubules because it does not mask the expected microtubule-binding regions and does not have the PDZ binding sequence and coiled coil region. In addition, βPix-d has 11 a.a. in the C terminal that βPix-a and βPix-b do not have, suggesting that11 a.a. is related to its microtubule localization, but the additional research is needed. In addition, we assume that the localization of βPix-d in stable microtubules contribute to enhancing the microtubule stability. Microtubule-associated proteins (MAPs) bind to and stabilize microtubules (Cleveland et al., 1977; Drewes et al., 1998). The MAP2/tau family is a unique class of structural MAPs that reduce microtubule depolymerization by stabilizing the Tubulin–Tubulin interfaces along protofilaments (Al-Bassam et al., 2002), suggesting that βPix-d stabilizes microtubules by binding them like MAP2 and Tau.

In the present study, we show that βPix-d stabilizes microtubules through inactivation of Stathmin1, a microtubule-destabilizing factor. Our findings suggest

that relationship between βPix-d, microtubule-stabilizing factor and Stathmin1, microtubule-destabilizing factor are involved in neurite outgrowth. Because the proper balance between counteracting activities of βPix-d and Stathmin1 is required for neurite outgrowth, we need to study the activity of βPix-d that inhibits Stathmin1. The activity of GEF-H1 is suppressed in the microtubule bound state, whereas GEF-H1 release caused by microtubule disruption stimulates Rho-specific GEF activity (Krendel et al., 2002). Specifically, in the endothelial cell, decrease in phosphorylated Stathmin which leads to Stathmin-dependent microtubule disassembly cause release from microtubules and activation of Rho-specific GEF-H1 (Tian et al., 2012). In addition, it was reported that βPix is activated by its phosphorylation in neurons. CaMKI-mediated phosphorylation of Ser516 in βPix-a (Saneyoshi et al., 2008) and Src-mediated phosphorylation of Tyr598 in βPix-b (Shin et al., 2019) regulate dendritic spine morphogenesis and synaptogenesis. Tau that stabilizes microtubules and promotes microtubule assembly, is phosphorylated at Thr245, Thr377, Ser262 or Ser409 by Rho-kinase and then decreases Tau's coupling with microtubules and may cause further microtubule disassembly (Amano et al., 2003). Altogether, we suggest that activity of βPix-d in microtubules may be regulated by its phosphorylation, leading to neurite outgrowth.

Among the GEFs, DOCK7 regulates Rac activity, inactivates the Stathmin1 and promotes neuronal polarization (Watabe-Uchida et al., 2006). This report focuses on a role of DOCK7 in axon formation during the early stage of neuronal development. Our data shows that endogenous βPix-d is localized in microtubules during neuronal development (Figure 47) and expression of βPix-d in neuronal βPix isoform KO neurons recovers neurite length and neurite complexity (Figure 50 and 52),

suggesting that βPix-d plays a role in morphogenesis of neurites containing axons and dendrites. There is no significant difference in neurite and axon numbers between WT and neuronal βPix isoform KO mice (Figure 40E and 41D), indicating that neuronal βPix isoforms are not essential for neurite formation and neuronal polarization. Stathmin family are highly expressed in the nervous system during brain development (Chauvin and Sobel, 2015), and regulate the development of axons (Watabe-Uchida et al., 2006) and dendrites (Ohkawa et al., 2007) by its phosphorylation at Ser16. These studies provide convincing evidences to support our findings that βPix-d is required for morphogenesis of neurites containing axons and dendrites via Stathmin1 phosphorylation at Ser16.

Knockout of Stathmin in mice resulted in mostly mild or no detected phenotype for neuronal development and structures (Chauvin and Sobel, 2015; Schubart et al., 1996), suggesting that βPix-d is a major effector in our signaling pathway of neurite outgrowth. Stathmin has been linked to fear, cognition and aging in rodent and human studies (Brocke et al., 2010; Ehlis et al., 2011; Martel et al., 2008; Saetre et al., 2011; Shumyatsky et al., 2005), and Stathmin-dependent changes in microtubule stability are involved in synaptic function and memory formation (Uchida et al., 2014). Until now, there has been no report on dysfunction of memory and behavior for deletion of βPix isoforms. We suggest that our neuronal βPix isoform KO mice may have impairments in memory formation and disease-related behavior. In Rodent studies, Kalirin, one of Rac/Cdc42 GEFs, exhibits robust deficits in working memory, sociability and hyperactivity accompanied by alteration in cortical spine density (Cahill et al., 2009). In addition, Ser16 in Stathmin1 can be phosphorylated by PAK and CaMII/IV, the kinases critically involved in memory formation (Hayashi et al.,

2004; Kang et al., 2001; Silva et al., 1992). Those studies might provide the basis of mechanism for memory function controlled by microtubule stability.

In conclusion, we elicit the novel pathway for neurite outgrowth and microtubule stabilization, and our findings offer insight into the function of βPix-d among neuronal βPix isoforms. βPix-d is critical for neurite development through the regulation of microtubule stability. βPix-d is localized in microtubules and stabilizes them by phosphorylation of Stathmin1 at Ser16. Our data link βPix-d to the local inactivation of the microtubule destabilizing protein, Stathmin1. Future studies involving real-time imaging of microtubule behaviors are also required to detail the contribution of βPix-d to microtubule dynamics. Various studies report that alterations in dendrite morphology or defects in neuronal development contribute to several neurological and neurodevelopmental disorders (Kulkarni and Firestein, 2012). In addition, given that microtubule stability is involved in not only neuronal structure (Witte et al., 2008) but also cognitive function and axonal regeneration after spinal cord injury (Hellal et al., 2011; Uchida et al., 2014), regulation of microtubule stability might be a useful approach to treatment of neurological disorders and central nervous system injury. Thus, our established mechanism for microtubule stabilization and neurite outgrowth by βPix-d may offer the basis for understanding the neuronal structure and function in those disease and injury states. Further studies for βPix-d are essential to reveal its specific involvement in neuronal development and regeneration.

REFERENCES

Ahn, S.J., Chung, K.W., Lee, R.A., Park, I.A., Lee, S.H., Park, D.E., and Noh, D.Y. (2003). Overexpression of betaPix-a in human breast cancer tissues. Cancer Lett *193*, 99-107.

Al-Bassam, J., Ozer, R.S., Safer, D., Halpain, S., and Milligan, R.A. (2002). MAP2 and tau bind longitudinally along the outer ridges of microtubule protofilaments. The Journal of cell biology *157*, 1187-1196.

Alvarez, V.A., and Sabatini, B.L. (2007). Anatomical and physiological plasticity of dendritic spines. Annual review of neuroscience *30*, 79-97.

Amano, M., Kaneko, T., Maeda, A., Nakayama, M., Ito, M., Yamauchi, T., Goto, H., Fukata, Y., Oshiro, N., Shinohara, A.*, et al.* (2003). Identification of Tau and MAP2 as novel substrates of Rho-kinase and myosin phosphatase. Journal of neurochemistry *87*, 780-790.

Antunes, M., and Biala, G. (2012). The novel object recognition memory: neurobiology, test procedure, and its modifications. Cogn Process *13*, 93-110.

Arimura, N., and Kaibuchi, K. (2007). Neuronal polarity: from extracellular signals to intracellular mechanisms. Nature reviews Neuroscience *8*, 194-205.

Audebert, S., Navarro, C., Nourry, C., Chasserot-Golaz, S., Lecine, P., Bellaiche, Y., Dupont, J.L., Premont, R.T., Sempere, C., Strub, J.M.*, et al.* (2004). Mammalian Scribble forms a tight complex with the betaPIX exchange factor. Current biology : CB *14*, 987-995.

Baas, P.W., Rao, A.N., Matamoros, A.J., and Leo, L. (2016). Stability properties of neuronal microtubules. Cytoskeleton (Hoboken, NJ) *73*, 442-460.

Bach, M.E., Hawkins, R.D., Osman, M., Kandel, E.R., and Mayford, M. (1995). Impairment of spatial but not contextual memory in CaMKII mutant mice with a selective loss of hippocampal LTP in the range of the theta frequency. Cell *81*, 905-915.

Bagrodia, S., Taylor, S.J., Jordon, K.A., Van Aelst, L., and Cerione, R.A. (1998). A Novel Regulator of p21-activated Kinases. Journal of Biological Chemistry *273*, 23633-23636.

Barch, D.M. (2005). The cognitive neuroscience of schizophrenia. Annu Rev Clin Psychol *1*, 321-353.

Beaudoin, G.M., 3rd, Lee, S.H., Singh, D., Yuan, Y., Ng, Y.G., Reichardt, L.F., and Arikkath, J. (2012). Culturing pyramidal neurons from the early postnatal mouse hippocampus and cortex. Nature protocols *7*, 1741-1754.

Benarroch, E.E. (2007). Rho GTPases: role in dendrite and axonal growth, mental retardation, and axonal regeneration. Neurology *68*, 1315-1318.

Blanco-Suarez, E., Fiuza, M., Liu, X., Chakkarapani, E., and Hanley, J.G. (2014). Differential Tiam1/Rac1 activation in hippocampal and cortical neurons mediates differential spine shrinkage in response to oxygen/glucose deprivation. J Cereb Blood Flow Metab *34*, 1898-1906.

Bos, J.L., Rehmann, H., and Wittinghofer, A. (2007). GEFs and GAPs: critical elements in the control of small G proteins. Cell *129*, 865-877.

Brigman, J.L., Wright, T., Talani, G., Prasad-Mulcare, S., Jinde, S., Seabold, G.K., Mathur, P., Davis, M.I., Bock, R., Gustin, R.M.*, et al.* (2010). Loss of GluN2B-containing NMDA receptors in CA1 hippocampus and cortex impairs long-term depression, reduces dendritic spine density, and disrupts learning. The Journal of

neuroscience : the official journal of the Society for Neuroscience *30*, 4590-4600.

Brocke, B., Lesch, K.P., Armbruster, D., Moser, D.A., Muller, A., Strobel, A., and Kirschbaum, C. (2010). Stathmin, a gene regulating neural plasticity, affects fear and anxiety processing in humans. American journal of medical genetics Part B, Neuropsychiatric genetics : the official publication of the International Society of Psychiatric Genetics *153b*, 243-251.

Cahill, M.E., Xie, Z., Day, M., Photowala, H., Barbolina, M.V., Miller, C.A., Weiss, C., Radulovic, J., Sweatt, J.D., Disterhoft, J.F.*, et al.* (2009). Kalirin regulates cortical spine morphogenesis and disease-related behavioral phenotypes. Proceedings of the National Academy of Sciences of the United States of America *106*, 13058-13063.

Cantwell, D.P., and Baker, L. (1991). Association between attention deficit-hyperactivity disorder and learning disorders. J Learn Disabil *24*, 88-95.

Carlisle, H.J., and Kennedy, M.B. (2005). Spine architecture and synaptic plasticity. Trends Neurosci *28*, 182-187.

Cassimeris, L. (2002). The oncoprotein 18/stathmin family of microtubule destabilizers. Current opinion in cell biology *14*, 18-24.

Chauvin, S., and Sobel, A. (2015). Neuronal stathmins: a family of phosphoproteins cooperating for neuronal development, plasticity and regeneration. Progress in neurobiology *126*, 1-18.

Chneiweiss, H., Cordier, J., and Sobel, A. (1992). Stathmin phosphorylation is regulated in striatal neurons by vasoactive intestinal peptide and monoamines via multiple intracellular pathways. Journal of neurochemistry *58*, 282-289.

Cleveland, D.W., Hwo, S.Y., and Kirschner, M.W. (1977). Physical and chemical

properties of purified tau factor and the role of tau in microtubule assembly. Journal of molecular biology *116*, 227-247.

Couture, S.M., Penn, D.L., and Roberts, D.L. (2006). The functional significance of social cognition in schizophrenia: a review. Schizophrenia bulletin *32 Suppl 1*, S44-63.

Cross-Disorder Group of the Psychiatric Genomics, C., Lee, S.H., Ripke, S., Neale, B.M., Faraone, S.V., Purcell, S.M., Perlis, R.H., Mowry, B.J., Thapar, A., Goddard, M.E.*, et al.* (2013). Genetic relationship between five psychiatric disorders estimated from genome-wide SNPs. Nature genetics *45*, 984-994.

Dailey, M.E., and Smith, S.J. (1996). The dynamics of dendritic structure in developing hippocampal slices. The Journal of neuroscience : the official journal of the Society for Neuroscience *16*, 2983-2994.

Daub, H., Gevaert, K., Vandekerckhove, J., Sobel, A., and Hall, A. (2001). Rac/Cdc42 and p65PAK regulate the microtubule-destabilizing protein stathmin through phosphorylation at serine 16. The Journal of biological chemistry *276*, 1677-1680.

De Filippis, B., Romano, E., and Laviola, G. (2014). Aberrant Rho GTPases signaling and cognitive dysfunction: in vivo evidence for a compelling molecular relationship. Neurosci Biobehav Rev *46 Pt 2*, 285-301.

Di Paolo, G., Antonsson, B., Kassel, D., Riederer, B.M., and Grenningloh, G. (1997). Phosphorylation regulates the microtubule-destabilizing activity of stathmin and its interaction with tubulin. FEBS Lett *416*, 149-152.

Dotti, C.G., Sullivan, C.A., and Banker, G.A. (1988). The establishment of polarity by hippocampal neurons in culture. The Journal of neuroscience : the official journal

of the Society for Neuroscience *8*, 1454-1468.

Doyle, A.E. (2006). Executive functions in attention-deficit/hyperactivity disorder. J Clin Psychiatry *67 Suppl 8*, 21-26.

Drewes, G., Ebneth, A., and Mandelkow, E.M. (1998). MAPs, MARKs and microtubule dynamics. Trends in biochemical sciences *23*, 307-311.

Dubey, J., Ratnakaran, N., and Koushika, S.P. (2015). Neurodegeneration and microtubule dynamics: death by a thousand cuts. Frontiers in cellular neuroscience *9*, 343.

Duncan, G.E., Moy, S.S., Perez, A., Eddy, D.M., Zinzow, W.M., Lieberman, J.A., Snouwaert, J.N., and Koller, B.H. (2004). Deficits in sensorimotor gating and tests of social behavior in a genetic model of reduced NMDA receptor function. Behav Brain Res *153*, 507-519.

Ehlis, A.C., Bauernschmitt, K., Dresler, T., Hahn, T., Herrmann, M.J., Roser, C., Romanos, M., Warnke, A., Gerlach, M., Lesch, K.P.*, et al.* (2011). Influence of a genetic variant of the neuronal growth associated protein Stathmin 1 on cognitive and affective control processes: an event-related potential study. American journal of medical genetics Part B, Neuropsychiatric genetics : the official publication of the International Society of Psychiatric Genetics *156b*, 291-302.

Eichler, S.A., and Meier, J.C. (2008). E-I balance and human diseases - from molecules to networking. Front Mol Neurosci *1*, 2.

Eitel, J., Krull, M., Hocke, A.C., N'Guessan, P.D., Zahlten, J., Schmeck, B., Slevogt, H., Hippenstiel, S., Suttorp, N., and Opitz, B. (2008). Beta-PIX and Rac1 GTPase mediate trafficking and negative regulation of NOD2. J Immunol *181*, 2664-2671.

Eldar, E., Cohen, J.D., and Niv, Y. (2013). The effects of neural gain on attention and

learning. Nat Neurosci *16*, 1146-1153.

Etienne-Manneville, S., and Hall, A. (2002). Rho GTPases in cell biology. Nature *420*, 629-635.

Fiuza, M., Gonzalez-Gonzalez, I., and Perez-Otano, I. (2013). GluN3A expression restricts spine maturation via inhibition of GIT1/Rac1 signaling. Proceedings of the National Academy of Sciences of the United States of America *110*, 20807-20812.

Flanders, J.A., Feng, Q., Bagrodia, S., Laux, M.T., Singavarapu, A., and Cerione, R.A. (2003). The Cbl proteins are binding partners for the Cool/Pix family of p21-activated kinase-binding proteins. FEBS Lett *550*, 119-123.

Flynn, K.C. (2013). The cytoskeleton and neurite initiation. Bioarchitecture *3*, 86-109.

Fradley, R.L., O'Meara, G.F., Newman, R.J., Andrieux, A., Job, D., and Reynolds, D.S. (2005). STOP knockout and NMDA NR1 hypomorphic mice exhibit deficits in sensorimotor gating. Behav Brain Res *163*, 257-264.

Germano, C., and Kinsella, G.J. (2005). Working memory and learning in early Alzheimer's disease. Neuropsychol Rev *15*, 1-10.

Geyer, M.A., McIlwain, K.L., and Paylor, R. (2002). Mouse genetic models for prepulse inhibition: an early review. Molecular psychiatry *7*, 1039-1053.

Glaven, J.A., Whitehead, I., Bagrodia, S., Kay, R., and Cerione, R.A. (1999). The Dbl-related protein, Lfc, localizes to microtubules and mediates the activation of Rac signaling pathways in cells. The Journal of biological chemistry *274*, 2279-2285.

Govek, E.E., Newey, S.E., and Van Aelst, L. (2005). The role of the Rho GTPases in neuronal development. Genes & development *19*, 1-49.

Grenningloh, G., Soehrman, S., Bondallaz, P., Ruchti, E., and Cadas, H. (2004). Role

of the microtubule destabilizing proteins SCG10 and stathmin in neuronal growth. Journal of neurobiology *58*, 60-69.

Gu, J., Lee, C.W., Fan, Y., Komlos, D., Tang, X., Sun, C., Yu, K., Hartzell, H.C., Chen, G., Bamburg, J.R.*, et al.* (2010). ADF/cofilin-mediated actin dynamics regulate AMPA receptor trafficking during synaptic plasticity. Nat Neurosci *13*, 1208-1215.

Haebig, K., Gloeckner, C.J., Miralles, M.G., Gillardon, F., Schulte, C., Riess, O., Ueffing, M., Biskup, S., and Bonin, M. (2010). ARHGEF7 (Beta-PIX) acts as guanine nucleotide exchange factor for leucine-rich repeat kinase 2. PLoS One *5*, e13762.

Hall, B., Limaye, A., and Kulkarni, A.B. (2009). Overview: generation of gene knockout mice. Curr Protoc Cell Biol *Chapter 19*, Unit 19.12 19.12.11-17.

Hammond, R.S., Tull, L.E., and Stackman, R.W. (2004). On the delay-dependent involvement of the hippocampus in object recognition memory. Neurobiol Learn Mem *82*, 26-34.

Hayashi, M.L., Choi, S.Y., Rao, B.S., Jung, H.Y., Lee, H.K., Zhang, D., Chattarji, S., Kirkwood, A., and Tonegawa, S. (2004). Altered cortical synaptic morphology and impaired memory consolidation in forebrain- specific dominant-negative PAK transgenic mice. Neuron *42*, 773-787.

Hellal, F., Hurtado, A., Ruschel, J., Flynn, K.C., Laskowski, C.J., Umlauf, M., Kapitein, L.C., Strikis, D., Lemmon, V., Bixby, J.*, et al.* (2011). Microtubule stabilization reduces scarring and causes axon regeneration after spinal cord injury. Science (New York, NY) *331*, 928-931.

Hong, S.T., and Mah, W. (2015). A Critical Role of GIT1 in Vertebrate and

Invertebrate Brain Development. Exp Neurobiol *24*, 8-16.

Humbert, P., Russell, S., and Richardson, H. (2003). Dlg, Scribble and Lgl in cell polarity, cell proliferation and cancer. BioEssays : news and reviews in molecular, cellular and developmental biology *25*, 542-553.

Jan, Y.N., and Jan, L.Y. (2001). Dendrites. Genes & development *15*, 2627-2641.

Janke, C., and Kneussel, M. (2010). Tubulin post-translational modifications: encoding functions on the neuronal microtubule cytoskeleton. Trends Neurosci *33*, 362-372.

Kang, H., Sun, L.D., Atkins, C.M., Soderling, T.R., Wilson, M.A., and Tonegawa, S. (2001). An important role of neural activity-dependent CaMKIV signaling in the consolidation of long-term memory. Cell *106*, 771-783.

Kapitein, L.C., and Hoogenraad, C.C. (2015). Building the Neuronal Microtubule Cytoskeleton. Neuron *87*, 492-506.

Kedzior, K.K., and Martin-Iverson, M.T. (2006). Chronic cannabis use is associated with attention-modulated reduction in prepulse inhibition of the startle reflex in healthy humans. J Psychopharmacol *20*, 471-484.

Kim, S., Kim, T., Lee, D., Park, S.H., Kim, H., and Park, D. (2000). Molecular cloning of neuronally expressed mouse betaPix isoforms. Biochem Biophys Res Commun *272*, 721-725.

Kim, T., and Park, D. (2001). Molecular cloning and characterization of a novel mouse betaPix isoform. Mol Cells *11*, 89-94.

Koh, C.G., Manser, E., Zhao, Z.S., Ng, C.P., and Lim, L. (2001). Beta1PIX, the PAK-interacting exchange factor, requires localization via a coiled-coil region to promote microvillus-like structures and membrane ruffles. Journal of cell science *114*, 4239-

4251.

Krendel, M., Zenke, F.T., and Bokoch, G.M. (2002). Nucleotide exchange factor GEF-H1 mediates cross-talk between microtubules and the actin cytoskeleton. Nature cell biology *4*, 294-301.

Kulkarni, V.A., and Firestein, B.L. (2012). The dendritic tree and brain disorders. Molecular and cellular neurosciences *50*, 10-20.

Kushima, I., Nakamura, Y., Aleksic, B., Ikeda, M., Ito, Y., Shiino, T., Okochi, T., Fukuo, Y., Ujike, H., Suzuki, M.*, et al.* (2012). Resequencing and association analysis of the KALRN and EPHB1 genes and their contribution to schizophrenia susceptibility. Schizophrenia bulletin *38*, 552-560.

Larsson, N., Marklund, U., Gradin, H.M., Brattsand, G., and Gullberg, M. (1997). Control of microtubule dynamics by oncoprotein 18: dissection of the regulatory role of multisite phosphorylation during mitosis. Molecular and cellular biology *17*, 5530-5539.

Lasser, M., Tiber, J., and Lowery, L.A. (2018). The Role of the Microtubule Cytoskeleton in Neurodevelopmental Disorders. Frontiers in cellular neuroscience *12*, 165.

Lawler, S. (1998). Microtubule dynamics: if you need a shrink try stathmin/Op18. Current biology : CB *8*, R212-214.

Liu, G. (2004). Local structural balance and functional interaction of excitatory and inhibitory synapses in hippocampal dendrites. Nat Neurosci *7*, 373-379.

Liu, J., Zeng, L., Kennedy, R.M., Gruenig, N.M., and Childs, S.J. (2012). betaPix plays a dual role in cerebral vascular stability and angiogenesis, and interacts with integrin alphavbeta8. Developmental biology *363*, 95-105.

Llano, O., Smirnov, S., Soni, S., Golubtsov, A., Guillemin, I., Hotulainen, P., Medina, I., Nothwang, H.G., Rivera, C., and Ludwig, A. (2015). KCC2 regulates actin dynamics in dendritic spines via interaction with beta-PIX. The Journal of cell biology *209*, 671-686.

Lopez Tobon, A., Suresh, M., Jin, J., Vitriolo, A., Pietralla, T., Tedford, K., Bossenz, M., Mahnken, K., Kiefer, F., Testa, G.*, et al.* (2018). The guanine nucleotide exchange factor Arhgef7/betaPix promotes axon formation upstream of TC10. Scientific reports *8*, 8811.

Lowery, L.A., and Van Vactor, D. (2009). The trip of the tip: understanding the growth cone machinery. Nat Rev Mol Cell Biol *10*, 332-343.

Luo, L. (2000). Rho GTPases in neuronal morphogenesis. Nature reviews Neuroscience *1*, 173-180.

Luo, L. (2002). Actin cytoskeleton regulation in neuronal morphogenesis and structural plasticity. Annu Rev Cell Dev Biol *18*, 601-635.

Luscher, C., and Malenka, R.C. (2012). NMDA receptor-dependent long-term potentiation and long-term depression (LTP/LTD). Cold Spring Harbor perspectives in biology *4*.

Ma, Q.L., Yang, F., Calon, F., Ubeda, O.J., Hansen, J.E., Weisbart, R.H., Beech, W., Frautschy, S.A., and Cole, G.M. (2008). p21-activated kinase-aberrant activation and translocation in Alzheimer disease pathogenesis. The Journal of biological chemistry *283*, 14132-14143.

Manna, T., Thrower, D.A., Honnappa, S., Steinmetz, M.O., and Wilson, L. (2009). Regulation of microtubule dynamic instability in vitro by differentially phosphorylated stathmin. The Journal of biological chemistry *284*, 15640-15649.

Manser, E., Leung, T., Salihuddin, H., Zhao, Z.S., and Lim, L. (1994). A brain serine/threonine protein kinase activated by Cdc42 and Rac1. Nature *367*, 40-46.

Manser, E., Loo, T.H., Koh, C.G., Zhao, Z.S., Chen, X.Q., Tan, L., Tan, I., Leung, T., and Lim, L. (1998). PAK kinases are directly coupled to the PIX family of nucleotide exchange factors. Molecular cell *1*, 183-192.

Martel, G., Nishi, A., and Shumyatsky, G.P. (2008). Stathmin reveals dissociable roles of the basolateral amygdala in parental and social behaviors. Proceedings of the National Academy of Sciences of the United States of America *105*, 14620-14625.

Martin, E., Ouellette, M.H., and Jenna, S. (2016). Rac1/RhoA antagonism defines cell-to-cell heterogeneity during epidermal morphogenesis in nematodes. The Journal of cell biology *215*, 483-498.

Matsuzaki, M., Ellis-Davies, G.C., Nemoto, T., Miyashita, Y., Iino, M., and Kasai, H. (2001). Dendritic spine geometry is critical for AMPA receptor expression in hippocampal CA1 pyramidal neurons. Nat Neurosci *4*, 1086-1092.

Matus, A., Ackermann, M., Pehling, G., Byers, H.R., and Fujiwara, K. (1982). High actin concentrations in brain dendritic spines and postsynaptic densities. Proceedings of the National Academy of Sciences of the United States of America *79*, 7590-7594.

Melander Gradin, H., Marklund, U., Larsson, N., Chatila, T.A., and Gullberg, M. (1997). Regulation of microtubule dynamics by Ca2+/calmodulin-dependent kinase IV/Gr-dependent phosphorylation of oncoprotein 18. Molecular and cellular biology *17*, 3459-3467.

Mendoza-Naranjo, A., Gonzalez-Billault, C., and Maccioni, R.B. (2007). Abeta1-42 stimulates actin polymerization in hippocampal neurons through Rac1 and Cdc42

Rho GTPases. Journal of cell science *120*, 279-288.

Merriam, E.B., Millette, M., Lumbard, D.C., Saengsawang, W., Fothergill, T., Hu, X., Ferhat, L., and Dent, E.W. (2013). Synaptic regulation of microtubule dynamics in dendritic spines by calcium, F-actin, and drebrin. The Journal of neuroscience : the official journal of the Society for Neuroscience *33*, 16471-16482.

Miller, M.B., Yan, Y., Eipper, B.A., and Mains, R.E. (2013). Neuronal Rho GEFs in synaptic physiology and behavior. Neuroscientist *19*, 255-273.

Momboisse, F., Lonchamp, E., Calco, V., Ceridono, M., Vitale, N., Bader, M.F., and Gasman, S. (2009). betaPIX-activated Rac1 stimulates the activation of phospholipase D, which is associated with exocytosis in neuroendocrine cells. Journal of cell science *122*, 798-806.

Moon, S.Y., and Zheng, Y. (2003). Rho GTPase-activating proteins in cell regulation. Trends in cell biology *13*, 13-22.

Naisbitt, S., Kim, E., Tu, J.C., Xiao, B., Sala, C., Valtschanoff, J., Weinberg, R.J., Worley, P.F., and Sheng, M. (1999). Shank, a novel family of postsynaptic density proteins that binds to the NMDA receptor/PSD-95/GKAP complex and cortactin. Neuron *23*, 569-582.

Newey, S.E., Velamoor, V., Govek, E.E., and Van Aelst, L. (2005). Rho GTPases, dendritic structure, and mental retardation. Journal of neurobiology *64*, 58-74.

Nimchinsky, E.A., Sabatini, B.L., and Svoboda, K. (2002). Structure and function of dendritic spines. Annu Rev Physiol *64*, 313-353.

Oh, W.K., Yoo, J.C., Jo, D., Song, Y.H., Kim, M.G., and Park, D. (1997). Cloning of a SH3 domain-containing proline-rich protein, p85SPR, and its localization in focal adhesion. Biochem Biophys Res Commun *235*, 794-798.

Ohkawa, N., Fujitani, K., Tokunaga, E., Furuya, S., and Inokuchi, K. (2007). The microtubule destabilizer stathmin mediates the development of dendritic arbors in neuronal cells. Journal of cell science *120*, 1447-1456.

Omelchenko, T., Rabadan, M.A., Hernandez-Martinez, R., Grego-Bessa, J., Anderson, K.V., and Hall, A. (2014). beta-Pix directs collective migration of anterior visceral endoderm cells in the early mouse embryo. Genes & development *28*, 2764-2777.

Park, E., Na, M., Choi, J., Kim, S., Lee, J.R., Yoon, J., Park, D., Sheng, M., and Kim, E. (2003). The Shank family of postsynaptic density proteins interacts with and promotes synaptic accumulation of the beta PIX guanine nucleotide exchange factor for Rac1 and Cdc42. The Journal of biological chemistry *278*, 19220-19229.

Park, J., Kim, Y., Park, Z.Y., Park, D., and Chang, S. (2012). Neuronal specific betaPix-b stimulates actin-dependent processes via the interaction between its PRD and WH1 domain of N-WASP. J Cell Physiol *227*, 1476-1484.

Parnas, D., Haghighi, A.P., Fetter, R.D., Kim, S.W., and Goodman, C.S. (2001). Regulation of postsynaptic structure and protein localization by the Rho-type guanine nucleotide exchange factor dPix. Neuron *32*, 415-424.

Peca, J., Feliciano, C., Ting, J.T., Wang, W., Wells, M.F., Venkatraman, T.N., Lascola, C.D., Fu, Z., and Feng, G. (2011). Shank3 mutant mice display autistic-like behaviours and striatal dysfunction. Nature *472*, 437-442.

Penzes, P., Cahill, M.E., Jones, K.A., VanLeeuwen, J.E., and Woolfrey, K.M. (2011). Dendritic spine pathology in neuropsychiatric disorders. Nat Neurosci *14*, 285-293.

Poirazi, P., and Mel, B.W. (2001). Impact of active dendrites and structural plasticity on the memory capacity of neural tissue. Neuron *29*, 779-796.

Poulain, F.E., and Sobel, A. (2010). The microtubule network and neuronal morphogenesis: Dynamic and coordinated orchestration through multiple players. Molecular and cellular neurosciences *43*, 15-32.

Ramakers, G.J., Wolfer, D., Rosenberger, G., Kuchenbecker, K., Kreienkamp, H.J., Prange-Kiel, J., Rune, G., Richter, K., Langnaese, K., Masneuf, S.*, et al.* (2012). Dysregulation of Rho GTPases in the alphaPix/Arhgef6 mouse model of X-linked intellectual disability is paralleled by impaired structural and synaptic plasticity and cognitive deficits. Human molecular genetics *21*, 268-286.

Ramos, J.M. (2000). Long-term spatial memory in rats with hippocampal lesions. Eur J Neurosci *12*, 3375-3384.

Rampon, C., and Tsien, J.Z. (2000). Genetic analysis of learning behavior-induced structural plasticity. Hippocampus *10*, 605-609.

Ravelli, R.B., Gigant, B., Curmi, P.A., Jourdain, I., Lachkar, S., Sobel, A., and Knossow, M. (2004). Insight into tubulin regulation from a complex with colchicine and a stathmin-like domain. Nature *428*, 198-202.

Ren, Y., Li, R., Zheng, Y., and Busch, H. (1998). Cloning and characterization of GEF-H1, a microtubule-associated guanine nucleotide exchange factor for Rac and Rho GTPases. The Journal of biological chemistry *273*, 34954-34960.

Rhee, S., Yang, S.J., Lee, S.J., and Park, D. (2004). betaPix-b(L), a novel isoform of betaPix, is generated by alternative translation. Biochem Biophys Res Commun *318*, 415-421.

Ryan, X.P., Alldritt, J., Svenningsson, P., Allen, P.B., Wu, G.Y., Nairn, A.C., and Greengard, P. (2005). The Rho-specific GEF Lfc interacts with neurabin and spinophilin to regulate dendritic spine morphology. Neuron *47*, 85-100.

Saetre, P., Jazin, E., and Emilsson, L. (2011). Age-related changes in gene expression are accelerated in Alzheimer's disease. Synapse (New York, NY) *65*, 971-974.

Saneyoshi, T., Wayman, G., Fortin, D., Davare, M., Hoshi, N., Nozaki, N., Natsume, T., and Soderling, T.R. (2008). Activity-dependent synaptogenesis: regulation by a CaM-kinase kinase/CaM-kinase I/betaPIX signaling complex. Neuron *57*, 94-107.

Santiago-Medina, M., Gregus, K.A., and Gomez, T.M. (2013). PAK-PIX interactions regulate adhesion dynamics and membrane protrusion to control neurite outgrowth. Journal of cell science *126*, 1122-1133.

Schmidt, A., and Hall, A. (2002). Guanine nucleotide exchange factors for Rho GTPases: turning on the switch. Genes & development *16*, 1587-1609.

Schubart, U.K., Yu, J., Amat, J.A., Wang, Z., Hoffmann, M.K., and Edelmann, W. (1996). Normal development of mice lacking metablastin (P19), a phosphoprotein implicated in cell cycle regulation. The Journal of biological chemistry *271*, 14062-14066.

Shin, E.Y., Shin, K.S., Lee, C.S., Woo, K.N., Quan, S.H., Soung, N.K., Kim, Y.G., Cha, C.I., Kim, S.R., Park, D.*, et al.* (2002). Phosphorylation of p85 beta PIX, a Rac/Cdc42-specific guanine nucleotide exchange factor, via the Ras/ERK/PAK2 pathway is required for basic fibroblast growth factor-induced neurite outgrowth. The Journal of biological chemistry *277*, 44417-44430.

Shin, M.S., Song, S.H., Shin, J.E., Lee, S.H., Huh, S.O., and Park, D. (2019). Src-mediated phosphorylation of betaPix-b regulates dendritic spine morphogenesis. Journal of cell science.

Shirafuji, T., Ueyama, T., Yoshino, K., Takahashi, H., Adachi, N., Ago, Y., Koda, K., Nashida, T., Hiramatsu, N., Matsuda, T.*, et al.* (2014). The role of Pak-interacting

exchange factor-beta phosphorylation at serines 340 and 583 by PKCgamma in dopamine release. The Journal of neuroscience : the official journal of the Society for Neuroscience *34*, 9268-9280.

Sholl, D.A. (1953). Dendritic organization in the neurons of the visual and motor cortices of the cat. Journal of anatomy *87*, 387-406.

Shumyatsky, G.P., Malleret, G., Shin, R.M., Takizawa, S., Tully, K., Tsvetkov, E., Zakharenko, S.S., Joseph, J., Vronskaya, S., Yin, D.*, et al.* (2005). stathmin, a gene enriched in the amygdala, controls both learned and innate fear. Cell *123*, 697-709.

Silva, A.J., Paylor, R., Wehner, J.M., and Tonegawa, S. (1992). Impaired spatial learning in alpha-calcium-calmodulin kinase II mutant mice. Science (New York, NY) *257*, 206-211.

Silverman, J.L., Yang, M., Lord, C., and Crawley, J.N. (2010). Behavioural phenotyping assays for mouse models of autism. Nature reviews Neuroscience *11*, 490-502.

Smith, K.R., Davenport, E.C., Wei, J., Li, X., Pathania, M., Vaccaro, V., Yan, Z., and Kittler, J.T. (2014). GIT1 and betaPIX are essential for GABA(A) receptor synaptic stability and inhibitory neurotransmission. Cell Rep *9*, 298-310.

Song, Y., and Brady, S.T. (2015). Post-translational modifications of tubulin: pathways to functional diversity of microtubules. Trends in cell biology *25*, 125-136.

Stevens, B.M., Folts, C.J., Cui, W., Bardin, A.L., Walter, K., Carson-Walter, E., Vescovi, A., and Noble, M. (2014). Cool-1-mediated inhibition of c-Cbl modulates multiple critical properties of glioblastomas, including the ability to generate tumors in vivo. Stem Cells *32*, 1124-1135.

Sun, Y., and Bamji, S.X. (2011). beta-Pix modulates actin-mediated recruitment of

synaptic vesicles to synapses. The Journal of neuroscience : the official journal of the Society for Neuroscience *31*, 17123-17133.

Takano, T., Xu, C., Funahashi, Y., Namba, T., and Kaibuchi, K. (2015). Neuronal polarization. Development (Cambridge, England) *142*, 2088-2093.

Tashiro, A., and Yuste, R. (2008). Role of Rho GTPases in the Morphogenesis and Motility of Dendritic Spines. *439*, 285-302.

Tay, H.G., Ng, Y.W., and Manser, E. (2010). A vertebrate-specific Chp-PAK-PIX pathway maintains E-cadherin at adherens junctions during zebrafish epiboly. PLoS One *5*, e10125.

Tian, X., Tian, Y., Sarich, N., Wu, T., and Birukova, A.A. (2012). Novel role of stathmin in microtubule-dependent control of endothelial permeability. FASEB journal : official publication of the Federation of American Societies for Experimental Biology *26*, 3862-3874.

Tolias, K.F., Bikoff, J.B., Burette, A., Paradis, S., Harrar, D., Tavazoie, S., Weinberg, R.J., and Greenberg, M.E. (2005). The Rac1-GEF Tiam1 couples the NMDA receptor to the activity-dependent development of dendritic arbors and spines. Neuron *45*, 525-538.

Tolias, K.F., Duman, J.G., and Um, K. (2011). Control of synapse development and plasticity by Rho GTPase regulatory proteins. Progress in neurobiology *94*, 133-148.

Totaro, A., Tavano, S., Filosa, G., Gartner, A., Pennucci, R., Santambrogio, P., Bachi, A., Dotti, C.G., and de Curtis, I. (2012). Biochemical and functional characterisation of alphaPIX, a specific regulator of axonal and dendritic branching in hippocampal neurons. Biology of the cell *104*, 533-552.

Uchida, S., Martel, G., Pavlowsky, A., Takizawa, S., Hevi, C., Watanabe, Y., Kandel,

E.R., Alarcon, J.M., and Shumyatsky, G.P. (2014). Learning-induced and stathmin-dependent changes in microtubule stability are critical for memory and disrupted in ageing. Nature communications *5*, 4389.

van Horck, F.P., Ahmadian, M.R., Haeusler, L.C., Moolenaar, W.H., and Kranenburg, O. (2001). Characterization of p190RhoGEF, a RhoA-specific guanine nucleotide exchange factor that interacts with microtubules. The Journal of biological chemistry *276*, 4948-4956.

Volinsky, N., Gantman, A., and Yablonski, D. (2006). A Pak- and Pix-dependent branch of the SDF-1alpha signalling pathway mediates T cell chemotaxis across restrictive barriers. Biochem J *397*, 213-222.

Walczak-Sztulpa, J., Wisniewska, M., Latos-Bielenska, A., Linne, M., Kelbova, C., Belitz, B., Pfeiffer, L., Kalscheuer, V., Erdogan, F., Kuss, A.W.*, et al.* (2008). Chromosome deletions in 13q33-34: report of four patients and review of the literature. Am J Med Genet A *146a*, 337-342.

Watabe-Uchida, M., John, K.A., Janas, J.A., Newey, S.E., and Van Aelst, L. (2006). The Rac activator DOCK7 regulates neuronal polarity through local phosphorylation of stathmin/Op18. Neuron *51*, 727-739.

Witte, H., Neukirchen, D., and Bradke, F. (2008). Microtubule stabilization specifies initial neuronal polarization. The Journal of cell biology *180*, 619-632.

Won, H., Mah, W., Kim, E., Kim, J.W., Hahm, E.K., Kim, M.H., Cho, S., Kim, J., Jang, H., Cho, S.C.*, et al.* (2011). GIT1 is associated with ADHD in humans and ADHD-like behaviors in mice. Nat Med *17*, 566-572.

Wyszynski, M., Lin, J., Rao, A., Nigh, E., Beggs, A.H., Craig, A.M., and Sheng, M. (1997). Competitive binding of alpha-actinin and calmodulin to the NMDA receptor.

Nature *385*, 439-442.

Xie, Z., Cahill, M.E., Radulovic, J., Wang, J., Campbell, S.L., Miller, C.A., Sweatt, J.D., and Penzes, P. (2011). Hippocampal phenotypes in kalirin-deficient mice. Molecular and cellular neurosciences *46*, 45-54.

Yan, Y., Eipper, B.A., and Mains, R.E. (2015). Kalirin-9 and Kalirin-12 Play Essential Roles in Dendritic Outgrowth and Branching. Cerebral cortex (New York, NY : 1991) *25*, 3487-3501.

Yogev, S., and Shen, K. (2017). Establishing Neuronal Polarity with Environmental and Intrinsic Mechanisms. Neuron *96*, 638-650.

Youn, H., Jeoung, M., Koo, Y., Ji, H., Markesbery, W.R., Ji, I., and Ji, T.H. (2007). Kalirin is under-expressed in Alzheimer's disease hippocampus. J Alzheimers Dis *11*, 385-397.

Za, L., Albertinazzi, C., Paris, S., Gagliani, M., Tacchetti, C., and de Curtis, I. (2006). betaPIX controls cell motility and neurite extension by regulating the distribution of GIT1. Journal of cell science *119*, 2654-2666.

Zhang, H., and Macara, I.G. (2006). The polarity protein PAR-3 and TIAM1 cooperate in dendritic spine morphogenesis. Nature cell biology *8*, 227-237.

Zhang, H., Webb, D.J., Asmussen, H., and Horwitz, A.F. (2003). Synapse formation is regulated by the signaling adaptor GIT1. The Journal of cell biology *161*, 131-142.

Zhang, H., Webb, D.J., Asmussen, H., Niu, S., and Horwitz, A.F. (2005). A GIT1/PIX/Rac/PAK signaling module regulates spine morphogenesis and synapse formation through MLC. The Journal of neuroscience : the official journal of the Society for Neuroscience *25*, 3379-3388.

Zhou, Y., Kaiser, T., Monteiro, P., Zhang, X., Van der Goes, M.S., Wang, D., Barak,

B., Zeng, M., Li, C., Lu, C.*, et al.* (2016). Mice with Shank3 Mutations Associated with ASD and Schizophrenia Display Both Shared and Distinct Defects. Neuron *89*, 147-162.

Zimprich, A., Biskup, S., Leitner, P., Lichtner, P., Farrer, M., Lincoln, S., Kachergus, J., Hulihan, M., Uitti, R.J., Calne, D.B.*, et al.* (2004). Mutations in LRRK2 cause autosomal-dominant parkinsonism with pleomorphic pathology. Neuron *44*, 601-607.

국문초록

βPix(beta-PAK (p21-activated kinase) interacting exchange factor)는 액틴 골격근(actin filament)과 미세소관(microutbule)의 핵심 조절 인자인 Rac1과 Cdc42 small GTPase를 활성화시키는 GEF(guanine nucleotide exchange factor)로 잘 알려져 있다. 신경세포에서 βPix는 축삭돌기(axon), 수상돌기가시(dendritic spine), 시냅스(synape) 형성을 조절한다고 알려져 있다. 본 연구에서는 지금까지 신경세포의 발달과정에 관여하는 βPix의 기능 연구가 *in vitro*에서 진행되었다는 점에 착안하여, 본 연구실에서 제작한 βPix heterozygous mouse와 신경세포 특이적 βPix isoform knockout mouse를 통해 신경세포 구조 발달과정에서 βPix의 *in vivo* 기능을 밝히고, 지금까지 알려지지 않은 신경세포 특이적 βPix isoform인 βPix-d의 기능을 밝히고자 하였다.

βPix heterozygous mice는 뇌를 포함한 다양한 조직에서 βPix의 발현이 반으로 감소되어 있다. βPix heterozygous mice로부터 배양한 해마 신경세포는 신경돌기(neurite)의 길이가 짧고 복잡성이 단순화 되어 있으며 수상돌기가시(dendritic spine)의 밀도도 감소 되어있었다. 나아가 골지 염색한 뇌의 신경세포에서 수상돌기(dendrite) 가지의 복잡성과 수상돌기가시(dendritic spine)의 밀도에 결함이 있음을 *in vivo*에서도 확인하였다. 또한, 12주령의 βPix heterozygous mice의 해마에 시냅스 기능을 위해 필요한 NMDA 수용체와 AMPA 수용체의 subunit들의 발현이 감소되어 있고 βPix의 강력한 결합 단백질이자 βPix와 함께 수상돌기가시(dendritic spine) 발달을 조절한

다고 알려진 Git1의 발현도 감소되어 있음을 관찰하였다. 종합하면, βPix가 신경돌기(neurite)와 수상돌기가시(dendritic spine)의 발달과정에 필수적임을 *in vitro*와 *in vivo*에서 확인하였다.

βPix는 선택적 스플라이싱에 의해 신경세포 특이적으로 βPix-b와 βPix-d isoform을 발현하고 있고, 이러한 신경세포 특이적 βPix isoform에 대한 *in vivo* 기능은 보고된 바 없다. 본 연구실에서 제작한 신경세포 특이적 βPix isoform knockout mice의 뇌에는 신경세포 특이적 βPix isoform의 발현이 감소되어 있고, 특히 해마 내 Rac1과 Cdc42의 활성이 감소되어 있다. 신경세포 특이적 βPix isoform knockout mice의 *in vivo* 특징을 규명하기 위한 골지 염색에서 해마 신경세포 수상돌기(dendrite)의 복잡성과 수상돌기가시(dendritic spine)의 밀도에 결함이 관찰되고, 특히 사춘기 단계인 5주령 쥐의 해마 조직에서 NMDA 수용체 subunit 중 GluN2B와 CaMKIIα의 발현이 일시적으로 증가되어 있음을 확인하였다. 또한 신경세포 특이적 βPix isoform knockout mice의 배양한 해마 신경세포의 신경돌기(neurite)와 수상돌기가시(dendritic spine) 구조 발달에 결함이 있음을 확인하였고 더 나아가 흥분성 시냅스와 억제성 시냅스의 밀도 및 이러한 시냅스를 이루는 시냅스 후 구조와 시내스 전 구조의 크기가 감소되어 있음을 관찰하였다. 신경세포 특이적 βPix isoform knockout mice에서 배양한 해마 신경세포에 신경세포 특이적 βPix-b와 βPix-d를 각각 발현시켰을 때, 결함을 보였던 신경돌기(neurite)와 수상돌기가시(dendritic spine)의 발달, 흥분성 시냅스와 억제성 시냅스의 형성이 회복되었다. 흥미롭게도, βPix-b가 수상돌

기가시(dendritic spine)와 흥분성 시냅스 발달에 βPix-d보다 더 필수적으로 작용하고, βPix-d는 신경돌기(neurite)와 억제성 시냅스 발달에 βPix-b보다 더 필수적으로 작용하는 것을 확인함으로써 신경세포 특이적 βPix isoform들간의 신경세포 내 차별화된 기능을 규명하였다.

신경돌기(neurite) 내 미세소관(microtubule) 안정화는 정상적인 신경돌기(neurite) 발달에 중요하고 이는 정상적인 신경망 형성에 필수적이다. 신경세포 특이적 βPix isoform knockout mice의 해마 신경세포는 발달과정 중 이른 시기에 신경돌기(neurite)의 길이와 복잡성에 결함을 보이고 신경돌기(neurite)를 구성하는 미세소관(microtubule)의 안정성도 떨어져 있음이 관찰되었다. 이들 신경세포에서 감소된 미세소관(microtubule)의 안전성을 taxol을 통해 회복시켰을 때 손상된 신경돌기(neurite)의 구조가 회복되는 것을 확인하였다. 또한, 신경세포 특이적 βPix isoform인 βPix-b와 βPix-d의 발현에 의해 미세소관(microtubule)의 안정성이 증가하였고 βPix-b보다 βPix-d에 의해 안정성이 더 크게 증가하였다. βPix-d의 세포 내 발현 위치는 미세소관(microtubule)과 일치하는 것을 확인하였다. 추가적으로 신경세포 특이적 βPix isoform knockout mice의 해마 신경세포에는 미세소관(microtubule)을 불안정화 시키는 단백질인 Stathmin1의 인산화가 감소되어 있음을 확인하였고, βPix-d에 의해 감소되었던 Stathmin1의 인산화가 회복됨도 확인하였다. 또한 같은 시기의 해마 신경세포의 구조도 신경세포 특이적 βPix isoform knockout mice에 βPix-d를 발현시키면 결함을 보였던 신경돌기(neurite)의 구조가 회복되는 것을 확인함으로써, βPix-d에 의

해 Stathmin1의 활성이 감소되어 미세소관(microtubule)의 안정화가 증가됨으로써 신경돌기(neurite) 구조가 발달되는 것을 확인하였다. βPix의 결합 단백질인 PAK1이 Stathmin1을 직접적으로 인산화를 시켜준다는 보고가 있다. 신경세포 특이적 βPix isoform knockout mice의 해마 신경세포에서 PID(PAK inhibitory domain)의 발현에 의해 PAK1의 활성을 저해시키면, βPix-d를 발현하더라도 Stathmin1의 인산화 증가가 관찰되지 않았다. 이 결과는 βPix-d에 의한 Stathmin1의 인산화가 PAK1의 활성을 통한 것임을 제시한다. 본 연구는 βPix-d가 PAK1을 활성화시켜 Stathmin1의 인산화를 증가시킴으로써 미세소관을 안정화시켜 신경돌기 발달을 조절하는 신호전달 기전을 제시한다.

주요어:

βPix; βPix heterozygous mouse; 신경세포 특이적 βPix isoform knockout mouse; βPix-d; 신경돌기; 수상돌기 가시; 미세소관 안정화; Stathmin1

학번:

2012-23056